Synthesis of Graphene by Chemical Vapor Deposition and Solid Phase Reaction Process towards Next Generation Energy Device Applications

化学気相法および固相反応法による次世代エネルギーデバイス用グラフェンの合成

A Thesis
Submitted to the Department of Frontier Materials of
Nagoya Institute of Technology
in partial fulfilment of the
requirements for the degree of
Doctor of Philosophy (PhD)

by
Muhammed Emre Ayhan
Nagoya Institute of Technology, 2014

TABLE OF CONTENTS

ABSTRACT

In this research I demonstrate the synthesis of graphene on Ag foil by the atmospheric pressure (AP) chemical vapor deposition (CVD) process as a tarnish resistant coating. Continuous graphene film on Ag foil is grown using the solid camphor as a carbon precursor with a gas mixture of Ar and H_2. The Raman spectroscopy and transmission electron microscopy studies revealed formation of few-layer graphene structure on Ag surface. Tarnishing of silver surface through sulfidation is investigated with and without coating the graphene film. It is observed that the bare Ag surface immediately react with sulfur vapor to turn black, whereas graphene coating passivates the Ag surface robustly and thereby restraining sulfur reaction to preserve from tarnishing. My findings show that large-area graphne film can be effectively grown on Ag surface by a CVD process as a tarnish and corrosion resistance barrier.

At the second step, formation of the silver nanoparticles (Ag-NPs) in chemical vapor deposited graphene by dissolving base Ag foil and their integration for Schottky junction fabrication was demonstrated an application work. Ag-NPs of the size 20-100 nm were directly obtained on graphene surface by dissolving the base Ag foil of as-synthesized graphene in a diluted nitric acid solution. A Schottky junction is fabricated by transferring the Ag-NPs incorporated graphene on Si substrate. Significant photoresponse is observed with illumination of 3.6, 5.1 and 2.1 mW/cm^2 of near-infrared (1000 nm), visible (550 nm) and near ultraviolet (350 nm) light, respectively. The graphene-Si Schottky junction shows photoresponse of 122, 98 and 78 mAW^{-1} at 550, 350 and 1000 nm, respectively. The strong photoresponce can be attributed to light interaction with the plasmonic Ag-NPs and effective graphene-Si

Schottky junction. My finding shows that enhancing the light absorption with plasmonic nanoparticles weakest of incident light can be detected for a broad-wavelength range.

Synthesis of transfer-free high quality graphene on arbitrary substrate by metal assisted graphitization with a control carbon diffusion process has lot of significant for device applications. In this work, I also demonstrate synthesis of a monolayer graphene using common triblock co-polymer ($EO_nPO_mEO_n$) as carbon source by the solid phase reaction approach. In the synthesis process, a Ni and NiO thin film were used as catalytic and carbon diffusion barrier layer, respectively on top of polymer deposited SiO_2/Si substrate. The long carbon chain of a triblock co-polymer pluronic F127 ($EO_{106}PO_{70}EO_{106}$) can be graphitized in presence of the Ni layer, where carbon diffusion to top surface is controlled by NiO thin layer. The effect of carbon diffusion, thickness of polymer layer and annealing process are studied to obtain high quality monolayer graphene. Findings reveal that the NiO/Ni stacked thickness of polymer layer and reaction process in H_2 atmosphere strongly influence the quality of synthesized graphene.

LIST of FIGURES

CHAPTER I

CHAPTER II

CHAPTER IV

CHAPTER V

CHAPTER VI

LIST of TABLES

LIST of SYMBOLS and ABBREVIATION

SWNT	Single wall nanotubes
MWNT	Multi wall nanotubes
a	Lattice constant for graphite
a_1, a_2	Unit vectors in two-dimensional hexagonal lattice
a_{c-c}	Bond length between two carbon atoms
C_h	Chiral vector
m,n	Integers
RT	Room Temperature
SPM	Scanning Probe Microscopy
CNT	Carbon Nanotube
CCNF	Corn-shaped carbon nanofiber
CVD	Chemical Vapor Deposition
EDS	Electron Diffraction Spectroscopy
AFM	Atomic Force Microscopy
SEM	Scanning Electron Microscopy
TEM	Transmission Electron Microscopy
HRTEM	High Resolution Transmission Electron Microscopy

SAED	Selected area electron diffraction
XPS	X-ray photoelectron spectroscopy
ITO	Indium tin oxide
HOPG	Highly oriented pyrolytic graphite
SiC	Silicon carbide
GO	Graphene Oxide
H_2S	Hydrogen sulfide
OCS	Carbonyl sulfide
sccm	Standard cubic centimeters per minute
FE	Field-effect
FET	Field-effect transistor
IR	Infrared
UV	Ultraviolet
J-V	Current density-voltage
EQE	External quantum efficiency
PMMA	Poly methyl methacrylate
HNO_3	Nitric acid
Ag-NPs	Silver nano particles

V_{oc}	Open circuit voltage
J_{sc}	Current density
FF	Fill factor
PLD	Pulsed laser deposition
FWHM	Full width at half maximum

CHAPTER I

INTRODUCTION

1.1. Study Motivation

1.1.1 Renewable Energy

Among the other living creators the neediest one is human being and demand of human being is endless. New and sustainable energies are the one of the main need of human being owing to decreasing amount of fossil fuels such as oil, coal, natural gas, etc. as well as high cost of conventional energy sources. This humble research may open a door to improve solar photovoltaic technologies towards clean and renewable energy applications.

Renewable energy also so-called clean or green energy is defined as the energy that comes from natural sources in the universe such as biomass, bio-fuel, hydropower, geothermal, wind power and solar power. 19% of global energy consumption of the world supplied from renewable energy in 2011 [1]. As shown in figure 1.1 renewable energy is a minor part of the total world energy consumption. The main obstacle is that compared to other energy sources, sustainable energies are expensive or inefficient to accomplish, and countries aren't really that into hurting their current productivity and global competitiveness for long term policy.

Biomass	9.30%
Bio-heat	3.78%
Bio-power generation	0.35%
Wind power	0.56%
Solar PV	0.08%
Solar CSP	0.004%
Ocean power	0.001%
Geothermal electricity	0.07%
Hydropower	3.73%
Solar hot water	0.22%
Geothermal heat	0.14%
Ethanol	0.55%
Biodiesel	0.23%

Total

Fossil	78.2%
Nuclear	2.8%
Renewable	19.0%

Total World Energy Consumption by Source (2011)
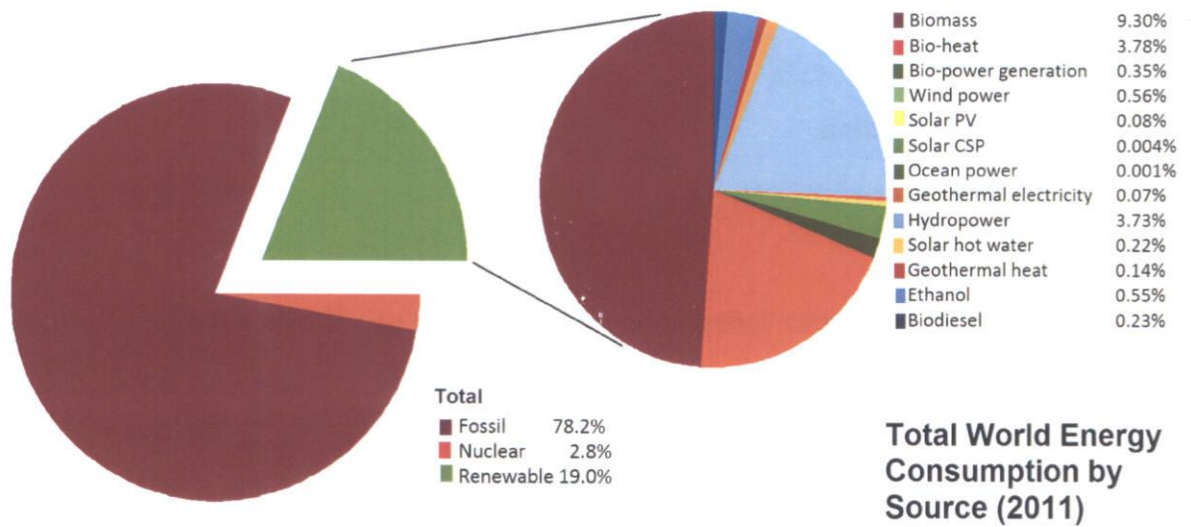
Figure 1.1   Total energy consumption by source in 2011, from REN21 Renewables 2013 Global Reports

According to Global Trends in Renewable Energy Investment 2014 which produced by the Frankfurt School-UNEP Collaborating Centre for Climate & Sustainable Energy Finance, the United Nations Environment Programme (UNEP) and Bloomberg New Energy Finance the investment descent $US35.1 billion was partly due to the falling down cost of solar photovoltaic systems. The other cause was the unstable energy policy in most countries a subject matter that bottled investment in fossil fuel stock in 2013.

1.1.2 Solar Photovoltaic (PV)

Photovoltaic related technologies which are related to converting solar energy into electric energy are the most progressive technologies in terms of solar energy. Solar photovoltaic (PV) improved its cost competitiveness in 2012 and installed from 31GW to 39GW. Renewable energy sources excluding hydro sources account for 43.6% of 2013's reinstalled production capacity. Investments of wind energy remained almost same scale, while solar photovoltaic outlays falled down 20% despite a record amount installed.

China for the first time invested in renewable energy more than Europe and renewable energy investment in Japan increased by 80% in 2013. The year of 2013 was a milestone for renewable energy. First time global solar photovoltaic installations (36.5GW) were greater than global wind power energy source installations (35.5GW). Record scales of new solar photovoltaic installation achieved in Japan, China and USA, while it was a down year in the wind energy industry [2].

According to Clean Edge 2014 energy trends, solar photovoltaics including modules, system components, and installation grew to $91.3 billion from $79.7 billion in 2012, with a record 36.5 GW installed globally. In contrast to 2011 and 2012, when photovoltaic panel costs plummeted more than 20% in both years, prices stabilized last

year, dropping just 3% to $2.50 per watt installed (less than one-third the cost 10 years earlier.) The advanced year in solar energy deployments translated into strong earnings gains as well. Although prices will continue to decrease an estimated 7% per year over the next decade, to $1.21 per watt by 2023 as shown in figure 1.2, double-digit annual growth in capacity will fuel strong income growth to $158.4 billion in 2023.

Global Clean-Energy Projected Growth 2013-2023 ($US Billions)

	2013	2023
Biofuels	$97.8	$145.6
Wind Power	$58.5	$93.8
Solar Power	$91.3	$158.4
TOTAL	$247.6	$397.8

Source: Clean Edge, Inc., 2014
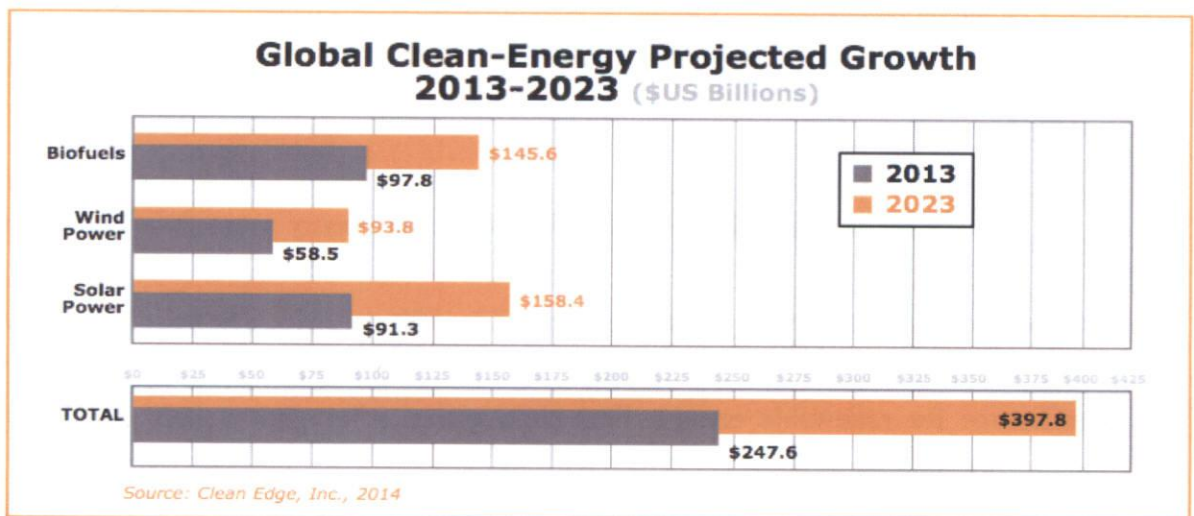
Figure 1.2   Growth of global clean energy project for 2013-2023[2]

The USA installed an estimated 4.2GW of new solar photovoltaic in 2013, deploying more than Germany (an estimated 3.3GW) for the first time in more than a decade. , According to Bloomberg New Energy Finance China installed 12 GW of solar photovoltaic in 2013 roughly as much as total cumulative solar photovoltaic

installations in the USA, and nearly triple the 4.5 GW deployed in China the year before. Before 2013, no any country had ever added more than 8 GW in year. Japan, continuing to replace most of its nuclear power, also installed a record amount of new solar photovoltaic capacity in 2013, approximately 7 GW.

According to above mentioned statistics solar photovoltaic one of the fastest growing technology for renewable energy sources. This next generation energy source can be remedy for the demand of human beings clean energy.

1.2 Purpose and Outline of Thesis

Graphene based composite nanomaterials can be used for various energy device applications. High speed transistors, semiconductors, transparent electrodes, optic lasers, hydrogen storage systems, nano electro-mechanical systems etc. have been widely demonstrated, considering unique electronic, optical, mechanical and chemical properties of graphene. Being electrically conductive and transparent and having to capability of absorbing different wavelength of light give an opportunity to be employed in solar energy device applications. Graphene also can be used in new generation batteries and super capacitors as electrodes. Compare to graphite anodes used commercial lithium-ion batteries, graphene based batteries almost 10 times faster. On

the other hand supercapacitors can be charged and discharged hundred thousands of times. Supercapacitors can store and deliver energy in a short time. Therefore graphene based super capacitors can be considered one of the most promising energy device applications.

Graphene has been isolated just 10 years ago, though remarkable synthesis methods and applications have been investigated and demonstrated. Thousands of different papers presented in last decade. However main issue in the graphene studies is the commercialization in the market. Furthermore synthesis of graphene with well-ordered structure and fabrication of graphene based nanomaterial devices have to be improve and modified according to proper functional applications.

Synthesis of graphene have been carried out by various approaches, including, micromechanical cleavage of highly oriented pyrolytic graphite (HOPG) [3], epitaxial growth on silicon carbide (SiC) [4], reduction of chemically exfoliated graphene oxide [5] and chemical vapor deposition (CVD) on transition metals [6-8]

Typically in a chemical vapor deposition (CVD) process to growth high quality graphene film, catalytic decomposition of hydrocarbons on metals such as nickel, copper and cobalt is the most essential method [9, 15]. Similarly, ruthenium, iridium, platinum, palladium and non-catalytic gold have been also investigated as a substrate

material for graphene synthesis in a CVD process [16-19]. However there was no report about synthesis of graphene on silver. Among the other materials the most electrically conductive metal is the silver. Furthermore unique optical, thermal and surface plasmonic properties of silver have attracted me to study on synthesis of graphene on noble metal silver.

In this thesis, synthesis of continuous graphene film on silver by thermal atmospheric pressure CVD process using solid carbon source has demonstrated for the first time, considering unique optical and electrical properties of silver. On the other hand silver can be extensively used in commercial optical devices like solar panel and electrical devices like ceramic capacitors, contacts, switches etc. However, sulfurization of Ag surface with formation of Ag_2S, also known as tarnishing is one of the main problem in many applications [20, 21]. The corrosion and formation of a rough surface with sulfidation can reduce optical properties and constraining various applications [22].

In these prospects, synthesis of graphene on Ag surface by a CVD approach can be very interesting. The synthesized continuous graphene film effectively passivates the Ag surface and restricts sulfurization to prevent from corrosion. Synthesized graphene film can supply effective preserving for many optical and electrical devices. Details of this study will be discussed in chapter IV.

To fabricate next generation energy device application graphene has to be modified or integrated with other materials. Combination of graphene based materials with other conventional semiconductors is of great interest for solar photovoltaic technologies [23-28]. In such type of applications, graphene not only act as a transparent conductor but also facilitate photo-exciton dissociation and charge separation. Graphene can also provide an efficient charge transportation owing to significant high carrier mobility property. Graphene with the ability to tune the Fermi energy can be also ideal material to fabricate high performance broadband photodetectors. However, in the previous studies optical absorption in a monolayer graphene was still considerably low, which can be overcome with integration of surface plasmonic nanoparticles. To design a photodetector with a simple device architecture and high light sensitivity can be critical in practical applications. In this aspect and contrast to previous reports, graphene based Schottky junction device with plasmonic metal nanoparticles can be a promising approach to achieve high photoresponsivity.

In this study CVD derived graphene was decorated with silver nanoparticles to fabricate a photodetector with high light sensitivity and simple device architecture, considering excellent properties of silver such as electrical and optical properties including strong interaction with light of silver. On the other hand if one-step approach

could be achieved to obtain silver nanoparticles is the ideal solution. Therefore in this work non-catalytic silver was used as catalyst and silver nanoparticles were directly obtained on graphene without using any other reagent in my demonstrated one-step approach for the first time.

In regards to practical device applications, high quality CVD graphene must be transferred to insulting substrates. To overcome drawback of the transfer process, direct synthesis of graphene on the required substrate has been explored for practically feasible device applications [29-32]. Previously, Ismach et al. has demonstrated direct growth of few-layer graphene on dielectric surface by a CVD approach owing to evaporation of Cu catalytic layer during growth process [33]. Similarly, direct graphene growth has been achieved on germanium (Ge) in a CVD process [34]. Previously, our group have also demonstrated synthesis of bi-layer and few-layer graphene on SiO_2/Si substrate by Co catalytic layer assisted crystallization of a-C thin film [35].

Transfer-free synthesis of few-layer graphene has been integrated with n-Si substrate to fabricate a Schottky junction. However, control carbon diffusion and graphitization process at the metal catalytic layer and substrate interface were inhomogeneous to obtain a monolayer graphene. Crystallization of the a-C thin film at the substrate interface remains a challenge to obtain high quality monolayer graphene.

For the first time a monolayer graphene growth was demonstrated using common type block co-polymer ($EO_nPO_mEO_n$) as carbon source by the solid phase reaction approach presence of carbon diffusion barrier. In this work, I used the Pluronic F127 ($EO_{106}PO_{70}EO_{106}$) co-polymer as the carbon source to synthesis graphene on a SiO_2/Si substrate, avoiding additional transfer step. The tri-block co-polymer can be easily dissolved in common organic solvents such as acetone, ethanol and methanol or water considering the low molecular weight. Furthermore block co-polymer can provide better graphitization during graphene growth process owing to long carbon chain structure.

1.3   References

[1]   REN21 Renewables 2013 Global Reports

[2]   Clean Energy Trends 2014 by Clean Edges

[3]   K. S. Novoselov, D. Jiang, F. Schedin, T. J. Booth, V. V. Khotkevich, S. V. Morozov, and A. K. Geim, *Proc. Natl. Acad. Sci.* **102, 10451** (2005).

[4]   C. Berger, Z. Song, X. Li, X. Wu, N. Brown, C. Naud, D. Mayou, T. Li, J. Hass, A. N. Marchenkov, E. H. Conrad, P. N. First, and W. A. de Heer, *Science* **312, 1191** (2006).

[5]   S. Stankovich, D. A. Dikin, G. H. B. Dommett, K. M. Kohlhaas, E. J. Zimney, E. A. Stach, R. D. Piner, S. T. Nguyen, and R. S. Ruoff, *Nature* **442, 282** (2006).

[6]   P. R. Somani, S. P. Somani and M. Umeno, *Chem. Phys. Lett.* **430, 56** (2006).

[7]   Q. Yu,J. Lian, S. Siriponglert, H. Li, Y. P. Chen and S. S. Pei, *Appl. Phys. Lett.* **93, 113103** (2008).

[8]   A. Reina, X. Jia, H. John, D. Nezich, H. Son, V. Bulovic, M.S. Dresselhaus, and J. Kong, *Nano Lett.* **9, 30** (2009).

[9]   B. C. Banerjee, T. J. Hirt and P. L. Walker, Nature **192, 450** (1961).

[10]   I. Alstrup, I. Chorkendorff, and S. Ullmann, *Surf. Science* **264, 95** (1992).

[11]   K. S. Kim, Y. Zhao, H. Jang, S. Y. Lee, J. M. Kim, K. S. Kim, J. H. Ahn, P. Kim, J. Y. Choi, and B. H. Hong, *Nature* **457, 706** (2009).

[12]   X. S. Li, W. W. Cai, J. H. An, S. Kim, J. Nah, D. X. Yang, R. Piner, A. Velamakanni, I. Jung, E. Tutuc, S. K. Banerjee, L. Colombo, and R. S. Ruoff, *Science* **324, 1312** (2009).

[13]   S. Bae, H. K. Kim, Y. Lee, X. Xu, J. Park, Y. Zheng, J. Balakrishnan, D. Im, T. Lei, Y. Song, Y. Kim, K. Kim, B. Ozyimaz, J. Ahn, B. Hong, and S. Iijima, *Nat. Nanotechnol.* **5, 574** (2010).

[14]   E. Sutter, P. Albrecht, and P. Sutter, *Appl. Phys. Lett.* **95, 133109** (2009).

[15]   R. Hirano, K. Matsubara, G. Kalita, Y. Hayashia, and Masaki Tanemura, *Nanoscale* **4, 7791** (2012).

[16]   J. Coraux, A. T. N'Diaye, M. Engler, C. Busse, D. Wall, N. Buckanie, F. Heringdorf, R. van Gastei, B. Poelsema and T. Michely, *New Jour. Phys.* **11, 023006** (2009).

[17]   J. Wintterlin, and M. L. Bocquet, *Surf. Science* **603, 1841** (2009).

[18]   L. Gao, J. R. Guest, and N. P. Guisinger, *Nano Lett.* **10, 3512** (2010).

[19]   T. Oznuluer, E. Pince, E. O. Polat, O. Balci, O. Salihoglu, and C. Kocabas, *Appl. Phys. Lett.* **98, 183101** (2011).

[20]   H. E. Bennett, R. L. Peck, D. K. Burge, J. M. Bennett, *J. Appl. Phys.* **40, 3351** (1969).

[21]   J. L. Elechiguerra, L. L. Lopez, C. Liu, D. G. Gutierrez, A. C. Bragado, and M. J. Yacaman, *Chem. Mater.* **17, 6042** (2005).

[22]   J. C. Reed, H. Zhu, A. Y. Zhu, C. Li, and E. Cubukcu, *Nano Lett.* **12, 4090** (2012).

[23]   X. Li, H. Zhu, K. Wang, A. Cao, J. Wei, C. Li, Y. Jia, Z. Li, X. Li and D. Wu, *Adv.Mater.,* **22, 2743,** (2010)

[24]   X. Miao, S. Tongay, M. K. Petterson, K. Berke, A. G. Rinzler, B. R. Appleton and A. F. Hebard, *Nano Lett.,* **12, 2745** ,(2012)

[25]   H. Yang, J. Heo, S. Park, H. J. Song, D. H. Seo, K. E. Byun, P. Kim, I. Yoo, H. J. Chung and K. Kim, *Science,* **336, 1140,** (2012)

[26]   Y. An, A. Behnam, E. Pop and A. Ural, *App. Phys. Lett.,* **102, 013110,** (2013)

[27]   X. An, F. Liu, Y. J. Jung and S. Kar, *Nano Lett. ,* **13, 909,** (2013)

[28]   X. Wang, Z. Cheng, K. Xu, H. Tsang and J. B. Xu, *Nature Photo.,* **7, 888,** (2013)

[29]   Yan Z, Peng Z, Sun Z, Yao J, Zhu Y, Liu Z, Ajayan P M andTour J M, *ACS Nano,* **5 8187** (2011)

[30]   Su C Y et al Nano *Lett.* **11 3612,** (2011)

[31]   GKalita, M SKayashta, K Wakita and M Umeno,*RSCAdv.,* **2 3225**(2012)

[32]   J Kwak et al,*Nature Commun.,* **3 1**(2012)

[33]   Ismach, A.; Druzgalski, C.; Penwell, S.; Schwartzberg, A.;Zheng, M.; Javey, A.; Bokor, J.; Zhang, Y.,*Nano Lett.,* **10, 1542–1548** (2010.)

[34]   Gang Wang et al., *Scientific Reports* **3, 10, 1038** (2013)

[35]   G. Kalita, R. Hirano, M.E.Ayhan, M.Tanemura, *J.Phys. D. Appl Phys.* **46, 455103** (2013)

CHAPTER II

LITERATURE SURVEY

2.1   An Overview of Frontier Carbon Materials

2.1.1   Fullerenes

A fullerene is a molecule composed of carbon in the form of a hollow sphere, tube or other shapes. Spherical fullerenes are also called buckyballs, and they resemble the balls used in soccer. Cylindrical fullerenes are called carbon nanotubes (CNTs) or Bucky tubes. Fullerenes are similar in structure to graphite, which is composed of stacked graphene sheets of linked hexagonal rings; but they may also contain pentagonal (or sometimes heptagonal) rings. The first fullerene molecule to be discovered, and the family's namesake, buck minister fullerene (C_{60}), was prepared at Rice University by Richard Smalley, Robert Curl, James Heath, Sean O'Brien, and Harold Kroto in 1985 [1].
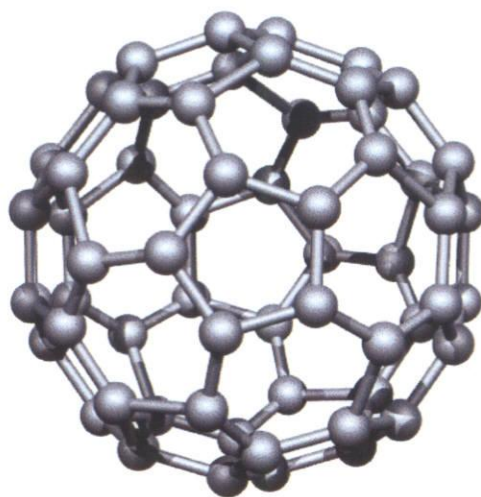
Figure 2.1.1   Fullerene C_{60} molecule structure

Figure 2.1.1 represents the fullerene C_{60} molecule structure. Fullerenes consist

of 20 hexagonal and 12 pentagonal rings as the basis of an icosahedral symmetry closed

cage structure. Each carbon atom is bonded to three others and is sp^2 hybridized. The

C_{60} molecule has two bond lengths - the 6:6 ring bonds can be considered "double

bonds" and are shorter than the 6:5 bonds. C_{60} is not "super aromatic" as it tends to avoid

double bonds in the pentagonal rings, resulting in poor electron delocalization. As a

result, C_{60} behaves like an electron deficient alkene, and reacts readily with electron rich

species. The geodesic and electronic bonding factors in the structure account for the

stability of the molecule. In theory, an infinite number of fullerenes can exist, their

structure based on pentagonal and hexagonal rings, constructed according to rules for

making icosahedra. Table 2.1.1 shows the physical properties of fullerene C_{60}.

Density	1.65 g cm-3
Standard heat of formation	9.08 kcal mol^{-1}
Index of refraction	2.2 (at 600nm)
Boiling point	800K
Resistivity	1014 ohms m^{-1}
Crystallinity form	Hexagonal cubic
Vapor pressure	5 x 10^{-6} torr at RT

Table 2.1.1   Physical properties of fullerene C_{60}

2.1.2 Carbon Nanotubes

A large percentage of academic and popular literature attributes the discovery of hollow, nanometer-size tubes composed of graphitic carbon which named as carbon nanotubes to Sumio Iijima of NEC in 1991. Carbon nanotubes are layers of graphite wrapped into cylinder in shape of few nanometers in diameters, and approximately 10-20 microns in length. There are two main types of nanotubes which are single wall nanotubes (SWNT) and multi wall nanotubes (MWNT). Rolling a single graphite sheet into a cylinder forms SWNT, several graphite sheet into a cylinder forms MWNT with an inner layer spacing of about 0.34 to 0.36nm^2 [2].

Structure of a nanotube is can be considered as similar to the structure of graphite, which consists of a single layer of carbon atoms arranged in a chicken wire structure. These honeycomb layers are stacked on top of each other. In graphite sp^2 hybridization three sp^2 orbitals are formed at 120^0 to each other within a plane and sigma bonds which is a covalent bond. This strong sigma bonds strongly bind the atoms in plane. Out of-plane that perpendicular to the plane called π bond is much weaker than the in plane sigma bonds. The structure of a carbon nanotube can be described by using a chiral vector. As shown in figure 2.1.2 three types of carbon nanotubes are possible, armchair, zigzag and chiral nanotubes, based on how the two-dimensional graphene sheet is rolled up [3].

Armchair   (n,n)
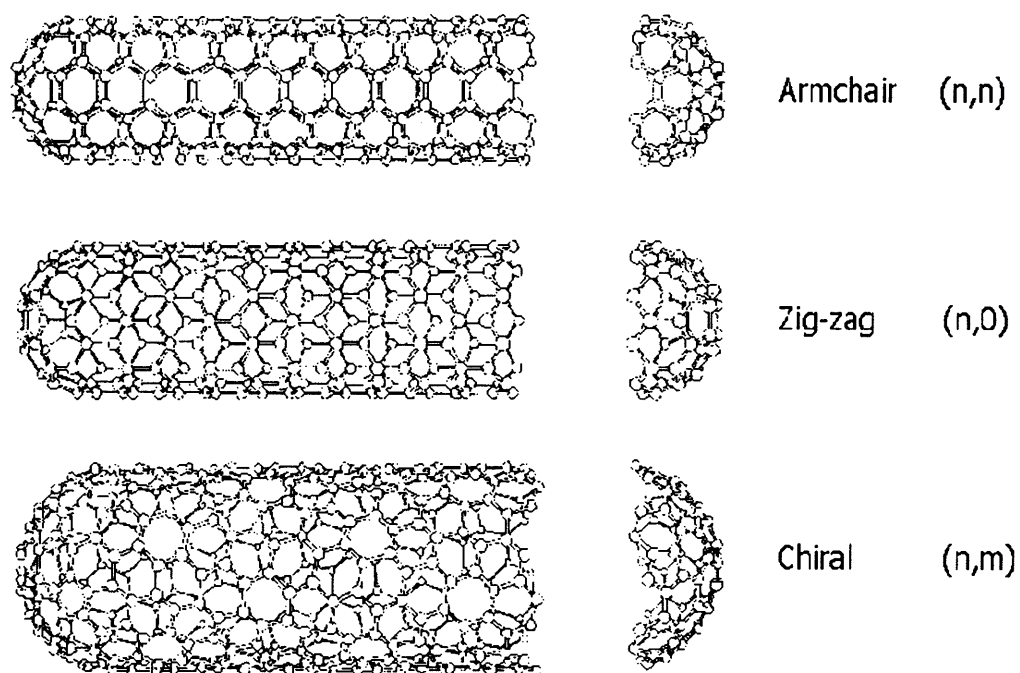
Zig-zag   (n,0)

Chiral   (n,m)

Figure 2.1.2   Armchair SWNT, zig-zag, and chiral nanotubes, respectively [3]

17

The types of carbon nanotubes can be easily defined in regards to the unit cell of

a carbon nanotube. The chiral vector of the carbon nanotube, *Ch* shown in figure 2.1.3,

is described by *Ch= na1+ma2* where *a1* and *a2* are unit vectors in the two-dimensional

hexagonal lattice, and *n* and *m* are integers [3]. The other important parameter is the

chiral angle that is the angle between *Ch* and *a1*. When a graphene sheet is rolled up to

formation of the cylindrical part of the carbon nanotube, the ends of the chiral vector

meet each other. The chiral vector forms the round of the carbon nanotube's circular

cross-section, and different values of *n* and *m* lead to different carbon nanotube

structures. As shown in figure 2.1.4, armchair carbon nanotubes are formed when *n=m*

and the chiral angle is 30°.

Zigzag carbon nanotubes are formed when either *n* or *m* is zero and the chiral

angle is 30°. Zigzag carbon nanotubes are formed when either *n* or *m* is zero and the

chiral angle is 0°. All other carbon nanotubes, with chiral angles intermediate between

0° and 30°, are known as chiral carbon nanotubes. For the hexagonal lattice a primitive

cell is made of two atoms. Also, *a1* and *a2* are described as two vectors with

120°openings [3]. In the figure *a1* and *a2* can be expressed using the Cartesian

coordinate (x, y) as shown in the figure 2.1.4.
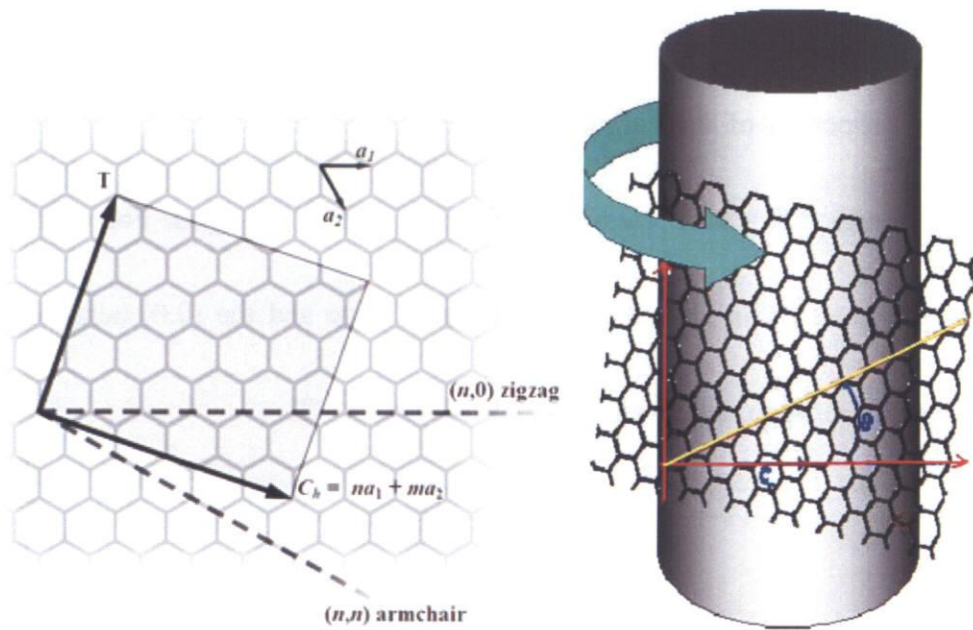
Figure 2.1.3   A layer of graphene sheet showing the chiral vector [4]
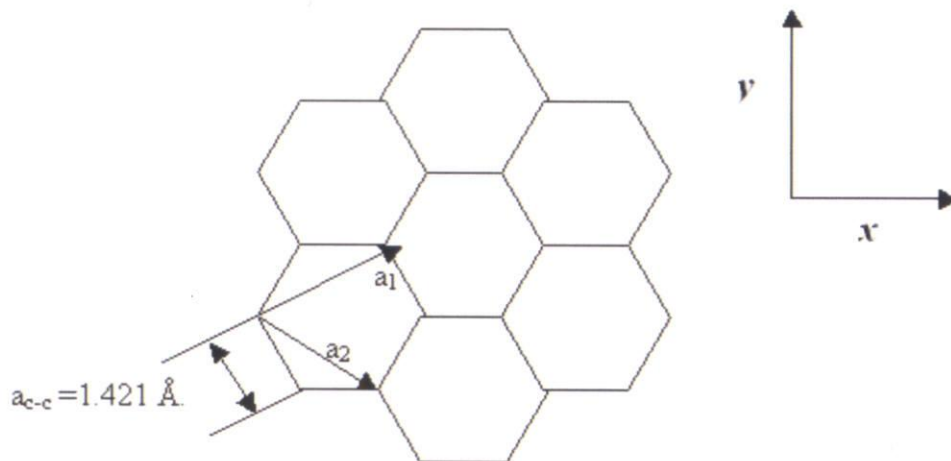
Figure 2.1.4   Unit cell of graphite

It turns inside out that the way in that the sheet is rolled up reconcile to the electronic properties of the carbon nanotube. Researchers quantify this by using the chiral vector to define that crossover with the starting hexagon. For example, if as shown in figure2.1.5 is printed on a transparent page and the (0,0) hexagon overlaps with the (8,0) hexagon, the result would be a (8,0) SWNT.
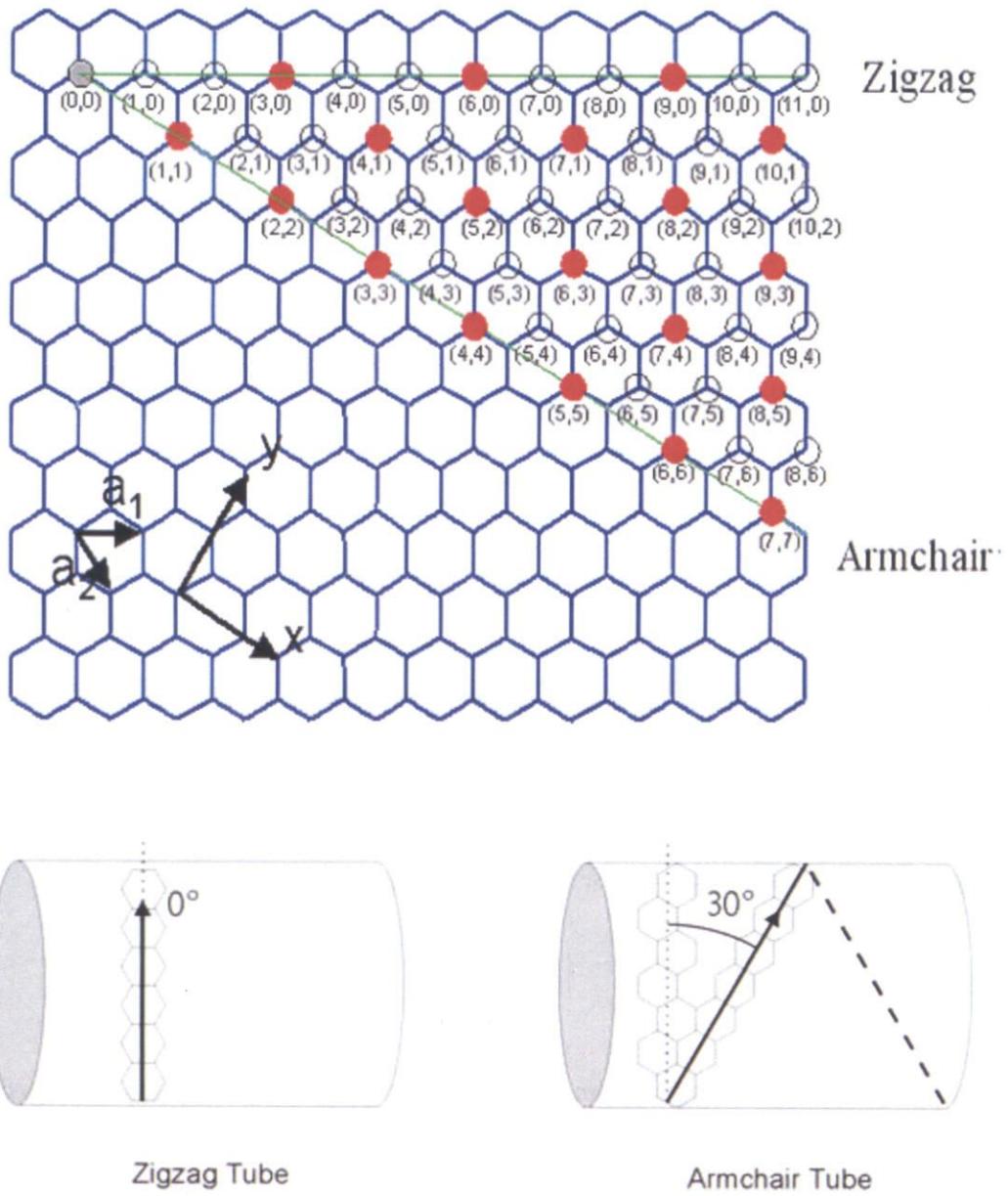
Figure 2.1.5   Vectors specified by the pairs of integers (n, m) for general carbon nanotubes, including armchair, zig-zag, and chiral tubes. The hollow denote metallic tubules while the small dots are for semi conducting tubules.

Carbon nanotubes (CNTs) are the most promising candidates for electrical and mechanical nano devices at present [5]. They offer useful field emission (FE) capability with moderate applied voltages because metallic nanotubes can be assimilated to nano scale tips and their large aspect ratio results in large field enhancement factors [6, 7]. In addition, CNTs have potential application for scanning probe microscopy (SPM) because of their mechanical strength [8]. Emitters or scanning probes using CNTs that bend laterally may be problematic. For example, thermal or mechanical vibration can cause a poor signal-to noise ratio (S/N). Therefore, the fabrication of the corn-shaped carbon nanofibers (CCNFs) with metal free tips to improve the radial rigidity required for improving the performance of SPM and FE flat panel displays [9].

2.2 Graphene

Graphene is a single atom thin layer of pure carbon atoms arranged in a honeycomb or a chicken wire structure. Among the other frontiers of materials, two dimensional (2D) graphene crystals are considered to be main building block of sp^2 hybridized carbon nanomaterials. [10-14]. As an analogy we can compare soil and graphene in terms of productivity. The soil provides the basis of all foods and biomass. Similarly all carbonaceous materials such as fullerenes (0D), carbon nanotubes (1D), graphite (3D) can be produced from 2D graphene. Figure 2.2.1 demonstrates the

different forms of graphene sheets.
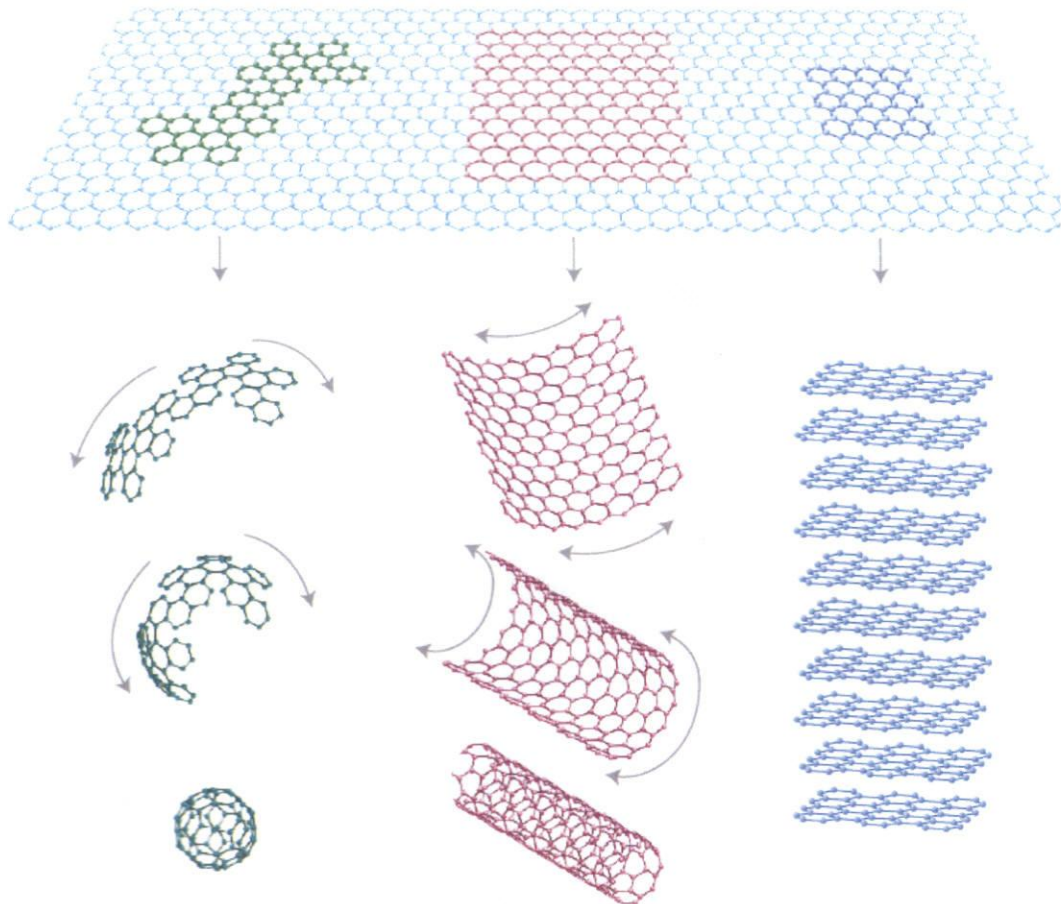
Figure 2.2.1   Representing structure of 0D fullerenes, 1D carbon nanotubes, 2D

graphene and 3D graphite.[12]

Philip R. Wallace was first time explored the theory of graphene in 1947 [15].

His limited work was to understanding the electronic properties of graphite. In 1984,

Gordon Walter Semenof, David DeVincenzo and Eugene J. Mele were attracted

attention to electric current would be carried out by effectively massless charge carriers

in graphene [16]. Attempts to epitaxial grow on top of other crystal surfaces from single

layer of graphite were started in 1970. The name of graphene was first pronounced by S.Mouras and co-workers in 1987. S.Mouras and Boehm et al. (1994) were described the graphite layers forming graphite intercalation compounds (GIC). Finally, in 2002 Andre Geim and Kostya Novoselov at the University of Manchester were began to work on graphene and get patent which entitled " Nano-scaled Graphene Plates" related with graphene production. Just two years later, in 2004 these researchers demonstrated successfully the first isolation of graphene flake from bulk graphite [17]. The key point of success was selection of proper substrate (SiO_2) which provides recognizable optical contrast. Andre Geim and Kostya Novoselov have received many awards for their epochal work on graphene including 2010 Nobel Prize in Physics.

2.2.1 Structure of graphene

Carbon atoms electron configuration is $1s^2 2s^2 2p$ which can hybridize to generate different hybrid orbitals. Thus various structural and morphological carbon nanomaterials can be produce. For example, tetrahedron structure via sp^3 hybridization, hexagonally structure like graphite or graphene via sp^2 hybridization and organic molecules via sp hybridization. Figure 2.2.2 shows the crystal structure of single layer graphene. As shown in figure 2.2.2 in single layer graphene, each primitive cell contains two carbon atoms (A and B). The position of these two atoms is not equal because

connection with a lattice vector (like R=$n_1a_1+n_2a_2$; where n_1 and n_2 are integers) is not

possible. Primitive lattice vectors a_1 and a_2 described as follows.

$$a_1 = \left(\frac{a}{2}, \frac{\sqrt{3}a}{2}\right) \qquad a_2 = \left(\frac{a}{2}, -\frac{\sqrt{3}a}{2}\right)$$

Where a= $|a_1|$ = $|a_2|$ = 0.246nm is the distance between adjacent primitive cells.

The lattice constant is 0.142nm which is the atomic distance between adjacent carbon

atoms.
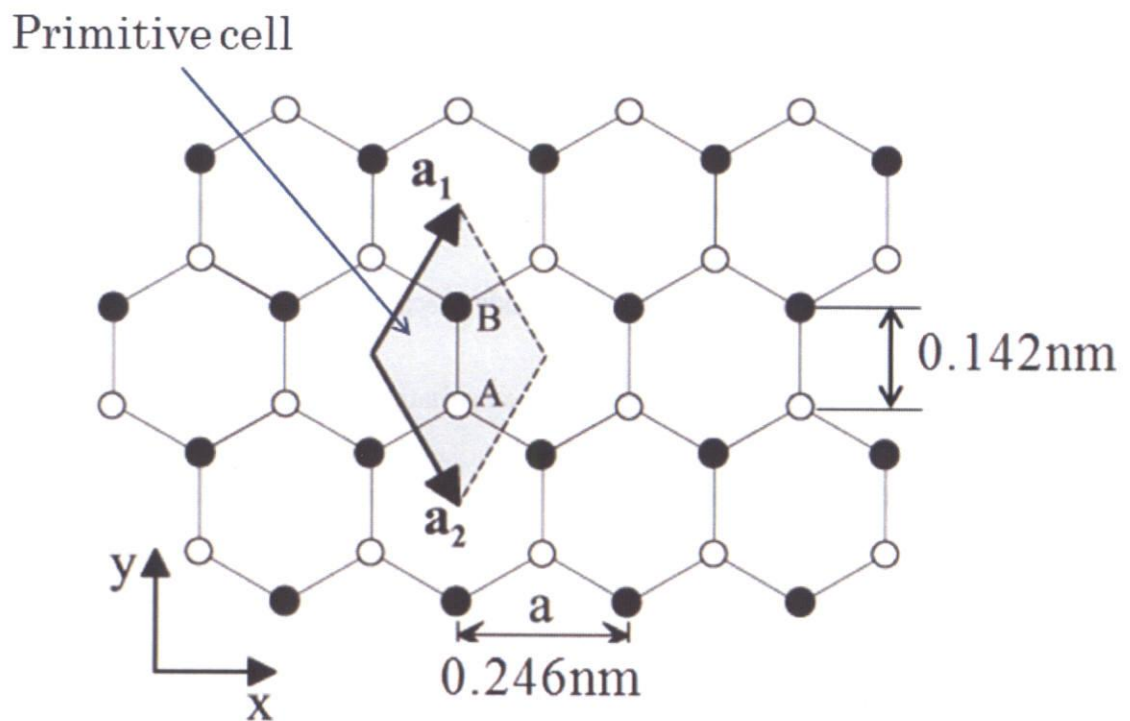
Figure 2.2.2   The crystal structure of single layer graphene.

2.2.2 Properties and Applications of Graphene

Graphene has many unique properties in many aspects. Structure of graphene may be reason for unusual electronic properties. Charge carrier properties of carbon nanotubes and graphens are in many respects familiar [18]. For instance, both of them have high electron mobility and ambipolar transport. However graphene is having 2D system allows the produce very large area device fabrication, especially in the semiconductor industry.

As shown in figure 2.2.3 the hexagonal lattice of graphene has two bands structure which was defined first by P.R. Wallace [15]. π -states generates the valance band and π^*-states generates the conduction band. The band structure forms K and K' valleys in the Brillouin zone. These two bands touch six neutrality points (Dirac points). Low energy in electron transport, electronic excitation (E) and momentum (k) exhibit a linear dispersion [19]. K and K' corners obey the Dirac equation instead of traditional Schrödinger equation that characterized by Fermi velocity (10^6 m s^{-1}, close to the speed of light) resulting zero band gap structure.
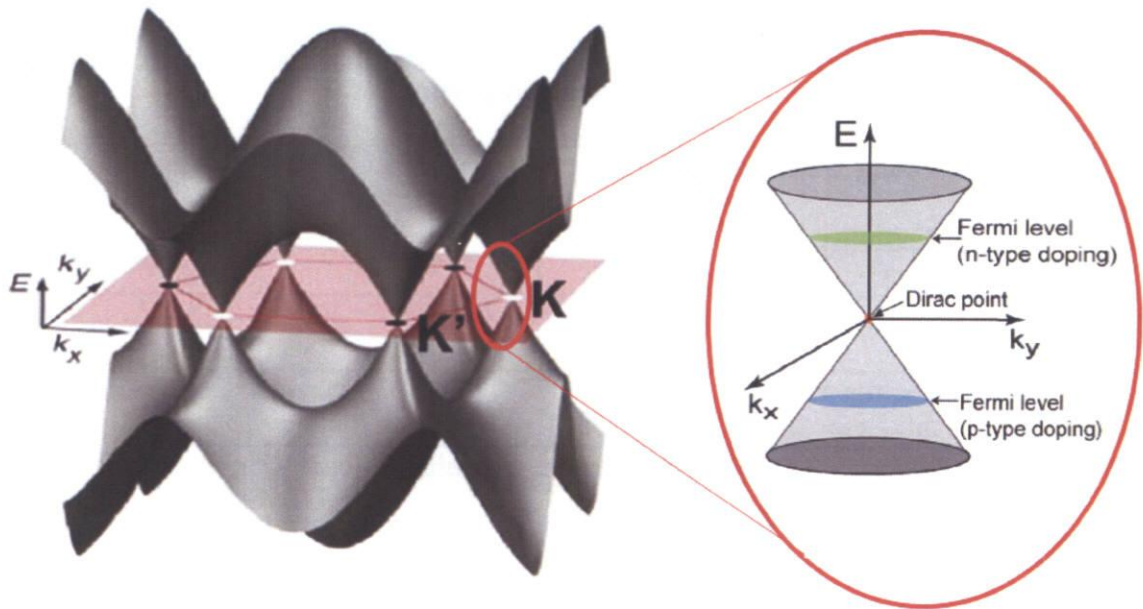
Figure 2.2.3 Electronic band structure of graphene.

Some properties of graphene are indexed in table 2.2.1. The zero band gap semiconductor shows exciting properties such as anomalous quantum hall effect [20], high carrier mobility (>200,000 $cm^2V^{-1}S^{-1}$) [21]. Graphene has optical transparency independent of wavelength (~97.7%) makes it effective option for optoelectronic devices [22]. In near future, graphene may replace indium tin oxide (ITO) because of high cost and fragility of ITO. Furthermore, graphene attracts the many researchers interest regarding to its mechanical strength (>1 TPa) which ~200 times greater than steel [23]. Graphene also has high thermal conductivity ((4.84 ± 0.44) × 10^3 to (5.30 ± 0.48) × 10^3 W/mK) which higher than CNTs or diamond. Above mentioned extraordinary properties are point out that graphene is one of the pioneer nanomaterial.

Properties	
Mechanical Properties	
✓ High Young 's Modulus (1TPa) ✓ High flexibility	
Electrical Properties	
✓ High electron mobility	

Material	Mobility at room temperature (cm^2 V^{-1} s^{-1})
Silicon	1.4×10^3
InSb	7.7×10^4
Graphene	2.0×10^5

✓ Anomolous Quantum Hall Effect

✓ Ambipolar electric field effect at room temperature (doping level of 6×10^{12} cm^{-2})

Physical and Chemical Properties	

✓ High surface area (>2600m^2/g)

✓ High optical transparency (~97.7%)

✓ High termal conductivity ($(4.84 \pm 0.44) \times 10^3$ to $(5.30 \pm 0.48) \times 10^3$ W/mK)

✓ Graphene can adsorb and desorb various atoms and molecules(NO_2, NH_3 etc)

Table 2.2.1   Some unique properties of graphene

The remarkable unique properties of graphene open up new possibilities for next generation nano electronic devices. Figure 2.2.4 represents the some novel applications of graphene.
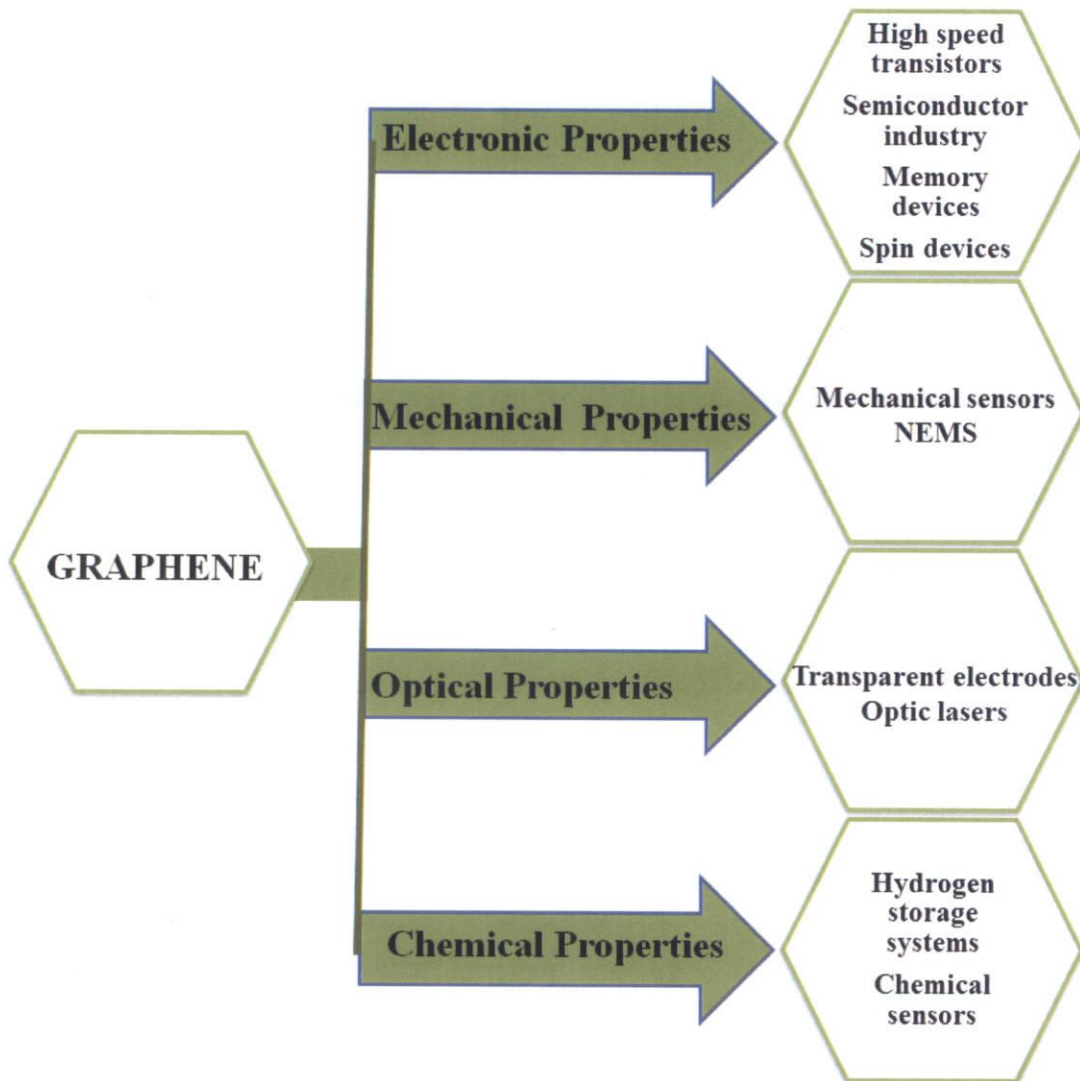
Figure 2.2.4   Some novel applications of graphene.

2.2.3 Synthesis Methods for Graphene

Graphene has been derived or synthesized by various approaches, including, micromechanical cleavage of highly oriented pyrolytic graphite (HOPG) [24], epitaxial growth on silicon carbide (SiC) [25], reduction of chemically exfoliated graphene oxide [26] and chemical vapor deposition (CVD) on transition metals [27-29]. In the following section above mentioned approaches will be discussed. Synthesis of graphene in a CVD process by hydrocarbon decomposition on transition metal surface, such as copper (Cu), nickel (Ni), and cobalt (Co) has been significantly investigated [30-33]. On the other hand, noble metals such as gold (Au) and silver (Ag) were also demonstrated as a possible substrate material for graphene growth [34, 35]. Thermal chemical vapor deposition technique using solid carbon source will be discussed in detail at chapter IV.

2.2.3.1 Micromechanical Cleavage of Highly Oriented Pyrolytic Graphite (HOPG)

Pyrolytic graphite is a graphite material with a high degree of preferred crystallographic orientation of the c-axes perpendicular to the surface of the substrate. Pyrolytic graphite can be obtained by graphitization heat treatment of pyrolytic carbon or by chemical vapor deposition at temperatures above 2500°K. Hot working of pyrolytic graphite by annealing under compressive stress at approximately 3300°K

results in highly oriented pyrolytic graphite (HOPG). Thus HOPG is a highly-ordered form of high-purity pyrolytic graphite. HOPG is characterized by the highest degree of three-dimensional ordering. The density, parameters of the crystal lattice, preferable orientation in a plane (0001) and anisotropy of the physical properties of the HOPG are close to those for natural graphite mineral.

A.K. Geim and K. S. Novoselov and their colleages were first time reported the synthesis of graphene by mechanical exfoliation (repeated peeling) of small mesas of highly oriented pyrolytic graphite. This approach has been found to be highly reliable and allowing to prepare few layer graphene films up to 100μm in size.

The starting material was 1-mm-thick platelets of highly oriented pyrolytic graphite (HOPG). They used commercially available HOPG of grades ZYH and HOPG-1. Using dry etching in oxygen plasma, first prepared 5 mm-deep mesas on top of the platelets (mesas were squares of various sizes from 20 mm to 2 mm). The structured surface was then pressed against a 1-mm-thick layer of a fresh wet photoresist spun over a glass substrate. After baking, the mesas became attached to the photoresist layer, which allows to cleave them off the rest of the HOPG sample. Then, using scotch tape they started repeatedly peeling flakes of graphite off the mesas. Thin flakes left in the photoresist were released in acetone. When a Si wafer was dipped in the solution and

then washed in plenty of water and propanol, some flakes became captured on the wafer's surface (as a substrate, n^+-doped Si with a SiO2 layer on top was used; in order to avoid accidental damage - especially during plasma etching - they have chosen to use relatively thick SiO2 with t =300nm). After this, they used ultrasound cleaning in propanol, which removed mostly thick flakes. Thin flakes (d < 10 nm) were found to attach strongly to SiO_2, presumably due to van der Waals and/or capillary forces.

2.2.3.2 Epitaxial Growth on Silicon Carbide (SiC)

Synthesis of graphene by mechanical cleavage of HOPG provides new opportunity to investigate physical and transport properties of single layer graphene, as well few layer graphene. However, in terms of electronic applications much more effective methods have to be used to obtain high quality monolayer and few layer graphene. Among the other synthesis approaches apitaxial growth of high quality graphene film on suitable substrate supplies the most effective approach towards to target. Monolayer and multi-layer graphene growth on SiC by thermal decomposition of SiC at high temperature in ultrahigh vacuum have been investigated by different groups [36-40].

2.2.3.3 Reduction of Graphite Oxide (GO)

Graphite oxide is a composition of carbon, oxygen and hydrogen atoms in variable ratios, obtained by treatment of graphite with strong oxidizers. Figure 2.2.4 shows the proposed image of graphite oxide with functional groups. A, B and C represents the epoxy bridges, hydroxyl groups and pairwise carboxyl groups respectively.
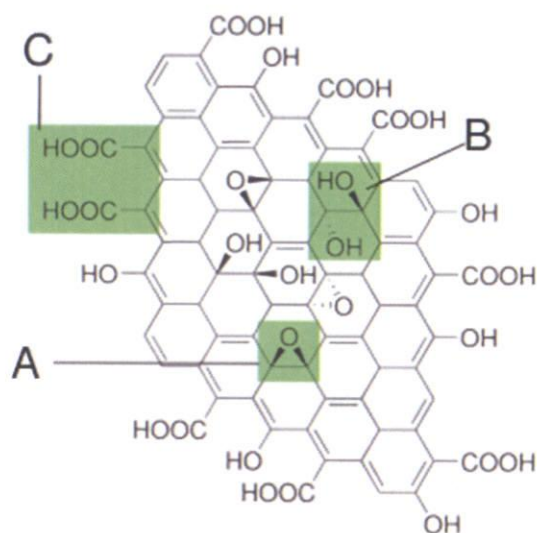
Figure 2.2.4   Proposed structure of graphite oxide

Generally, graphite oxide is produced by the oxidative treatment of graphite via three principal methods demonstrated by Brodie [41], Hummers [42], and Staudenmeier [43], respectively.

The reduction process of GO results in gradual decrease in hydrophilic character, often leading to irreversible agglomeration and precipitation [44, 45]. To solve this problem of agglomeration an anionic water-soluble polymer was used during the reduction process, giving rise to stable dispersion [44]. A new method was also proposed to achieve the reduction of GO without any assistance of surfactant polymer [46]. Based on the study on surface charge, the formation of stable GO colloid was attributed to the electrostatic repulsion, rather than just the hydrophilicity of GO. Since the carboxyl groups are difficult to be reduced by hydrazine under certain conditions, the graphene sheets in aqueous solution should still be charged after reduction [47]

2.2.3.4 Chemical Vapor Deposition

Chemical vapor deposition (CVD) is a chemical reaction process used to fabricate high-purity, effective solid materials. CVD process is mainly used in the semiconductor technologies to produce thin film. In a typical CVD process, the substrate material is exposed to one or more precursors, which decompose on the substrate surface to produce the desired deposit. Frequently, volatile products are also produced, which are removed by gas flow through the reaction chamber. Types of CVD process are as follows;

➢ Atmospheric Pressure Chemical Vapor Deposition (APCVD)

➢ Low Pressure Chemical Vapor Deposition (LPCVD)

➢ Metal-Organic Chemical Vapor Deposition (MOCVD)

➢ Plasma Assisted Chemical Vapor Deposition (PACVD)

➢ Plasma Enhanced Chemical Vapor Deposition (PECVD)

➢ Laser Chemical Vapor Deposition (LCVD)

➢ Photochemical Vapor Deposition (PCVD)

➢ Chemical Vapor Infiltration (CVI)

➢ Chemical Beam Epitaxy (CBE)

Table 2.2.2 shows some of the CVD process types including their advantages, disadvantages and applications.

CVD Process Type	Advantages	Disadvantages	Applications
APCVD	Simple Fast deposition Low temperature	Poor step coverage Contamination	Low temperature oxides
LPCVD	High purity Excellent uniformity Good step coverage	Slow deposition High temperature	High temperature oxides Silicon Nitride Poly-Silicon W and WSi_2
PECVD	Good step coverage Low temperature	Chemical and particle contamination	Low temperature insulators over metals Nitride passivation

Table 2.2.2   Some chemical vapor deposition process and their properties and

possible applications.

In a typicall CVD process various kind of precursor metals have been used such as halides ($TiCl_4$, $TaCl_5$, WF_6, etc), hydrides (SiH_4, GeH_4, $AlH_3(NMe_3)_2$, NH_3, etc), metal organic compounds, metal alkyls ($AlMe_3$, $Ti(CH_2tBu)_4$, etc), metal alkoxides ($Ti(OiPr)_4$, etc), metal dialylamides ($Ti(NMe_2)_4$, etc), metal diketonates ($Cu(acac)_2$, etc), metal arbonyls ($Ni(CO)_4$, etc).

CVD is an extremely versatile process that can be used to produce almost any metallic or ceramic compound. Some of these including elements, metals and alloys, carbides, nitrides, borides, oxides, intermetallic compounds. An often neglected by-product of the CVD process are volatile gases. However, these gases may be toxic, flammable or corrosive so must be treated appropriately. Analysis of the off-gases can also lead to a better understanding of the CVD reaction mechanisms and the information used to refine the process.

CVD has many applications towards a wide range of industries such as:

✓ **Coatings-** coatings for a variety of applications such as wear resistance, corrosion resistance, high temperature protection, erosion protection and combinations thereof.

✓ **Semiconductors and related devices** – Integrated circuits, sensors and optoelectronic devices

✓ **Dense structural parts** – CVD can be used to produce components that are difficult or uneconomical to produce using conventional fabrication techniques. Dense parts produced via CVD are generally thin walled and maybe deposited onto a mandrel or former.

✓ **Optical Fibres** – For telecommunications.

✓ **Composites** – Preforms can be infiltrated using CVD techniques to produce ceramic matrix composites such as carbon-carbon, carbon-silicon carbide and silicon carbide-silicon carbide composites. This process is sometimes called chemical vapor infiltration or CVI.

✓ **Powder production** – Production of novel powders and fibres

✓ **Catalysts**

✓ **Nano machines**

In this thesis I demonstrate synthesis of few-layer graphene film on Ag foil by the AP-CVD process using solid precursor camphor as carbon source. As carrier gas combination of Ar and H_2 was utilized. Details of AP-CVD process will be discussed in chapter 3.

2.3 References

[1]   Kroto H.W. et al., *Nature*, **318 (6042) 162-163**, (1985)

[2]   Alan C., Colin P., Terry R., Baker K and. Rodriguez N.M., *J.Phys.Chem.B*, **102 (22), 4253-4256.**

[3]   Saito R., Dresselhaus G., Dresselhaus M.S., Physical properties of nanotubes, *Imperial College Press*, (2003).

[4]   Maruyama's molecular dynamics and nano heat website.

[5]   R.H. Baughman, A.A. Zakhidov, W.A. de Heer, *Science,* **297, 787,** (2002)

[6]   Y. Saito, K. Hamaguchi, K. Hata, K. Uchida, Y. Tasaka, F. Ikazaki, M.Yumura, A. Kasuya, Y. Nishina, *Nature* **389, 554,** (1997)

[7]   W.B. Choi, D.S. Chung, J.H. Kang, H.Y. Kim, Y.W. Jin, I.T. Han, Y.H. Lee, J.E. Jung,   N.S. Lee, G.S. Park, J.M. Kim, *Appl. Phys. Lett.* **75,3129,** (1999)

[8]   S.S. Wong, E. Joselevich, A.T. Woolley, C.L. Cheung, C.M. Lieber, *Nature* **394 52,** (1998)

[9]   Y. Hayashi, T. Tokunaga, Y. Yogata, S. Toh, K. Kaneko, T. Soga, T. Jimbo, *Appl. Phys. Lett.* **84, 2886,** (2004)

[10]   K. S. Novoselov, A. K. Geim, S. V. Morozov, D. Jiang, Y. Zhang, S. V. Dubonos, I. V. Grigorieva and A. A. Firsov, *Science,* **306, 666,** (2004).

[11]   Y. Zhang, Y. W. Tan, H. L. Stormer and P. Kim, *Nature,* **438**, 201 (2005).

[12]   A. K. Geim and K. S. Novoselov, *Nature mater.* **6**, 183 (2007).

[13]   C. Lee, X. Wei, J. W. Kysar, and J. Hone, *Science,* **321**, 385 (2008).

[14]   S. Chen, L. Brown, M. Levendorf, W. Cai, S.Y. Ju, J. Edgeworth, X. Li, C.W. Magnuson, A. Velamakanni, R.R. Piner, J. Park and R.S. Ruoff, *ACS Nano*, **5, 1321,** (2011).

[15]   Wallace, P. R. The band theory of graphite. *Phys. Rev.,* **71, 622-634** (1947).

[16]   Semenoff, G.W. Condensed-matter simulation of a three-dimensional anomaly. *Phys. Rev. Lett.* **53, 2449-2452,** (1984)

[17]   P. Avouris, *Nano Letters,* **10, 4285- 4294,** (2010)

[18]   F. Giannazzo, V. Raineri and E. Rimini, in *Scanning Probe Microscopy in Nanoscience and Nanotechnology*, ed. B. Bhushan, *Springer-Verlag, Berlin*, **pp. 247–285,** (2011)

[19]   L. A. Ponomarenko, F. Schedin, M. I. Katsnelson, R. Yang, E. W. Hill, K. S. Novoselov and A. K. Geim, *Science*, **320, 356–358,** (2008)

[20]   Zhang Y, Tan YW, Stormer HL, Kim P. *Nature,* **438: 201-4,** (2005)

[21]   Morozov SV, Novoselov KS, Katsnelson MI, Schedin F, Elias DC, et al. *Phys Rev Lett,* **100: 016602,** (2008)

[22]   Nair RR, Blake P, Grigorenko AN, Novoselov KS, Booth TJ, Stauber T, et al.

        Science, **320: 1308**, (2008)

[23]   Lee C, Wei X, Kysar J, Hone , *J. Science*, **321(5887):385–8**, (2008)

[24]   K. S. Novoselov, D. Jiang, F. Schedin, T. J. Booth, V. V. Khotkevich, S. V.

        Morozov, and A. K. Geim, *Proc. Natl. Acad. Sci.***102, 10451** (2005).

[25]   C. Berger, Z. Song, X. Li, X. Wu, N. Brown, C. Naud, D. Mayou, T. Li, J.

        Hass, A. N. Marchenkov, E. H. Conrad, P. N. First, and W. A. de Heer,

        *Science***312, 1191**(2006).

[26]   S. Stankovich, D. A. Dikin, G. H. B. Dommett, K. M. Kohlhaas, E. J. Zimney,

        E. A. Stach, R. D. Piner, S. T. Nguyen, and R. S. Ruoff, *Nature* **442, 282**

        (2006).

[27]   P. R. Somani, S. P. Somani and M. Umeno, *Chem. Phys. Lett.***430, 56** (2006).

[28]   Q. Yu,J. Lian, S. Siriponglert, H. Li, Y. P. Chen and S. S. Pei, *Appl. Phys.*

        *Lett.***93, 113103** (2008).

[29]   A. Reina, X. Jia, H. John, D. Nezich, H. Son, V. Bulovic, M.S. Dresselhaus,

        and J. Kong, *Nano Lett.***9, 30** (2009).

[30]   K. S. Kim, Y. Zhao, H. Jang, S. Y. Lee, J. M. Kim, K. S. Kim, J. H. Ahn, P.

        Kim, J. Y. Choi, and B. H. Hong, *Nature* **457, 706** (2009).

[31]   X. S. Li, W. W. Cai, J. H. An, S. Kim, J. Nah, D. X. Yang, R. Piner, A.

        Velamakanni, I. Jung, E. Tutuc, S. K. Banerjee, L. Colombo, and R. S. Ruoff,

Science **324**, **1312** (2009).

[32]   S. Bae, H. K. Kim, Y. Lee, X. Xu, J. Park, Y. Zheng, J. Balakrishnan, D. Im, T. Lei, Y. Song, Y. Kim, K. Kim, B. Ozyimaz, J. Ahn, B. Hong, and S. Iijima, *Nat. Nanotechnol.* **5, 574,** (2010).

[33]   E. Sutter, P. Albrecht, and P. Sutter, *Appl. Phys. Lett.* **95, 133109,** (2009).

[34]   T. Oznuluer, E. Pince, E. O. Polat, O. Balci, O. Salihoglu, and C. Kocabas, *Appl. Phys. Lett.* **98, 183101,** (2011).

[35]   M. E. Ayhan, G. Kalita, S. Sharma, M. Tanemura, *Phys. stat. sol. RRL*, **7, 1076,** (2013)

[36]   Berger C., Song Z. M., Li T. B., Li X. B., Ogbazghi A. Y, Feng R., Dai Z.T., Marchenkov A. N., Conrad E.H., First P. N., De Heer W. A., *Journal of Physical Chemistry B*, **vol. 108, no. 52, pp. 199912-19916**, (2004)

[37]   Berger C., Song Z. M., Li X. B., wu X. S., Brown N., Maud D., Naud C., De Heer W. A., *Physica Status Solidi a- Applications and Materials Science,* vol. **204, no. 6, pp. 1746-1750**, (2007)

[38]   Berger C., Song Z. M., Li X. B., wu X. S., Brown N., Naud C, Mayo D., Li T. B, Hass J., Marchenkov A. N., Conrad E.H., First P. N., De Heer W. A., *Science*, **vol.12, no. 5777, pp. 1191-1196**, (2006)

[39] Charrier A., Coati A., Argunova T., Thibaudau F., Garreau Y., Pinchaux R., Forbeaux I., Debever J. M., Sauvage Simkin M., Themlin J. M., *Journal of Applied Physics*, vol. **92, no. 5, pp. 2479-2484**, (2002)

[40] Forbeaux I., Themlin J. M., Charrier A., Thibaudau F., Debever J. M., *Applied Surface Science,* vol. **162, pp. 406-412**, (2000)

[41] Brodie BC. Sur. *Ann Chim Phys*; **59:466–72**, (1860)

[42] Hummers W, Offeman R. Preparation of graphitic oxide. *J Am Chem Soc* ; **80:1339**, (1958)

[43] Staudenmaier L. Verfahren zur darstellung der graphitsaure. *Ber Dtsch Chem Ges*; **31:1481–99**, (1898)

[44] S. Stankovich, R. D. Piner, X. Chen, N. Wu, S. T. Nguyen, R. S. Ruoff, *J. Mater. Chem.* **16, 155**, (2006),

[45] S. Stankovich, D.A. Dikin, R. D. Piner, K. A. Kohlhaas, A. Kleinhammes, Y. Jia, Y. Wu, S.T. Nguyen, R. S. Ruoff, *Carbon* **45, 1558**, (2007)

[46] D. Li, M. B. Müller, S. Gilje, R. B. Kaner, G. G. Wallace, *Nat. Nanotechnol.* **3, 101**, (2008)

[47] Yan Geng, Shu Jun Wang, Jang-Kyo Kim, *Journal of Colloid and Interface Science* **336, 592**, (2009)

CHAPTER III

Experimental Set-up

In this chapter the information on the experimental facilities utilized in this study are discussed. In this work synthesis of graphene was carried out with various approaches using different kind of carbon sources. Synthesis of graphene, device fabrication and their characterization techniques were analyzed in Chapter III. The precursor materials and electrode materials were also presented in following chapter.

3.1 Experimental Facilities

3.1.1 Thermal Chemical Vapor Deposition (CVD)

In this work catalytic decomposition of hydrocarbon on noble metal silver carried out by thermal chemical vapor deposition process using botanical derivative camphor as carbon precursor. As shown in figure 3.1.1 two different furnaces were utilized for thermal chemical vapor deposition process in this study. The first furnace was used for evaporation of pure solid precursor camphor and second furnace was used for growth zone to heat Ag substrate. As a carrier gas different composition of Ar and H_2 gases were used. A typical CVD system consists of the following parts;

- ➢ Sources of and feed lines for gases

- ➢ Mass flow controllers for metering the gases into the system

- ➢ A reaction chamber or reactor as growth zone

- ➢ A system for heating up the wafer on which the film is to be deposited

- ➢ Temperature sensors

Our atmospheric pressure (AP)-CVD process consist of following stages;

1) Specified gas compositions of Ar and H_2 was introduced to growth zone

2) Gases moved to Ag substrate

3) Slowly introducing the pure solid camphor to growth zone

4) Reactant agents get adsorbed on the surface of Ag foil

5) Chemical reactions with the Ag substrate to formation of thin film

6) Out diffusion of by-product gases from growth zone
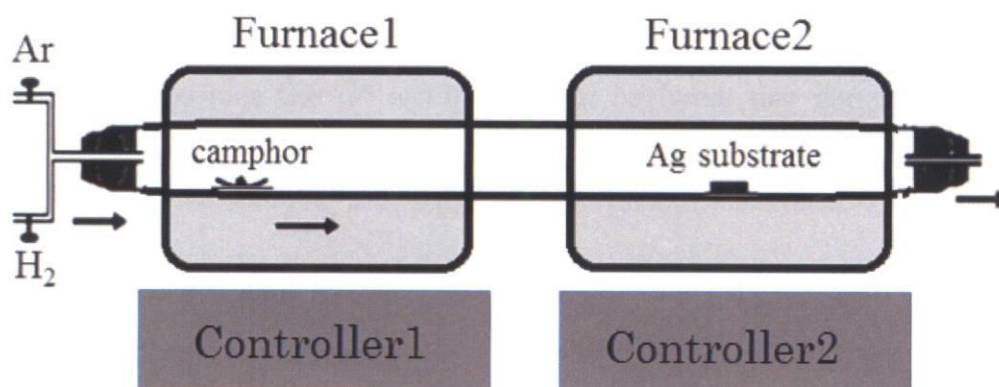
Figure 3.1.1   Schematic diagram of thermal CVD system

Details of graphene synthesis experiments will be discussed in Chapter IV.

Experimental conditions of synthesis of graphene on Ag foil are shown in table 3.1.1.

Carrier gases	Ar/H_2(85/5sccm)
Carbon source	Camphor(10mg)
Temperature	945°C
Annealing time	15min
Deposition time	~20min
Substrate	Ag foil(30μm thick, 99.98% pure)

Table 3.1.1   Experimental conditions of synthesis of graphene on Ag foil

3.1.2 Spin Coating

In this research water soluble tri-block copolymer Pluronic F127 was used as carbon source. Among the other polymer coating methods to obtain much uniform and thin layer spin coating technic was carried out using Micasa Opticoat MS-A100 spin coater. Co-polymer was dissolved in water (0.1wt %) and spin coated onto SiO_2/Si substrate at 5000 rpm for 2 min. The thickness of thin film can be controlled by changing the rotation speed and time, as well as changing amount and concentration of precursor. Our results showed that 100 μl of triblock co-polymer are not enough for

uniform graphene formation. To obtain much thinner layer, rotation speed and rotation time can be increased. Table 3.1.2 shows the spin coating conditions.

Concentration of co-polymer	0.2 wt %
Amount of co-polymer	200 μl
Rotation speed	5000 rpm
Rotation time	120sec

Table 3.1.2   Spin coating conditions

3.1.3   Pulsed Laser Deposition (PLD)

Lasers have some unique properties such as high power density, coherence, narrow band frequency, etc. Generally laser light beams have ability to vaporize the hard materials surface. By pulsed laser deposition technic polycomponent materials can be deposited onto arbitrary substrate to produce thin film [1-4].

PLD is a very simple method. Only laser energy density, wavelength and repetition rate have to be controlled during deposition process. Compare to other sputtering approaches very small size targets are utilized in PLD method. Thickness of layer can be controlled easily by PLD. The deposition rate was calculated as 3.8nm/h. On the other hand stoichiometry of the Ni target can be kept in the deposited thin films.

In this study pulse laser beam was focused onto the surface of solid Ni target using Nd:YAG laser (λ = 355 nm, energy density of 30mJ and f=10 Hz). Rapid evaporation of Ni catalytic materials carried out easily by strong absorption of electromagnetic radiation. Figure 3.1.2 shows the photograph image of PLD and figure 3.1.3 presents the corresponding illustration of solid phase reaction approach.
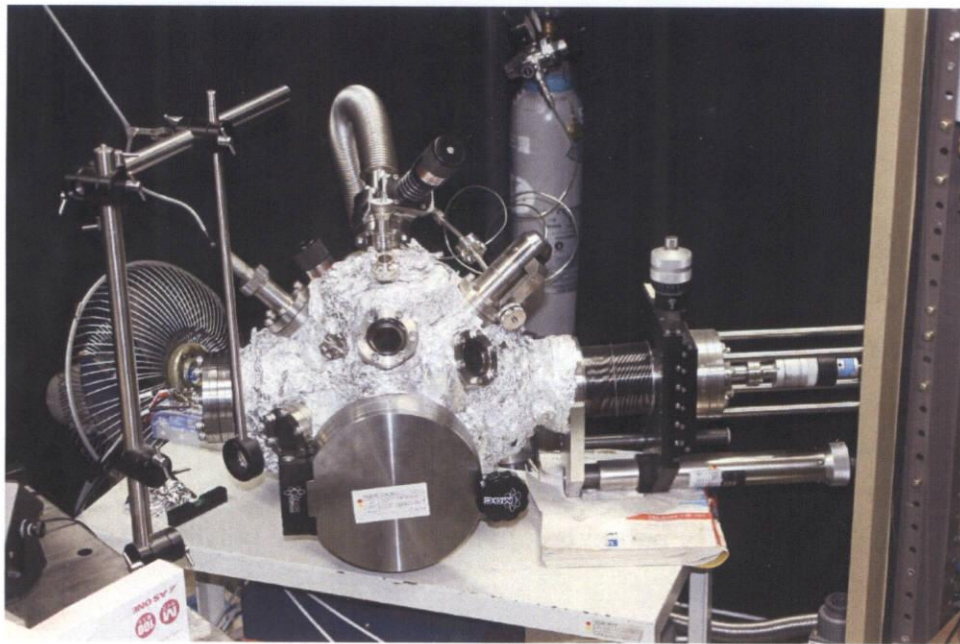
Figure 3.1.2   The photograph image of pulse laser deposition system.
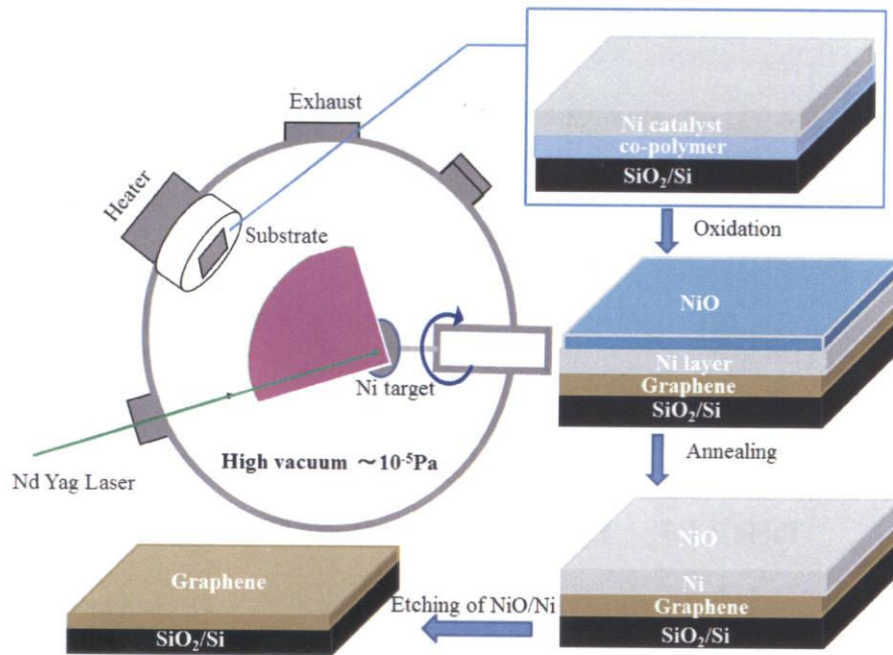
Figure 3.1.3   Schematic diagram of solid phase reaction process

In despite of advantages of PLD some back drawback such as undesirable particles depositions and splashing on the films. These large particles (sometimes may be few micrometer sizes) highly affect the formation of graphene and dramatically reduce the electrical properties. To overcome this problem, inserting a mask is can be effective way to prevent unwanted large particles. Another problem of PLD technic is the narrow angle distribution of Ni catalytic deposition which is restricts the fabrication of large area continuous thin films. Rotating the Ni target and choosing suitable distance (40mm) between target and substrate can lead to much larger uniform thin films fabrication. The mechanism of PLD consists of following steps;

●   Laser radiation with the catalytic Ni target

●   Gas-dynamic of the ablation material

●   Decomposition of the Ni metals onto SiO/Si substrate

●   Nucleation and formation of thin film on SiO/Si substrate

Type of parameter	Nd:YAG laser
Beam diameter	$\leqq 8$ mm
Wavelength	355 nm
Laser output	150 mW
Pulse repetition	0.1 ns
Pulse width	14-15 ns
Distance between target and substrate	40 mm

Table 3.1.3   Experimental parameter for PLD process

3.1.4 Thermal Evaporation

Graphene-Si Schottky junction photodetector was fabricated by transferring the Ag-NPs decorated graphene on Au electrode deposited SiO_2/n-Si substrates. Au electrode and Au:Sn back ohmic contact layers were deposited by Ulvac Kiko Inc. thermal evaporator at higher pressure than 10^{-3}Pa. Figure 3.1.4 shows the photograph image of thermal evaporator and figure 3.1.5 shows schematic diagram of thermal evaporation system, respectively. The substrate materials were placed in a holder. Materials were inserted on a tungsten plate for deposition. The tungsten plate is connected to electrodes. The thicknesses of the deposited electrodes were controlled by monitoring the rate of deposition.
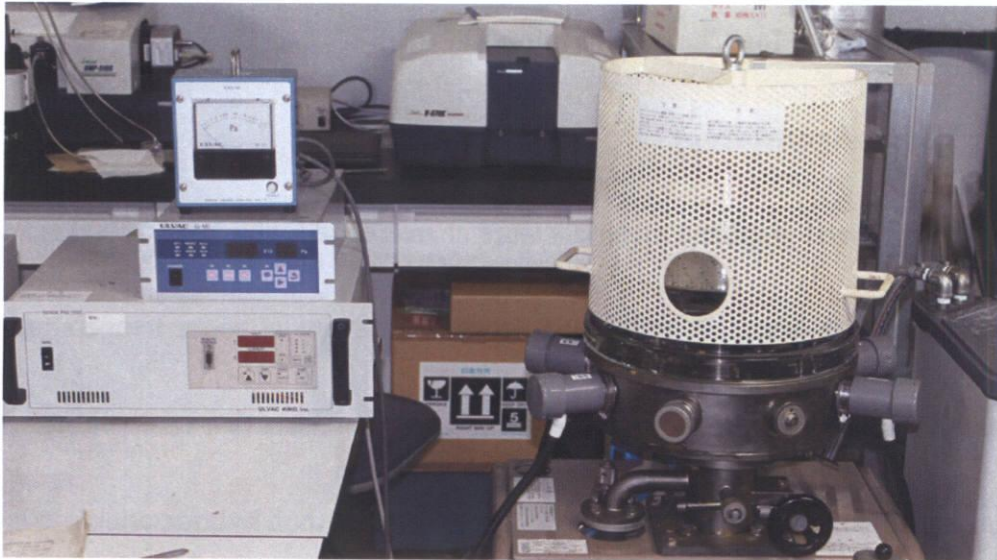
Figure 3.1.4   The photograph image of thermal evaporator.
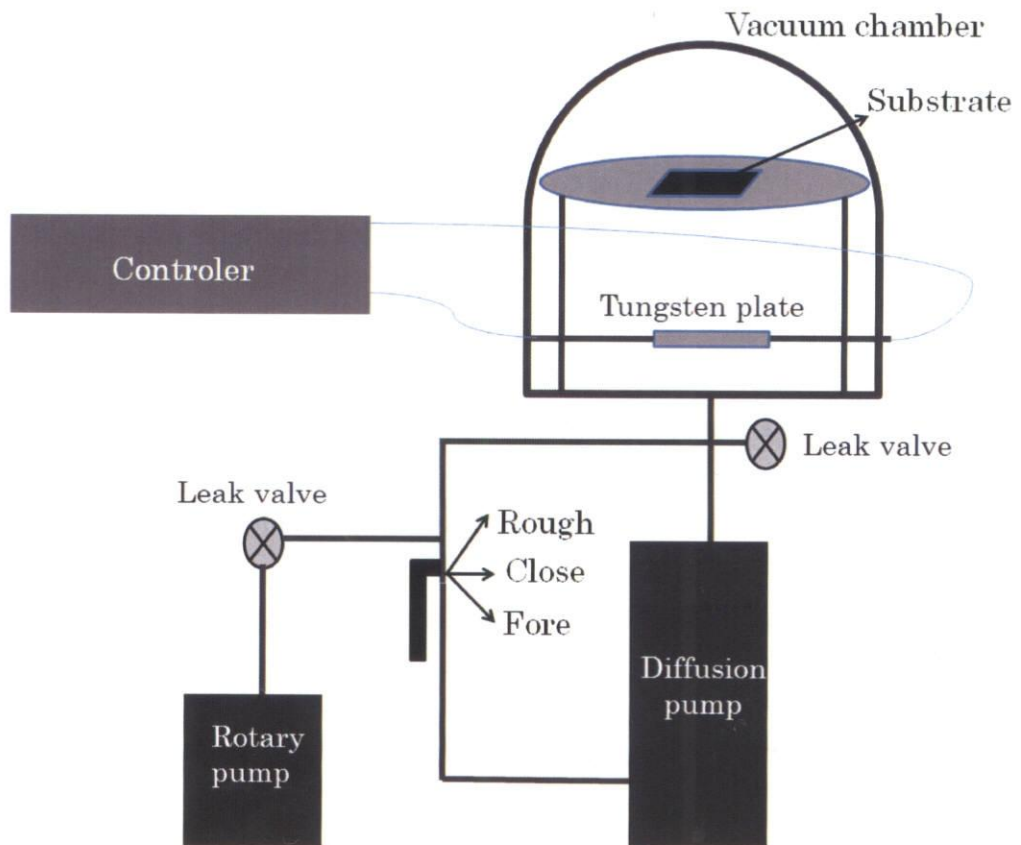
Figure 3.1.5   Schematic diagram of the thermal evaporator for deposition of Au and

Au:Sn electrodes.

3.2 Instruments for Characterization

3.2.1 Raman Spectroscopy

Synthesized graphene materials were characterized with NRS 3300 laser Raman spectrometer with laser excitation energy of 532.08 nm at room temperature in the spectral range from 500 to 3500 cm^{-1}. The main information that can be obtained from Raman spectra of graphene-like materials is in the sp^2 carbon hybridization.

Raman spectroscopy is very effective spectroscopic measurement technique that used to analyse low-frequency modes in a system. Measurement of the Raman spectrum is based on the phenomenon of light scattering rather than absorption of light due to oscillation. When light incident is scattered on the material, to analyse the scattered light having a frequency different from the frequency of incident light included in the scattered light, and identify the substance. Generally Raman spectroscopy relies on inelastic scattering and Raman scattering of monochromatic light due to a laser in visible, near infrared (NIR) and near ultraviolet (NUV) range.

To explain principle of Raman spectroscopy, a molecule consisting the atom A and B with a mass (m_1 、 m_2 respectively) can be given as an example. The constant (F) represents the intensity of binding atom A and B. The restoring force (f) is expressed

by equation (3.2.1). Here average interatomic distance (r_0) with a displacement (Δr) from the by Hooke's Law.

$$f = -F\Delta r \qquad\qquad \text{eq. (3.2.1)}$$

The relation between the restoring force f and oscillation potential energy U expressed in equation (3.2.2)

$$\frac{dU}{d(\Delta r)} = -f = F(\Delta r) \qquad\qquad \text{eq. (3.2.2)}$$

To seek oscillation potential (U) by integration this;

$$U = \frac{1}{2}F(\Delta r)^2 \qquad\qquad \text{eq. (3.2.3)}$$

On the other hand the kinetic energy of atom A and atom B is as follows;

$$T = \frac{1}{2}m_1\dot{r}_1^2 + \frac{1}{2}m_2\dot{r}_2^2 \qquad\qquad \text{eq. (3.2.4)}$$

Here r_1, r_2 are coordinates of atom A and atom B respectively. If we modify the equation (2-1.4) we can obtain equation (3.2.5).

$$T = \frac{1}{2}\frac{(m_1\dot{r}_1 + m_2\dot{r}_2)^2}{m_1 + m_2} + \frac{1}{2}\frac{m_1 m_2}{m_1 + m_2}(\dot{r}_1 - \dot{r}_2)^2 \qquad\qquad \text{eq. (3.2.5)}$$

Here in, first term of this expression is the kinetic energy of whole molecule. Since molecular oscillation is an independent constant, the kinetic energy of oscillation is as follows;

53

$$T = \frac{1}{2} \frac{m_1 m_2}{m_1 + m_2} \left(\dot{r}_1 - \dot{r}_2 \right)^2 = \frac{1}{2} \mu \left(\dot{r} \right)^2 \qquad\qquad \text{eq. (3.2.6)}$$

Here μ is the reduced mass which is defined in equation (3.2.7)

$$\mu \equiv \frac{m_1 m_2}{m_1 + m_2} \qquad\qquad \text{eq. (3.2.7)}$$

In this research Raman spectroscopy was used to characterize the quality of graphene and number of layers. Figure 3.2.1 shows Raman spectra of comparison of different carbonaceous materials including graphene [5].

In a Raman spectra vertical axis presents the intensity of peak and horizontal axis presents the Raman shift. As shown in figure 3.2.1 from top to bottom, graphene, highly oriented pyroltic graphite (HOPG), single walled carbon nanotube (SWCNT), damaged graphene, single walled carbon nanohorn and amorphous carbon spectra are presented, respectively. Most pronounced peaks in Raman spectra are defect related peak D appears around 1300 cm^{-1}, graphitic G peak appears around 1580 cm^{-1} and second order 2D peak also known as G' peak appears around 2700 cm^{-1}.

Generally, crystallinity of graphene characterize by comparing to the ratio of intensity of D peak and intensity of G peak (I_D/I_G) as well as the ratio of G peak

intensity and 2D peak intensity. In case of damaged graphene a shoulder peak appears

next to G peak and 2D peak shifts to around 2900 cm^{-1} [6]. In case of single layer

graphene (I_G/I_{2D}) evaluate less than 0.5 and full width half maximum (FWHM) of 2D

peak is around 30~40 cm^{-1} [7]. In case of bilayer graphene (I_G/I_{2D}) evaluate between 0.9

and 1.6 and full width half maximum (FWHM) of 2D peak is around ~45 cm^{-1} [8].
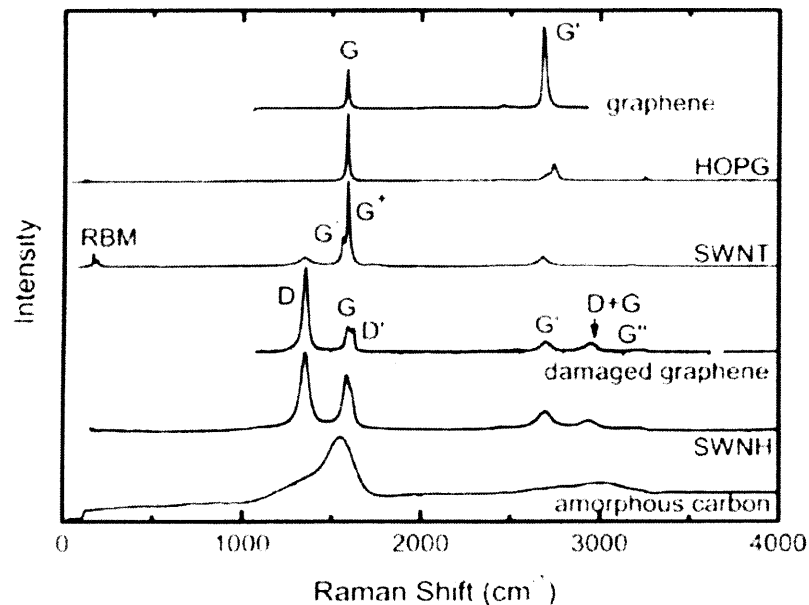
Figure 3.2.1   Raman spectra of comparison of different nano carbon materials [5]

3.2.2 Atomic Force Microscopy (AFM)

Surface analysis studies was carried out JEOL JSPM-5200TM atomic force

microscope (AFM). AFM is a kind of high resolution scanning probe microscopy on the

order of component of nano size, more than 1000 times higher limit than optical

diffraction limit. Figure 3.2.2 present the schematic diagram of basic principle of AFM measurement. As a basic principle of AFM consist of a cantilever with a sharp tip at its end that is used for scanning the target sample surface. The cantilever usually made up by silicon or silicon nitride with a probe radius of curvature in nanometer size. When the probe approached into proximity of substrate surface forces between the probe and sample surface lead to deflection of cantilever according to Hooke's law as shown in equation 3.2.8. Here F is the force, k is the spring constant and x represents the cantilever deflection. Forces which are measured in AFM including electrostatic forces, mechanical and magnetic forces, van der Waals forces, chemical bonding, etc.

$$F=-kx \qquad\qquad \text{eq. (3.2.8)}$$
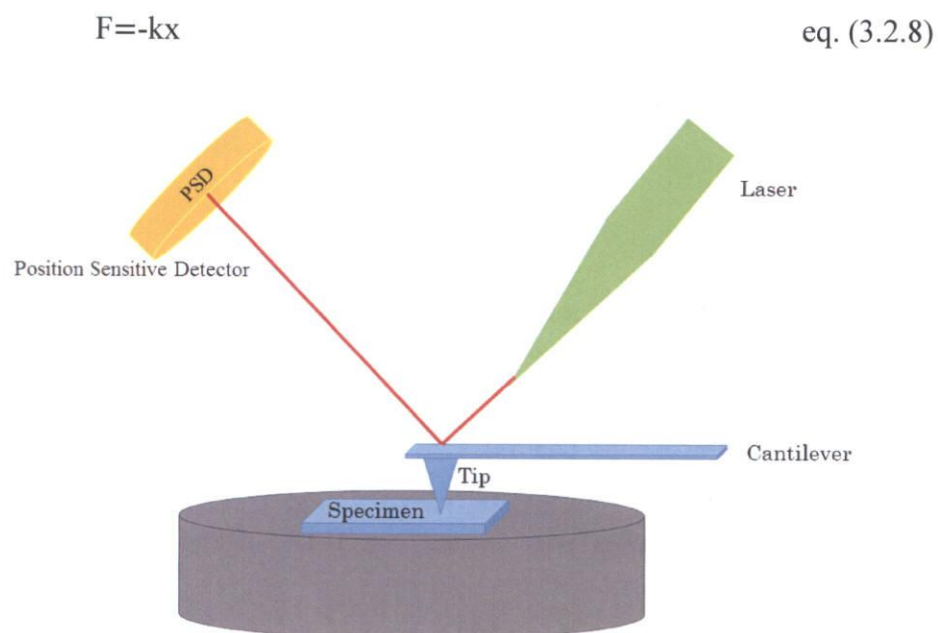
Figure 3.2.2 Corresponding schematic diagram of basic principle of AFM measurement.

The position of the cantilever is detected by bouncing a laser off its back onto a position-sensitive photodetector (PSPD). The system can detect sub-angstrom vertical movement of the cantilever tip because the ratio of the path length between the cantilever and the detector to the length of the cantilever itself produces a mechanical amplification. The computer stores the distance the scanner moves vertically at each (x,y) data point. This data point is used to form the topographic image of the sample surface.

AFM has various advantages compare to scanning electron microscope (SEM). Unlike the electron microscope, which provides a two-dimensional projection or a two-dimensional image of a specimen. AFM provides a three-dimensional surface profile. In addition, samples viewed by AFM do not require any special treatments (such as metal/carbon coatings) that would irreversibly change or damage the sample, and does not typically suffer from charging artifacts in the final image.

A disadvantage of AFM compared with the scanning electron microscope (SEM) is the single scan image size. In one pass, the SEM can image an area on the order of square millimeters with a depth of film on the order of millimetres. However AFM can only image a maximum height on the order of 10-20 micrometers

and a maximum scanning area of about 150×150 micrometers.

On the other hand the scanning speed of an AFM is also very limited. Traditionally, an AFM cannot scan images as fast as a SEM, requiring several minutes for a typical scan, while a SEM is capable of scanning at near real-time, although at relatively low quality. The relatively slow rate of scanning during AFM imaging often leads to thermal drift in the image making the AFM less suited for measuring accurate distances between topographical features on the image [9-11].

3.2.3 Scanning Electron Microscopy (SEM)

Morphological analyses were carried out by scanning electron microscopy (SEM) studies with JEOL JSM 5600 scanning electron microscope. The scanning electron microscope (SEM) uses a focused beam of high-energy electrons to generate signals at the surface of substrate. The signals that derive from electron substrate interactions display information about the substrate having external morphology, crystal structure, uniformity of material, chemical composition and so on. Information about sample are collected from a selected area of the surface and two dimensional image is obtained. Scanning are ranges from about 1 to 5 microns in width can be imaged using conventional SEM with magnification range of 20X to about 30.000X and spatial resolution of 50 to 100nm.

3.2.3.1 The Principles of SEM

Accelerated electrons in an SEM carry considerable amounts of kinetic energy, and this energy is distributed as a various signals produced by electron-specimen interactions the incident electrons are decelerated in the solid sample. These signals include secondary electrons which produce SEM images, backscattered electrons (BSE), and diffracted backscattered electrons (EBSD) that are used to describe crystal structures and orientations of minerals, photons, visible light cathodoluminesence (CL) and heat. Secondary electrons and backscattered electrons are commonly used for imaging samples. Secondary electrons are most valuable for showing morphology and topography on samples and backscattered electrons are most valuable for illustrating contrasts in composition in multiphase samples.

X-ray generation is produced by inelastic collisions of the incident electrons with electrons in discrete orbitals of atoms in the sample. As the excited electrons return to lower energy states, they yield X-rays that are of a fixed wavelength (that is related to the difference in energy levels of electrons in different shells for a given element). Thus, characteristic X-rays are produced for each element in a mineral that is "excited" by the electron beam. SEM analysis is considered to be "non-destructive"; that is, x-rays generated by electron interactions do not lead to volume loss of the sample, so it is

possible to analyze the same materials repeatedly.

3.2.3.2 Essential Parts of Scanning Electron Microscopes (SEMs)

All scanning electron microscopes are consist of some essential parts as follows;

- ✓ Electron source (gun)

- ✓ Electron lenses

- ✓ Specimen stage

- ✓ Electron detectors

- ✓ Display and data output systems

- ✓ Infrastructure materiality such as power supply, vacuum and cooling systems, etc.
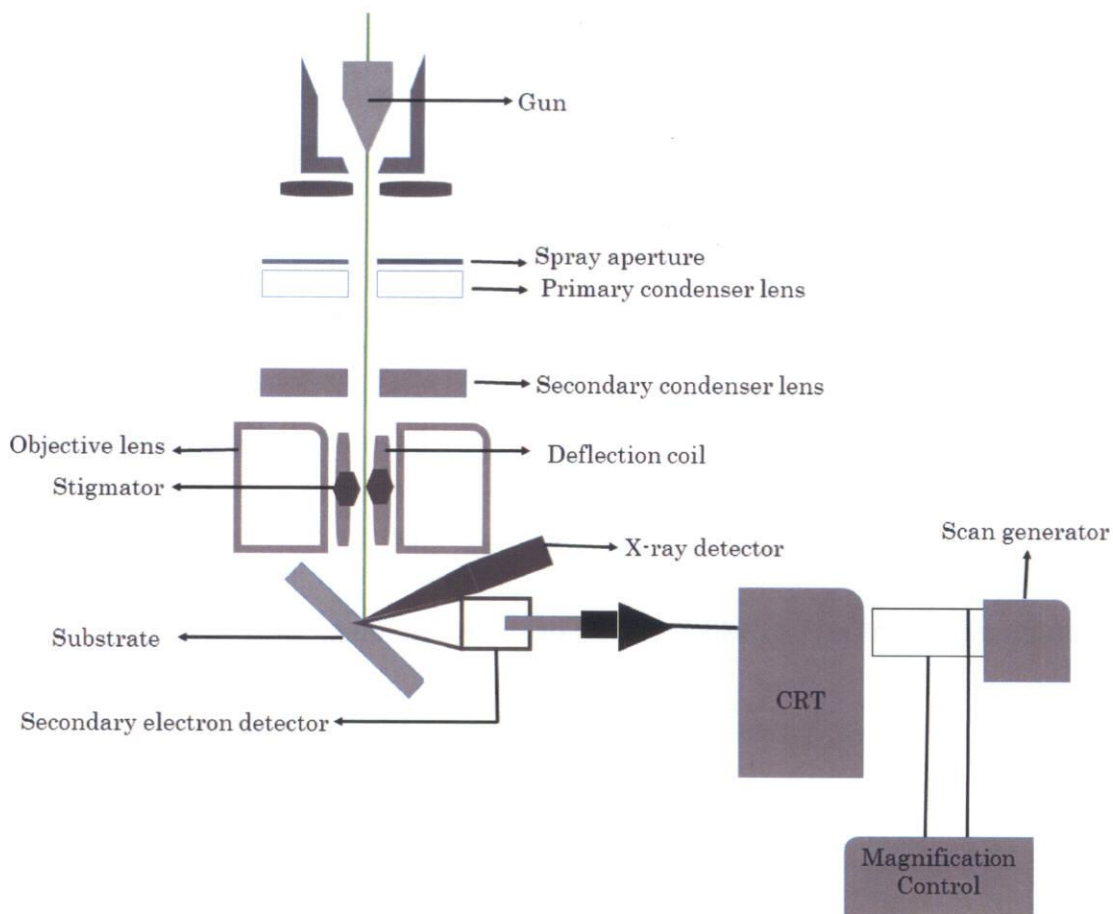
Figure 3.2.3   Schematic diagram of scanning electron microscopy (SEM)

3.2.4   Transmission Electron Microscopy (TEM)

In this research, conventional transmission electron microscope (TEM) studies were carried out by JEOL JEM 2100, operated at 200kV along with EDX analyzer to determine the structure and chemical nature of the chemical vapor deposited graphene and Ag-NPs. From the next section, the theory of electron microscope imaging, EDS, etc. are introduced.

Transmission electron microscopy (TEM) is a microscopy method that utilize a beam of electron is transmitted through an ultra-thin specimen, interacting with the specimen as it passes through. An image is acquired from the interaction of the electrons transmitted through the specimen. TEMs are capable of imaging at a significantly higher resolution than light microscopes, owing to the small de Broglie wavelength of electrons. This enables the instrument to be able to examine fine detail even as small as a single column of atoms, which is tens of thousands times smaller than the smallest resolvable object in a light microscope.

TEM forms a major analysis method in a range of scientific fields, in both physical and biological sciences. TEMs find application in cancer research, virology, materials science as well as pollution and semiconductor research. At smaller magnifications TEM image contrast is due to absorption of electrons in the material, due to the thickness and composition of the material. At higher magnifications complex wave interactions modulate the intensity of the image, requiring expert analysis of observed images.

3.2.4.1 The Concept of Resolution

The smallest distance between two points that can be figured out by our eyes is about 0.1-0.2 mm, depending on our vision ability. This distance is the resolution or resolving power of our eyes. The instrument that shows pictures revealing detail finer than 0.1 mm could be described as a microscope. The Rayleigh criterion describes the resolution of light microscope as:

$$\delta = \frac{0.61\lambda}{\mu \sin \beta}$$

eq. (3.2.9)

Where λ is the wavelength of the radiation, μ is the refractive index of the view medium and β is the semi-angle of collection of the magnifying lens. The variable of refractive index and semi-angle is small, thus the resolution of light microscope is mainly determined by the wavelength of the radiation source. Taking green light as an example, its 550nm wavelength (visible) gives 300nm resolution, which is not high enough to separate two nearby atoms in solid-state materials. The distance between two atoms in solid is around 0.2nm. Based on wave-particle duality, we know that electron has some wave-like properties:

$$\lambda = \frac{h}{p}.$$

eq. (3.2.10)

If an electron is accelerated by an electrostatic potential drop eU, the electron

wavelength can be described as:

$$\lambda = \frac{h}{\sqrt{2m_0 e U (1 + \frac{eU}{2m_0 c^2})}}$$

3.2.4.2 The Part of Transmission Electron Microscope

Figure 3.2.4 presents the essential instruments of a traditional transmission

electron microscope. The illumination system of TEM takes the electrons from the gun

and transfers them to the sample giving either a broad beam or focused beam. As shown

in figure 3.2.4 the parts above the specimen belong to illumination system. The

combination of objective lens and stage is the main part of TEM. Physically, the TEM

imaging system consist the intermediate lenses and projector lens.
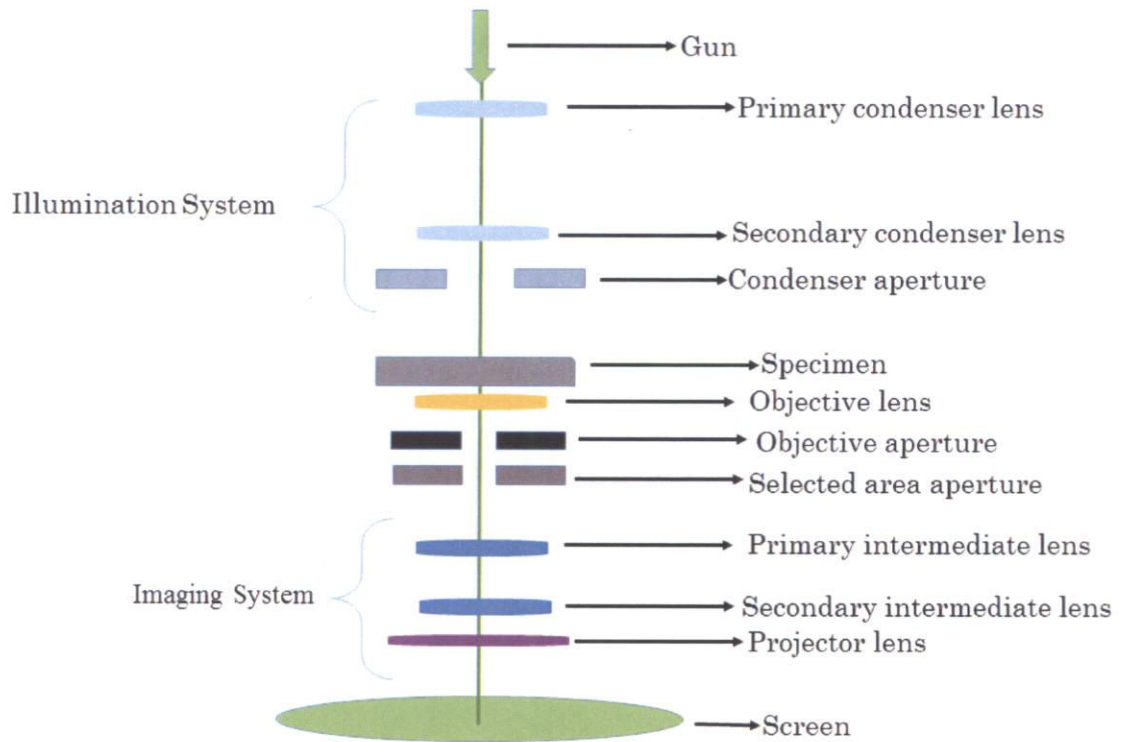
Figure 3.2.4.　　Parts of TEM

The diffraction pattern and image are obtained at the back focus plane and image plane of the objective lens. If we take the back focus plane as the objective plane of the intermediate lens and projector lens, we can obtain the diffraction pattern on the screen. It is said that the TEM works in diffraction mode. If we take the image plane of the objective lens as the objective plane of the intermediate lens and projector lens, we will form image on the screen which is the image mode.

3.2.4.3 Electron Diffraction Pattern in TEM

There are two basic modes of TEM operation, firstly the bright-field mode, where the (000) transmitted beam contributes to the image, secondly the dark-field imaging mode, in which the (000) beam is externalized. The size of the objective aperture in bright-field mode directly determines the information to be emphasized in the final image. When the objective size is selected so as to externalize the diffracted beams, one has the configuration normally used for low-resolution defect studies, called diffraction contrast. In this case, a crystalline specimen is oriented to excite a particular diffracted beam and the image is sensitive to the differences in specimen thickness, distortion of crystal lattices due to defects, strain and bending.

3.3 Materials

3.3.1 Solid carbon source camphor ($C_{10}H_{16}O$)

To synthesis continuous graphene film on noble metal Ag by chemical vapour deposition process a botanical derivative pure solid camphor ($C_{10}H_{16}O$) was used as carbon source rather than gaseous carbon source. The amount of solid precursor camphor can be controlled easily. Because of chemically hexagonal structure of camphor much better graphitization can be obtained. Handling of camphor is very easy

and no need to utilize extra equipment for its evaporation. Furthermore camphor is very cheap and environmental friendly owing to be botanical derivative. Figure 3.2.5 shows the photograph image of commercial camphor and molecular structure of camphor.
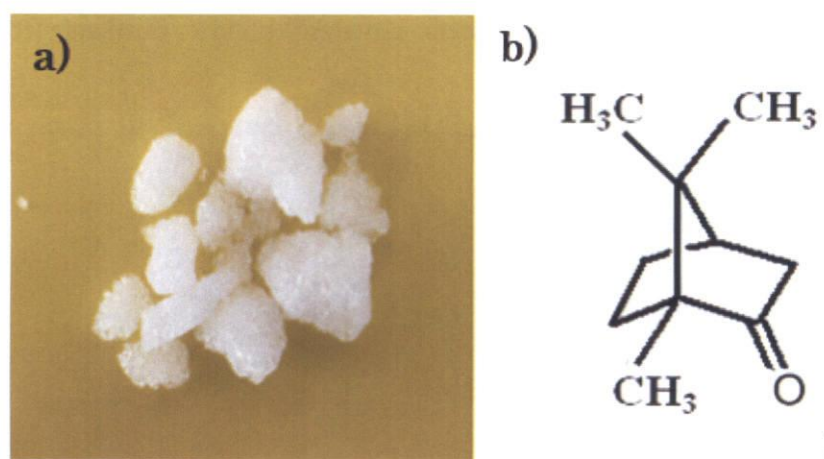
Figure 3.2.5   (a) Photograph image of commercial camphor and (b) molecular structure of camphor ($C_{10}H_{16}O$)

3.3.2   Tri-block copolymer Pluronic F127

Transfer-free synthesis of graphene on SiO (100nm) patterned Si substrate by solid phase reaction process was carried out by using triblock co-polymer Pluronic F127 ($EO_{106}PO_{70}EO_{106}$) as carbon source. The co-polymer can be easily dissolved in common organic solvents such as acetone, ethanol and methanol or water considering the low molecular weight. Pluronic F127 ($EO_{106}PO_{70}EO_{106}$) is a nonionic, water

soluble, 100% active and comparatively nontoxic surfactant which is environmental friendly. On the other hand F127 is also thermally decomposable. A triblock copolymer surfactant terminating in primary hydroxyl groups (-OH) which can increase the water solubility. The plenty of hydroxyl groups and non-substitute carbon atoms can provide an opportunity to link each other with covalent bonds. Furthermore long chain precursors like Pluronic F127 ($EO_{106}PO_{70}EO_{106}$) can lead to much more bigger graphene domain formation.

$$H-\left[O\underset{CH_2}{\overset{CH_2}{\diagdown}}\right]_a\left[O\underset{CH_2}{\overset{CH_3}{\underset{|}{CH}}}\right]_b\left[O\underset{CH_2}{\overset{CH_2}{\diagdown}}\right]_a-OH$$
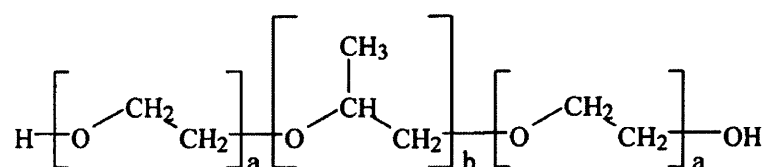
Figure 3.2.5   Chemical formula of triblock co-polymer Pluronic F127

3.4 References

[1]   O. Tsuyoshi, S. Keisuke, Y. Takahisa, L. Mikk, *Journal of Applied Physics* **103-10**, (2008)

[2]   Ferguson J. D., Arikan G., Dale D. S., Woll A. R., Brock J. D., *Physical Review Letters* **103-25**, (2009)

[3]   K. Gertrjan, Kropman B. L., Rijinders G., Blank D., Rogolla H., *Applied Physics Letters* **73-20**, (1998)

[4]   Ohtomo A., Hwang H.Y., *Journal of Applied Physics* **102 (8): 083704**, (2007)

[5]   A. Jorio, M. Dresselhaus, R. Saito, and G. F. Dresselhaus, *WILEY-VCH*, (2011).

[6]   A. C. Ferrari, J. C. Meyer, V. Scardaci, C. Casiraghi, M. Lazzeri, S. Piscanec, D. Jiang, K. S. Novoselov, S. Roth, A. K. Geim: *Phys. Rev. Let.*, **97, 187401**, (2006)

[7]   Seunghyun Lee,† Kyunghoon Lee,† and Zhaohui Zhong, *Nano Lett.*, **10, 4702–4707**,(2010)

[8]   Ahmad Umair and Hassan Raza, *nanoscale research letters*, **7:437,** (2012)

[9]   R. V. Lapshin *Nanotechnology* (UK: IOP) **15(9): 1135-1151,** (2004).

[10]   R. V. Lapshin.Measurement Science and Tech. **18 (3): 907–927,** (2007).

[11]   V. Y. Yurov, A. N. Klimov *Review of Scientific Instruments* (USA: AIP) **65 (5): 1551–1557,** (1994)

CHAPTER IV

Synthesis of Graphene on Noble Metal Silver via Chemical Vapor

Deposition Process and its Applications

4.1 Chemical Vapor Deposited Graphene on Ag Foil as Corrosion Resistant Coating

In a chemical vapor deposition (CVD) process catalytic decomposition of hydrocarbons on transition metals nickel, copper and cobalt have been significantly investigated as a catalytic layer to achieve high quality graphene growth [1-7]. Similarly, other metals, like ruthenium, iridium, platinum and palladium have been also demonstrated as a substrate material for graphene synthesis in a CVD process [8-10]. Growth of graphene on a non-catalytic gold substrate has been also reported [11]. The ability to synthesis of graphene on various metal substrates has many significant opportunities for wide range of innovative applications.

On the other hand, Ag nanoparticles have been integrated with graphene sheets to development of composite materials considering unique properties of silver such as, optical properties, surface plasmon resonance, high electrical and thermal conductivity [12-17].

It has been demonstrated that combination of Ag with graphene remarkable increasing in electrical conductivity can be achieved, as compared to graphene oxide film [18]. However, one of the main obstacle in many applications is sulfurization of Ag surface with formation of Ag_2S, also known as tarnishing or corrosion [19, 20]. In the atmospheric conditions sulfidation of Ag surface has been extensively investigated and demonstrated that sulfur-containing gaseous compounds, such as hydrogen sulfide (H_2S) and carbonyl sulfide (OCS) are prominent silver corrodents. The corrosion and formation of a rough surface with sulfidation reduce the optical properties and restricting many applications [21].

In these aspects, synthesis of graphene on Ag substrate by a CVD approach can be very interesting. A direct integration process of graphene on Ag surface can be very promising owing to unique optical, electrical and thermal properties of Ag. In this chapter, I demonstrate synthesis of few-layer graphene film on silver foil by the atmospheric pressure CVD process using solid carbon source. To prevent from tarnishing and corrosion of silver surface, synthesized graphene film can be effective covering material.

4.2 Experimental

In this study commercially available Ag foil with a thickness of 30 μm and purity of 99.98% was used for graphene synthesis by the thermal AP-CVD technique. Ag foils were cleaned with acetone and without any further treatment was used for graphene growth. 10 mg of botanical derivative solid camphor ($C_{10}H_{16}O$) was used as carbon source for graphene synthesis. Ag foils were heated up to 945 °C (below melting point~961.8 °C) in a tubular furnace under 100 standard cubic centimeters per minute (sccm) H_2 atmosphere. The graphene growth was investigated with different gas composition of Ar and H_2. The pure solid camphor was slowly evaporated and introduced in the growth zone along with a gas mixture of H_2 and Ar. Finally, the CVD furnace was slowly cooled down to room temperature. Tarnishing of bare and graphene-coated Ag foil were investigated with introduction sulfur vapor in atmospheric conditions. Pure sulfur (98.0+ %) purchased from Wako chemical was vaporized and exposed the samples for 15 min duration.

Synthesized graphene were characterized with NRS 3300 laser Raman spectrometer with laser excitation energy of 532.08 nm from a green laser. Transmission electron microscope (TEM) images were taken by JEOL JEM 2100, operated at 200kV along with EDX analyzer. Optical reflectance measurements of the graphene film were

carried out with the UV–Vis–NIR on JASCO-V570 spectrophotometer. Contact angle measurements were carried out with contact angle system OCA. The bare and graphene-coated Ag foils before and after the sulfur exposure were characterized by optical microscopy using VHX-500 digital microscope. Similarly, samples were characterized by scanning electron microscopy (SEM) studies with JEOL JSM 5600. X-ray photoelectron spectroscopy (XPS) data was acquired to determine the chemical composition of the Ag and graphene films using SSX-100 photoelectron spectrometer with photoemission stimulated by a monochromated Al K_α radiation source (1486.6 eV).

4.3 Results and Discussion

The synthesized continuous carbon films were properly examined by Raman spectroscopy, optical microscopy and scanning electron microscopy studies. Figure 4.3.1 shows Raman spectra of the deposited carbon films at three different gas compositions compared with camphor molecules. A strong Raman peak at 652 cm^{-1}, is observed for the solid precursor, corresponding to the carbon rings in the camphor molecule. The peak observed at 1741 cm^{-1} corresponds to the C=O stretching vibration band. Other weak peaks at 857 cm^{-1}, 1093 cm^{-1} and 1447 cm^{-1} correspond to various modes of hydrocarbon (C-H) in camphor. The carbon film deposited in Ar atmosphere

shows a broad splitted peak with peak centers at 1598 and 1367 cm^{-1}, corresponding to graphitic G and defect related D peak. The presence of broad G and D peaks and none appearance of a peak in the higher wave numbers indicate no graphene formation. Introducing 2 sccm of H$_2$ along with 88 sccm of Ar in the growth process, second order 2D Raman peak at 2682 cm^{-1} appeared along with much sharper G and D peaks at 1583 and 1340 cm^{-1}, respectively. Subsequently, increasing the amount of H$_2$ gas to 5 sccm much better graphitization was achieved with much more intense G and 2D peak intensities. The presence of an intense 2D Raman peak confirms that the synthesized carbon materials contains graphene like structure.
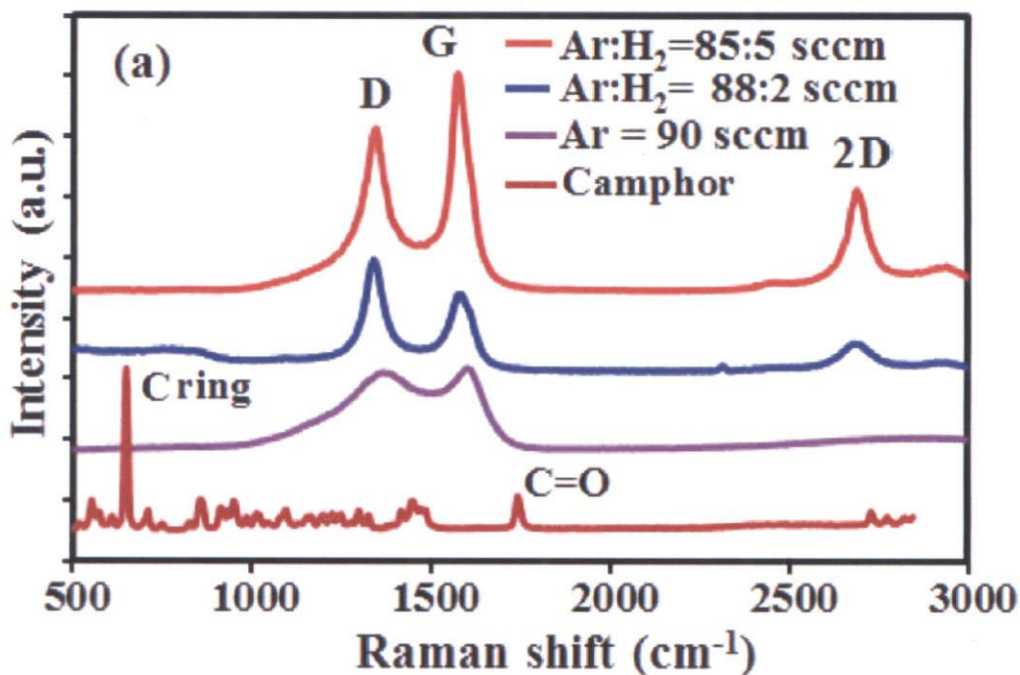
Figure 4.3.1   Raman spectra of solid camphor and as-synthesized carbon films with

different gas compositions of Ar and H$_2$.

Figure 4.3.2 a_b shows optical microscope and SEM images of the graphene on silver foil, respectively. Twins of polycrystalline Ag surface and grain boundaries and are evidently visible. The results clearly signify that H_2 has very a significant role in synthesis of graphene on silver as that of Cu substrate [22, 23]. The H_2 atoms can act as an activator agent of the carbon radicals promoting graphene nucleation on the non-catalytic noble metal Ag surface. Again, hydrogen absorption on Ag can stimulate surface reconstruction thus enhancing graphene nucleation and growth activities [24].
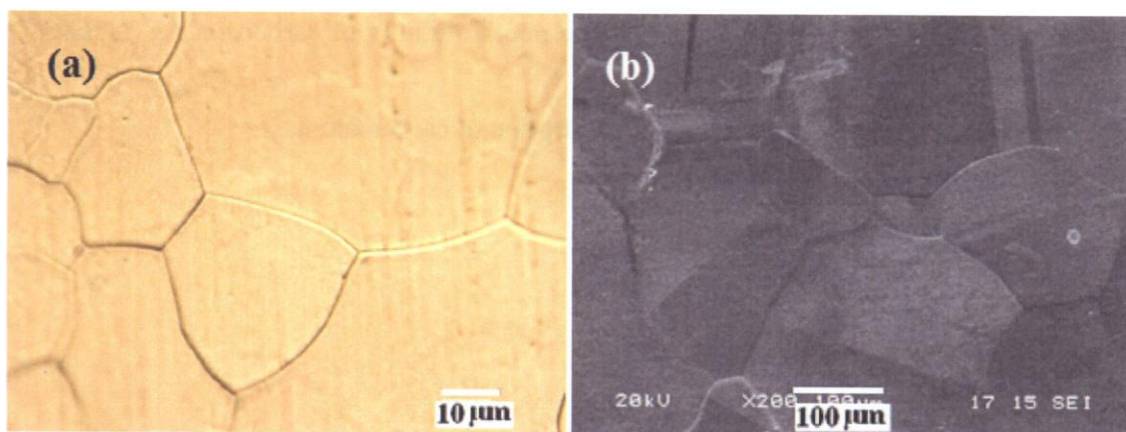
Figure 4.3.2   (a) Optical microscope and (b) SEM image of synthesized graphene

on Ag foil

4.3.1 TEM studies of CVD growth graphene on silver

The formation of few-layer graphene on Ag foil was further confirmed by transmission electron microscopy (TEM) studies. Figure 4.3.3a shows a TEM image of synthesized graphene sheets after chemically etching from Ag foil. TEM observation of

the sheet edges reveled few-layer graphene formation. Figure 4.3.3b_c shows TEM images at the graphene sheet edges, presenting three and five layers of graphene sheet, respectively. Inset of figure 4.3.3c_d shows the intensity profile images. From this intensity pattern, an interplaner spacing of about 0.34 nm is estimated, corresponding to graphitic d(002) spacing, confirming formation graphene structures. The polycrystalline Ag foil with micron order grain contains graphene domains with different number of layers. Carbon solubility in Ag (fcc) at its melting point is around 0.036 at%, which is almost similar to that of Cu 0.04 at%. The poor solubility of carbon on Ag as that of Cu indicates graphene growth with surface adsorption of carbon atoms.
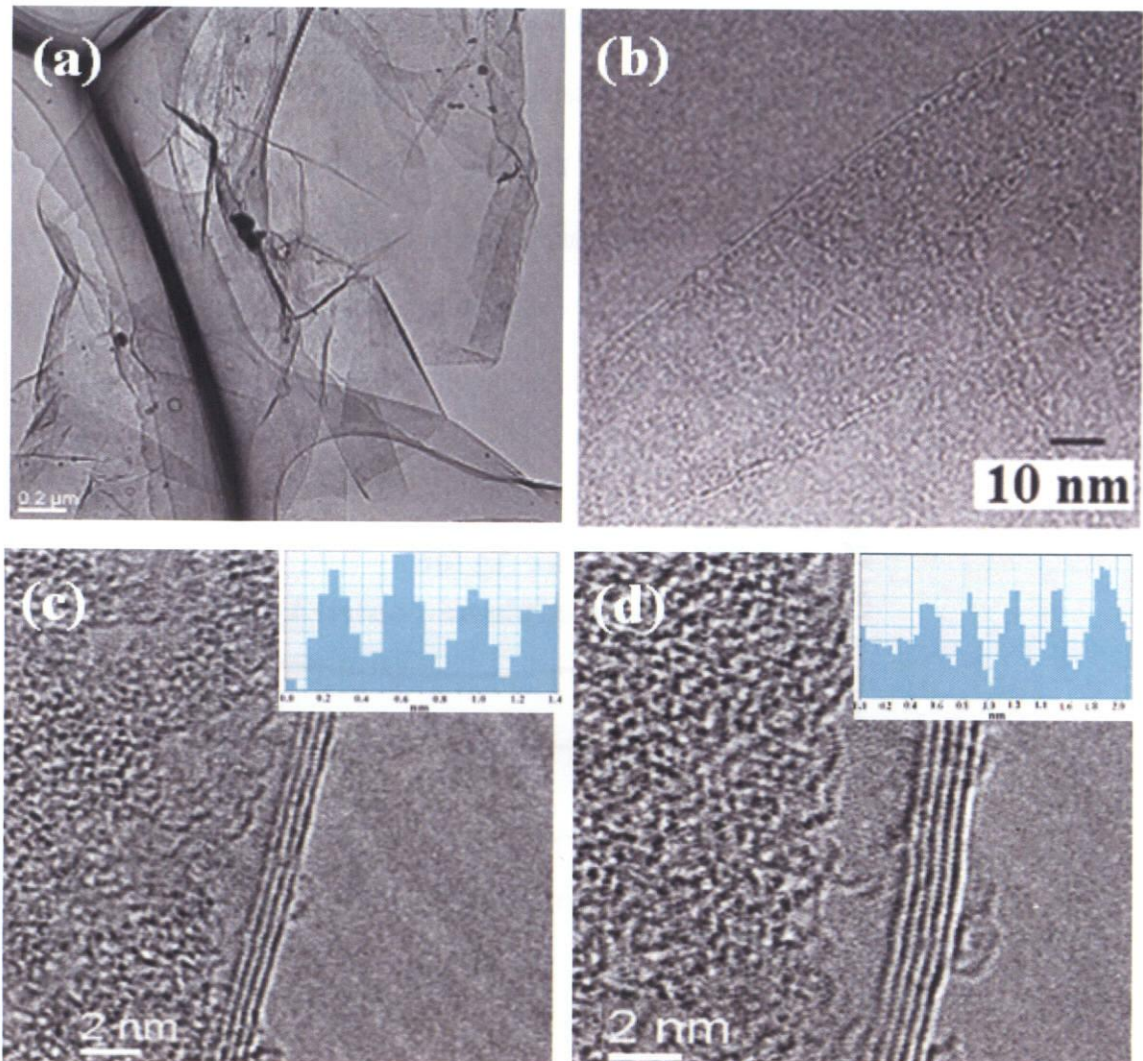
Figure 4.3.3   TEM images of (a) graphene sheets, (b) mono-layer, (c) three-layer

and (d) five layer graphene synthesized on Ag foil by CVD process.

(Inset of figure 2c_d shows the intensity profile images)

4.3.2 Reflectivity Test

Figure 4.34a shows optical reflectance of the bare and graphene-coated Ag foil

measured with UV–Vis–NIR spectrophotometer. Coating a graphene film, reflectivity of

the Ag surface reduces by around 23 % at 550 nm wavelength. The synthesized few-

layer graphene film absorbs some of the incident light and thus reducing reflectance of Ag surface. Figure 4.3.4b_c shows water droplet images on bare and graphene-coated Ag foil, respectively. Contact angle of the bare Ag foil increases from 82.5° to 96.7° with coating a graphene film. The increase in contact angle presents hydrophobic nature of the graphene-coated Ag foil. The less wettability with graphene coating can protect Ag surface from harsh chemical atmosphere.
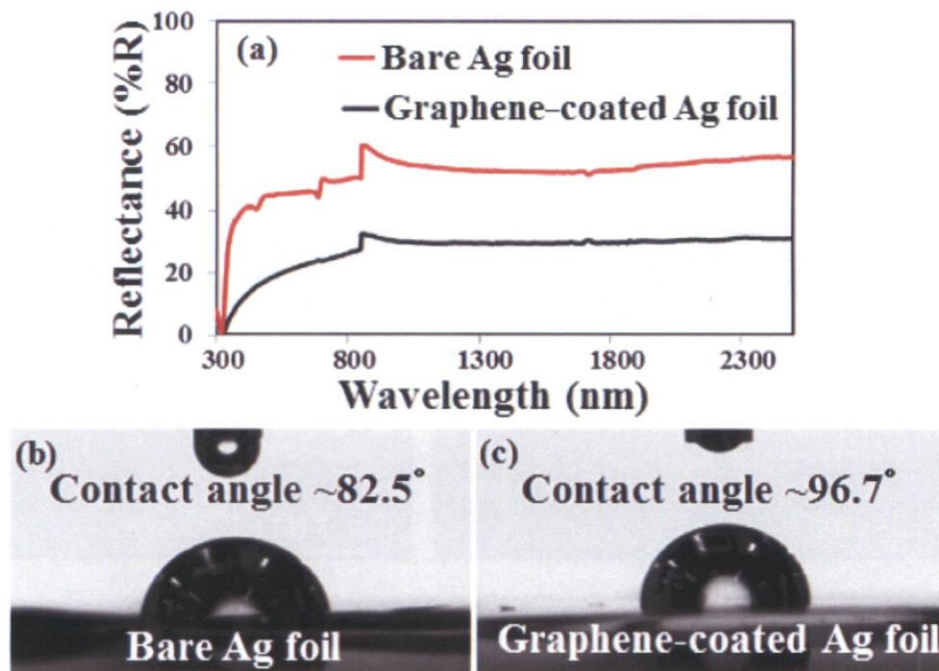
Figure 4.3.4   (a) Reflectance and (b), (c) contact angles of bare and graphene-coated Ag foil respectively.

4.3.3 Sulfurization Effect

The synthesized graphene film on Ag foil by the CVD process was explored as a tarnish-resistance coating. Tarnishing of bare and graphene-coated Ag foil was investigated introducing sulfur vapor in atmospheric conditions. Figure 4.3.5a shows photograph images of Ag foil surface with and without graphene coating, before and after sulfur vapor exposure. The graphene-coated Ag surface shows only small change after the treatment, however, uncoated Ag surface turn almost black. The sulfidation resistance of the graphene coating on Ag was analyzed by optical microscopy and SEM studies. Figure 4.3.5b_c shows optical microscopy images of bare and graphene-coated Ag foil before and after sulfur exposure. A visible change can be observed of the bare Ag foil with sulfidation. The color of the bare Ag turns black with large particles formation, whereas the color of the graphene-coated Ag remained almost unchanged. However, residue of sulfur as small particles was observed on the top of graphene-coated Ag foil. SEM studies also showed a visible difference between the bare Ag and the graphene-coated Ag foil after sulfidation. Figure 4.3.5d_e shows morphology of bare and graphene-coated Ag foil before and after sulfur exposure. Sulfidation significantly corrodes the Ag creating holes and removing Ag from surface to form particle like structure, whereas only small impact on graphene-coated Ag foil is

observed.
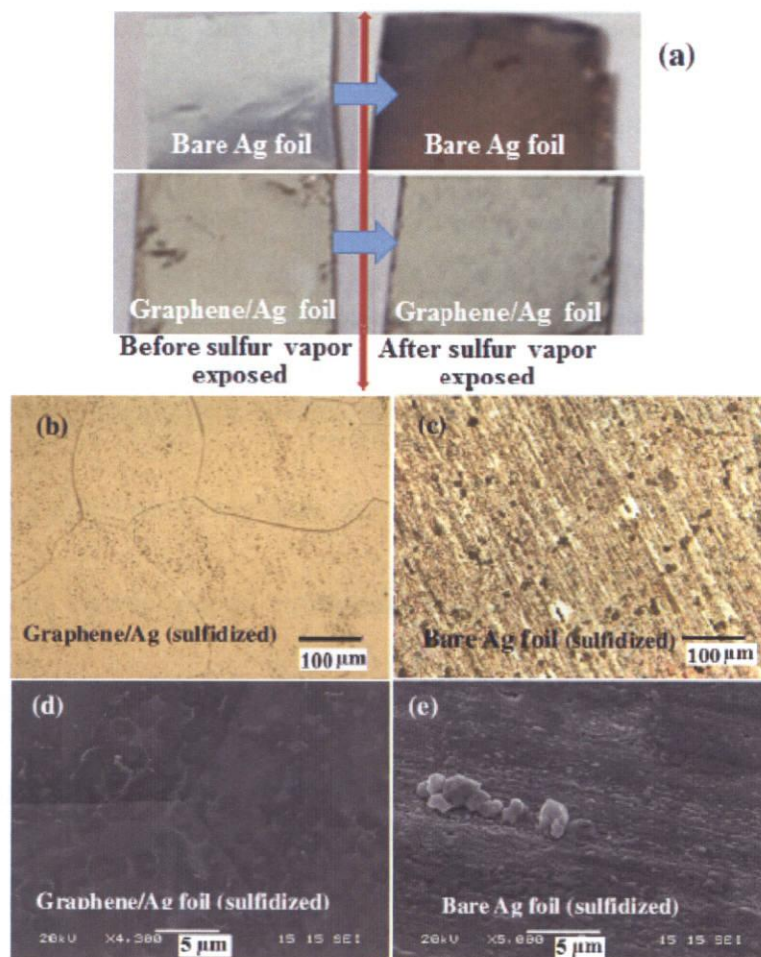
Figure 4.3.5   (a) Photographs of bare and grapheme-coated Ag foils before and after

sulfidation. (b, c) Optical microscope (with same brightness level) and

(d, e) SEM images of bare and graphene-coated Ag foils before and

after sulfidation, presenting the surface morphology.

4.3.4 X-ray Photoelectron Spectroscopy Studies of Graphene Coated Silver Foil vs Bare Silver Foil

Figure 4.3.6a presents wide XPS spectra of sulfidized bare and graphene-coated Ag surface. Sulfur was detected along with Ag and small amount of oxygen and carbon for the sulfidized bare Ag foil. The presence of oxygen and carbon atoms may be due to surface chemisorption during the sulfidation reaction in atmosphere. Figure 4.3.6b shows XPS core level spectra of C$1s$ with a peak-centre at 283.5 eV for the graphene-coated Ag foil after sulfidation. The C$1s$ peak intensity is much higher than that of small carbon peak detected in sulfidized bare Ag foil. The presence of a strong C$1s$ peak shows that the graphene film remain intact after sulfidation. Again, no clear shift of C$1s$ peak is observed, indicating undisturbed sp^2 hybridized carbon atom. Figure 4.3.6c shows XPS core level spectra of Ag $3d$ for the sulfidized bare Ag foil. Two splitted peaks at 367.2 and 372.9 eV were observed, corresponding to Ag $3d_{3/2}$ and Ag $3d_{5/2}$, respectively.

Figure 4.3.6d shows XPS S$2p$ spectra of the bare Ag foil with a peak-centre at 160.7 eV, in comparison to graphene-coated Ag foil. The high amount of sulfur content on the bare Ag foil and XPS peaks corresponding to the values for Ag bonded sulfur presents Ag$_2$S formation. The XPS analysis clearly indicates sulfidation of the bare Ag

foil; while the graphene-coated Ag foil remains intact. The XPS results can be correlated with optical and morphological evidence obtained with optical microscope and SEM analysis. The finding shows that the CVD grown graphene film effectively preserve the Ag foil surface form degradation and tarnishing.
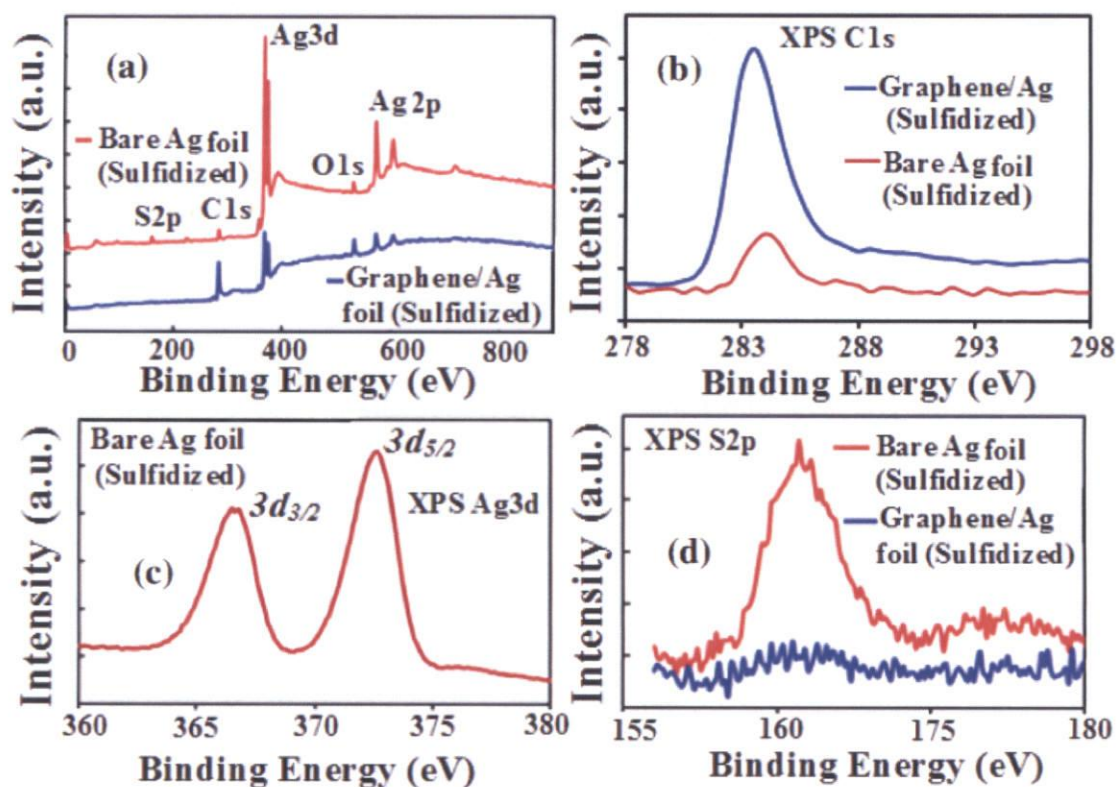
Figure 4.3.6   (a) X-ray photoelectron spectroscopy (XPS) survey spectra, (b) C1s, (c) Ag3D, and (d) S2p spectra for the bare and graphene-coated Ag foils after sulfidation.

4.3 Conclusion

In conclusion, I demonstrated synthesis of graphene on silver foil by the atmospheric pressure CVD process as a tarnish-resistant coating. Continuous graphene film on Ag foil was grown using the pure solid camphor ($C_{10}H_{16}O$) as a carbon source with a gas mixture of Ar (85 sccm) and H_2 (5 sccm). The Raman spectroscopy and TEM analyses revealed few-layer graphene formation on Ag surface. A thin graphene coating makes the Ag surface more hydrophobic with a reduction in reflectivity. Tarnishing of the silver surface in presence of sulfur vapor exposure was investigated with and without coating the graphene film. Findings show that the bare Ag surface immediately reacts with sulfur vapor to turn black, whereas graphene-coated Ag surface restrained reacting with the sulfur vapor and effectively preserved the silver surface. My findings signify that graphene film can be effectively grown on non-catalytic silver substrate to resist tarnishing and corrosion with sulfidation.

4.4 References

[1]   B. C. Banerjee, T. J. Hirt and P. L. Walker, Nature **192**, 450 (1961).

[2]   I. Alstrup, I. Chorkendorff, and S. Ullmann, Surf. Science **264**, 95 (1992).

[3]   K. S. Kim, Y. Zhao, H. Jang, S. Y. Lee, J. M. Kim, K. S. Kim, J. H. Ahn, P. Kim, J. Y. Choi, and B. H. Hong, Nature **457**, 706 (2009).

[4]   X. S. Li, W. W. Cai, J. H. An, S. Kim, J. Nah, D. X. Yang, R. Piner, A. Velamakanni, I. Jung, E. Tutuc, S. K. Banerjee, L. Colombo, and R. S. Ruoff, Science **324**, 1312 (2009).

[5]   S. Bae, H. K. Kim, Y. Lee, X. Xu, J. Park, Y. Zheng, J. Balakrishnan, D. Im, T. Lei, Y. Song, Y. Kim, K. Kim, B. Ozyimaz, J. Ahn, B. Hong, and S. Iijima, Nat. Nanotechnol. **5**, 574 (2010).

[6]   E. Sutter, P. Albrecht, and P. Sutter, Appl. Phys. Lett. **95**, 133109 (2009).

[7]   R. Hirano, K. Matsubara, G. Kalita, Y. Hayashia, and Masaki Tanemura, Nanoscale **4**, 7791 (2012).

[8]   J. Coraux, A. T. N'Diaye, M. Engler, C. Busse, D. Wall, N. Buckanie, F. Heringdorf, R. van Gastei, B. Poelsema and T. Michely, New Jour. Phys. **11**, 023006 (2009).

[9]   J. Wintterlin, and M. L. Bocquet, Surf. Science **603**, 1841 (2009).

[10] L. Gao, J. R. Guest, and N. P. Guisinger, Nano Lett. **10**, 3512 (2010).

[11] T. Oznuluer, E. Pince, E. O. Polat, O. Balci, O. Salihoglu, and C. Kocabas, Appl. Phys. Lett. **98**, 183101 (2011).

[12] J. B. Liu, S. H. Fu, B. Yuan, Y. L. Li, and Z. X. Deng, J. Am. Chem. Soc. **132**, 7279 (2010).

[13] X. Z. Tang, Z. W. Cao, H. B. Zhang, J. Liu, and Z. Z. Yu, Chem. Comm. **47**, 3084 (2011).

[14] S. Link, and M. A. El-Sayed, *Int. Rev. in Phys. Chem.* **19**, 409 (2000).

[15] S.Sun, P.Wu, *Phys. Chem. Chem. Phys.* **13**, 21116 (2011).

[16] X. Q. Zou, and S. J. Dong, J. Phys. Chem. B **110**, 21545 (2006).

[17] W. Yang, J. Li, Y. Zhong, H. Qian, Z. Li, and Y. Hu, *CrystEngComm* **15**, 2598 (2013).

[18] R. Pasricha, S. Gupta, and A. K. Srivastava, *Small*, **5**, 2253 (2009).

[19] H. E. Bennett, R. L. Peck, D. K. Burge, J. M. Bennett, J. Appl. Phys. **40**, 3351 (1969).

[20] J. L. Elechiguerra, L. L. Lopez, C. Liu, D. G. Gutierrez, A. C. Bragado, and M. J. Yacaman, Chem. Mater. **17**, 6042 (2005).

[21] J. C. Reed, H. Zhu, A. Y. Zhu, C. Li, and E. Cubukcu, Nano Lett. **12**, 4090

(2012).

[22]   I. Vlassiouk, M. Regmi, P. Fulvio, S. Dai, P. Datskos, G. Eres, and S. Smirnov,

ACS Nano **5**, 6069 (2011).

[23]   M. Losurdo, M. M. Giangregorio, P. Capezzuto and G. Brunoa, Phys. Chem.

Chem. Phys. 13, 20836 (2011).

[24]   G. Lee, Phys. Rev. B **51**, 7250 (1995).

CHAPTER V

Fabrication of Ag-NPs Decorated Graphene-Si Photodetector

Fabrication of graphene based photodetectors has been developed by employing the absorption (monolayer graphene~2.3%) of incident light in a broad wavelength range and high mobility for ultrafast detection [1-3]. A photoresponsivity of 10 mAW^{-1} has been succeeded with graphene based photodetectors in a field-effect transistor (FET) configuration [4-7]. Recently, Zhang et al., demonstrated very high photoresponsivity in a monolayer graphene photodetector by introducing electron trapping centers and creating a bandgap[8]. However, light absorption in a monolayer graphene can be still considerably low, which can be overcome by surface plasmonic nanoparticles integration. Liu et al. has reported multi-color photodetectors by integrating gold plasmonic nanostructures with graphene [9]. A maximum photoresponsivity of 6.1 mA W^{-1} at visible wavelength is obtained presence of gold plasmonic nanoparticles, which is still quite low. In terms of production of a photodetector, high light sensitivity and design of simple device architecture can be critical for solar energy device applications. From this perspective and contrast to previously demonstrated devices, graphene/n-Si based Schottky junction device with plasmonic metal nanoparticles can be a promising approach to achieve high

photoresponsivity.

In this chapter, I demonstrate fabrication of a graphene based Schottky junction photodetecotor with silver nanoparticles (AgNPs) decorated CVD synthesized graphene and n-Si. Ag-NPs were directly obtained on the graphene by dissolving the base Ag foil in diluted HNO_3 (25% concentration) without using any other reagents, reductants and stabilizers. A remarkable photoresponse is achieved in near-infrared (IR), visible and near ultraviolet (UV) wavelengths, attributing to light interaction with the plasmonic Ag-NPs in the demonstrated device.

5.1   Experimental

In this experiment commercially available Ag foil with a thickness of 30 μm and purity 99.98% was used for graphene synthesis by the thermal CVD technique. 10 mg of solid camphor ($C_{10}H_{16}O$) was used as carbon source for graphene synthesis. Graphene growth was carried out at 945 °C (below melting point~961.8°C of Ag) in a tubular furnace with a gas composition of Ar and H_2. The flow rate of Ar and H_2 was optimized as 85 and 5 standard cubic centimeters per minute (sccm), respectively. The solid carbon source was slowly evaporated and introduced in the growth zone along with the Ar and H_2 gas mixture. Finally, the CVD furnace was gradually cooled down to room temperature under the flow of 80 sccm H_2. The base Ag foil used for graphene

synthesis was dissolved in a diluted HNO_3 solution to create the surface assisted Ag-NPs on graphene. Graphene-Si Schottky junction photodetector was fabricated by transferring the Ag-NPs decorated graphene on Au electrode deposited SiO_2/n-Si substrates.

Synthesized graphene materials were characterized with NRS 3300 laser Raman spectrometer with laser excitation energy of 532.08 nm. The optical microscopy studies were carried out with VHX-500 digital microscope. Scanning electron microscopy (SEM) studies were carried out with JEOL JSM 5600. Transmission Electron Microscope (TEM) images were taken by JEOL JEM 2100, operated at 200kV equipped with an element analyzer. The Au electrodes were deposited by thermal evaporation technique using ULVAC VPC-260F. Current density-voltage (J-V) and external quantum efficiency (EQE) characteristics measurements were carried out at room temperature (25 °C) using a solar simulator (Bukokeiki, Japan) in the dark and under illumination with air mass (AM) 1.5 simulated solar radiation. The time dependent photo response characteristics were measured using a xenon lamp unit (SM-25, Bukokeiki, Japan) with a monochromator.

5.2   Results and Discussion

Synthesized continuous carbon films on silver foil were characterized by

Raman spectroscopy and optical microscopy to confirm graphene growth. Figure 5.2.1

shows the Raman spectra of as-synthesized graphene by the atmospheric pressure CVD

process. Most prominent peaks in the spectra *are* observed at 1346, 1584 and 2696 cm^{-1},

corresponding to disorder-induced D, graphitic G and second order 2D peak,

respectively. Presence of a strong 2D peak confirmed growth of graphene on the Ag foil.

Previously, I have demonstrated that synthesis of few-layer graphene is possible by the

CVD process on a noncatalytic Ag foil [10].
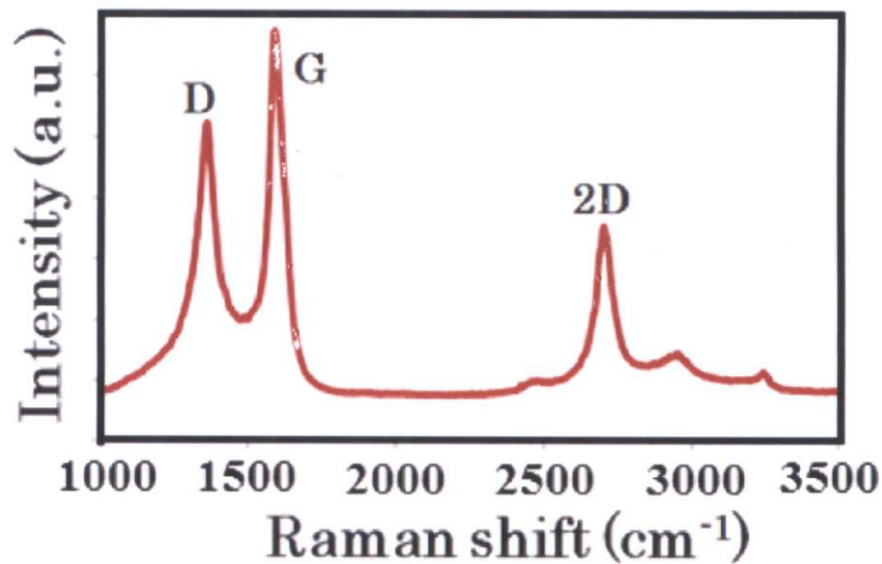
Figure 5.2.1   Raman spectra of as-synthesized graphene on Ag foil by an
atmospheric pressure CVD process.

Figure 5.2.2 shows an optical microscope image of the graphene grown on Ag

foil. Polycrystalline Ag grain of few microns and grain boundaries are evidently visible.

The Ag foil with micron order grain size contains graphene domain with different number of layers. Recently, decoupled synthesis of graphene on single-crystal Ag (111) substrate has been also reported by a CVD process using solid carbon source [11]. The possibility of synthesis of graphene on non-catalytic Ag foil can be significant to open up new possibilities for energy device applications considering the interesting optical and electrical properties of Ag.
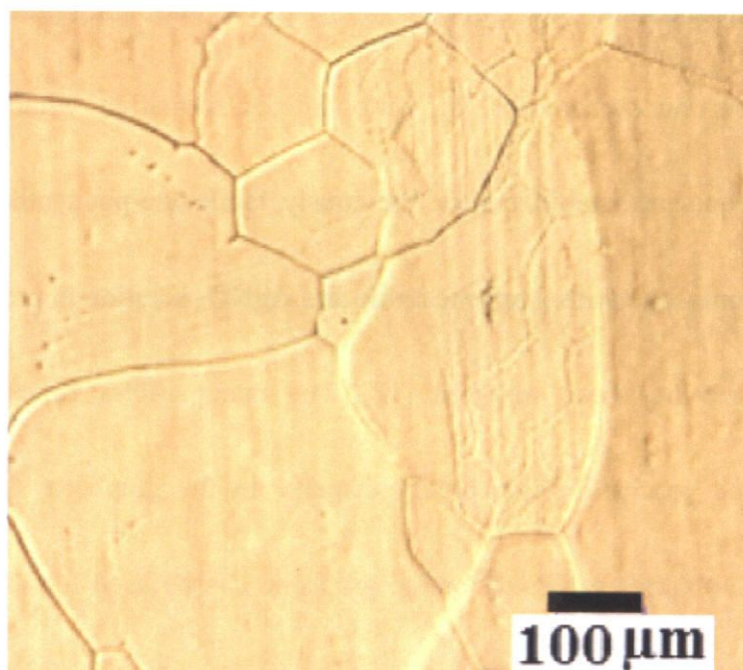
Figure 5.2.2   Optical microscope image of as-synthesized graphene on Ag foil by an atmospheric pressure CVD process.

5.2.1   Transfer of Graphene Film And Ag-Nps Decoration

The graphene synthesized on Ag foil was dissolved in a diluted HNO_3 (25% concentration) solution as shown in figure 5.2.3. Before dissolving the Ag base, graphene was coated with a very thin poly (methyl methacrylate) (PMMA) layer to transfer on SiO_2/Si substrate without any structural distortion. I observed that the Ag

foil dissolved gradually in the acid solution and leading to formation of Ag nanoparticles on the graphene surface. HNO_3 is an oxidizing agent and will oxidize Ag metal to Ag^+ ions, itself being reduced to a lower oxidation state. Most of the Ag dissolved during reaction process, where some nanoparticles were formed at the graphene surface in the acid solution. In the Ag foil dissolving process, graphene sheets act a supporting surface for Ag nanoparticles formation without using any other reagents, reductants, stabilizers etc. Previously, facile one-pot synthesize of Ag-NPs and graphene composite with graphene oxide and $AgNO_3$ solution in presence of a reductant and stabilizer has been reported [12]. The nanoparticles directly obtained in my demonstrated process remain highly disperse in the graphene sheets. The one step approach to obtain Ag-NPs decorated graphene can be used for various energy device applications such as solar panels, photodetectors, photodiodes, etc.

$$2Ag(s) + 2HNO_3(aq) \longrightarrow 2AgNO_3(aq) + H_2(g)$$
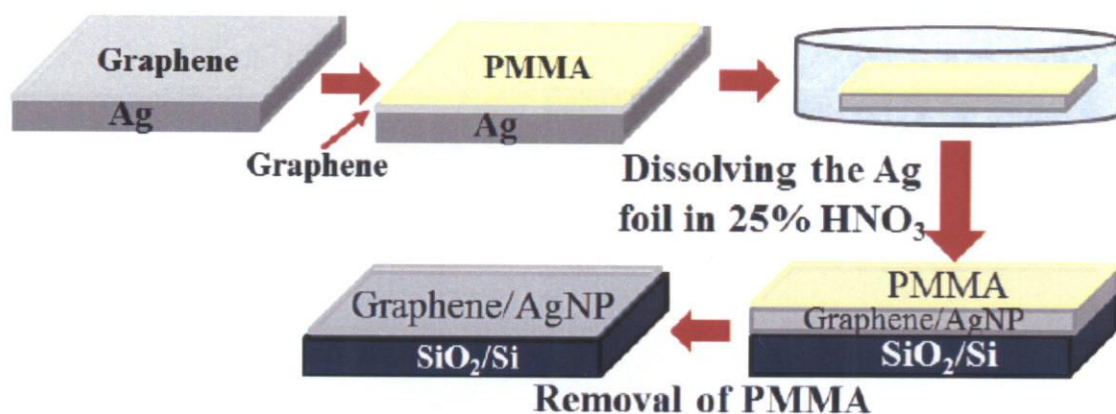
Figure 5.2.3   Ag-NPs formation on the as-synthesized CVD graphene by dissolving

base Ag foil in a diluted HNO_3 solution.

5.2.2   TEM Analyses of Single Crystal Ag-NP

The formation of Ag-NPs in the graphene sheet was analyzed and confirmed by

Transmission electron microscopy (TEM) studies. Figure 5.2.4a shows TEM image of a

single layer graphene synthesized on silver foil by the CVD process, however, few-layer

graphene formation is also observed. Figure 5.2.4b shows formation of Ag-NPs in the

CVD graphene by dissolving the base Ag substrate. Ag-NPs with a size distribution of

20-100 nm is uniformly coated in the graphene sheets. Most of the nanoparticles are

roughly round in shape, whereas some of them are rectangular in shape. Inset of figure

5.2.4b shows a high resolution TEM (HRTEM) image of a round shape nanoparticle,

presenting high crystalline nature.
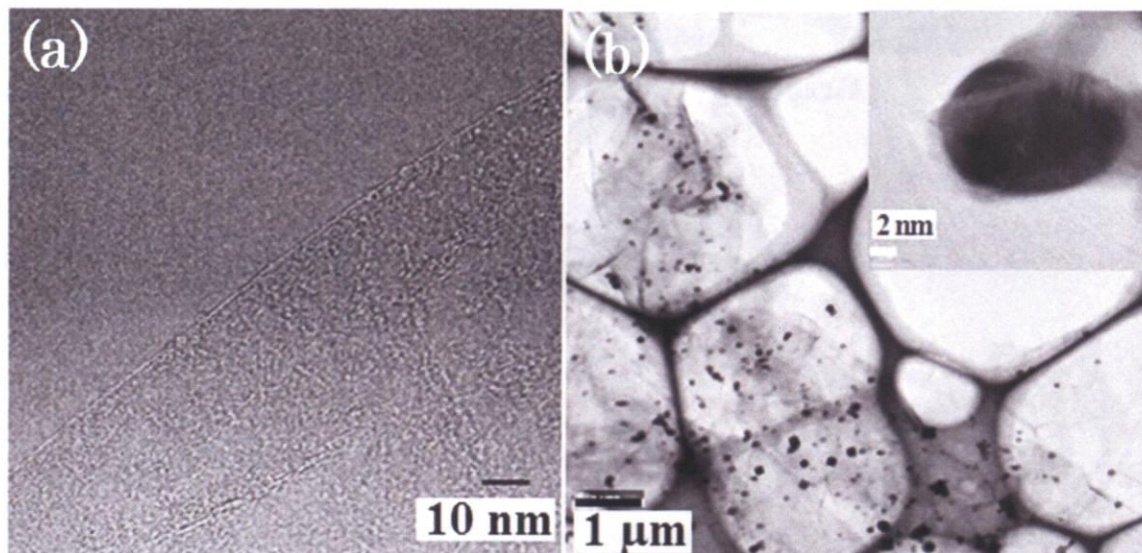
Figure 5.2.4   **(a)** TEM image at the edge of a graphene sheet synthesized on Ag foil by CVD process. **(b)** Formation of Ag-NPs decorated graphene by dissolving the Ag base substrate in a HNO_3 solution (inset shows a round shape Ag-NP)

The crystalline structure is further analyzed by HRTEM studies as shown in figure 5.2.5a. The lattice-fringe distance is measured as 0.24 nm, which corresponding to the spacing of (111) plane of cubic Ag. The selected area electron diffraction (SAED) pattern of a nanoparticle shows excellent single crystalline structure as shown Figure 5.2.5b. The SAED pattern spots can be indexed as the (111), (200), (220) and (311) plane for Ag cubic lattice structure [14-16].
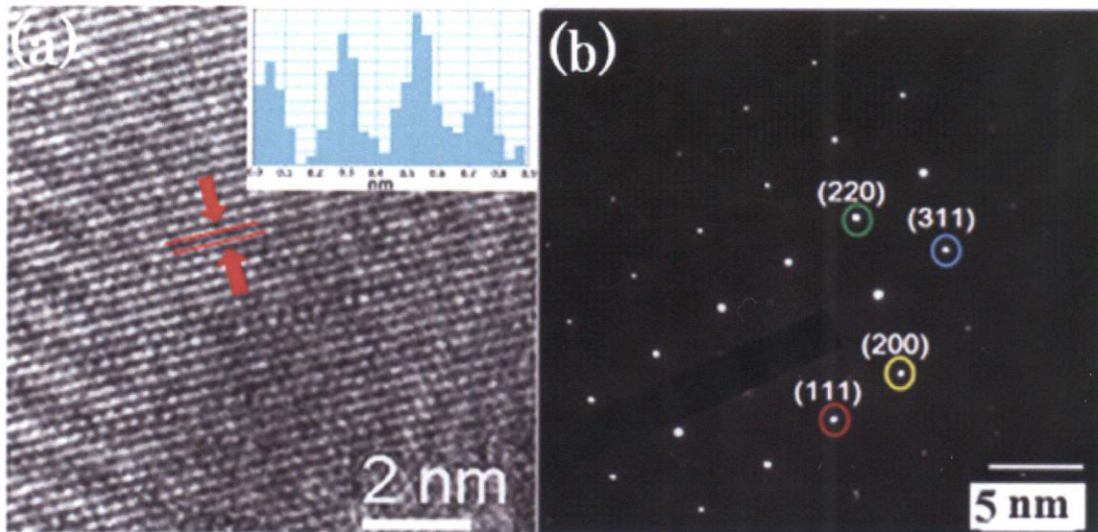
Figure 5.2.5   **(a)** HRTEM image and **(b)** SAED pattern of an Ag-NP, presenting

high crystalline nature and cubic lattice structure.

5.2.3   Fabrication of Schottky Junction Device

A Schottky junction photodetector device is fabricated with as-derived Ag-NPs

decorated graphene. Figure 5.2.6 shows a schematic diagram of the Ag-NPs decorated

graphene-Si Schottky junction device. An ohmic back contact was created with

deposition of Au:Sn on Si surface. SiO_2 was patterned on the front side of the n-Si

substrate for the Schottky junction fabrication with the Ag-NPs coated graphene.

Incident light in the device transmits through the graphene and absorbs in the Si

substrate to generate photo-exciton. Meanwhile, the Ag-NPs can enhance light

absorption with the surface plasmonic effect.
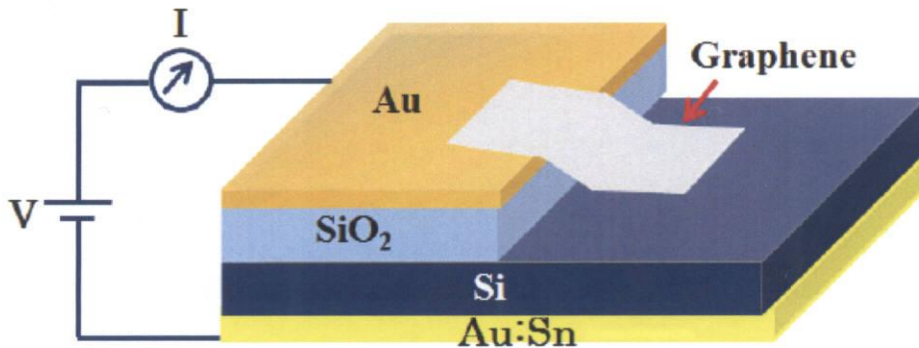
Figure 5.2.6   Schematic diagram of the fabricated Schottky junction with the transferred Ag-NPs incorporated graphene on n-Si substrate.

Figure 5.2.7a_b shows optical microscope and scanning electron microscope (SEM) image of the fabricated device, presenting the transferred graphene on Si substrate. The graphene is transferred like that it is extended from the bare Si to SiO_2 patterned surface. Efficient photo-exciton dissociation and charge transportation can be obtained at the interface of graphene and n-Si. Previously, our group have been demonstrated formation of a suitable potential barrier at the graphene/n-Si junction for efficient charge separation [13].
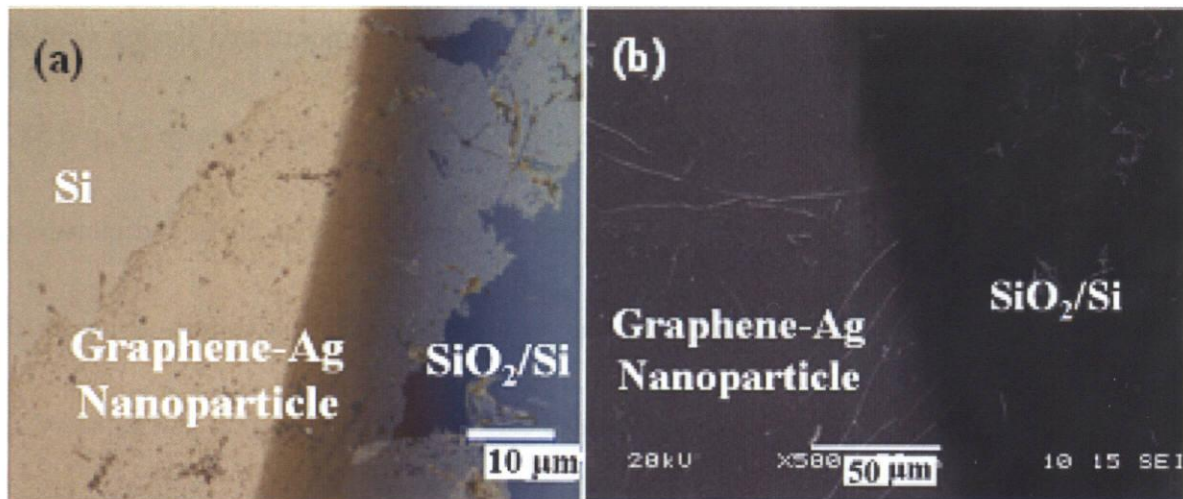
Figure 5.2.7   **(a)** Optical microscope and **(b)** SEM images of Ag-NPs coated graphene transferred to the SiO₂ patterned Si substrate.

5.2.4   Electrical Characteristic of AgNPs Decorated Graphene Based Schottky Junction Photodetector

Figure 5.2.8a shows current density- voltage (J-V) characteristic of the graphene/n-Si heterojunction device under dark condition. Rectifying J-V characteristics and ohmic back contact confirm formation of a Schottky junction at the graphene/n-Si interface. Figure 5.2.8b shows a log plot of the dark light characteristic. The fabricated Schottky junction shows a good rectification characteristic with an 'on/off' ratio of around 10^2 at ±1 V. However dark current is still not so low compare to conventional photodetectors. Photo-response property of the fabricated graphene/n-Si Schottky junction were also investigated with illumination of 100 mW/cm².

Figure 5.2.8c shows J-V characteristic of the demonstrated device with and without light illumination. A photovoltaic action with open circuit voltage (V_{oc}) 0.38 V, short circuit current density (J_{sc}) 3.5 mA/cm^2, fill factor (FF) of 20 % and conversion efficacy of 0.27 % is obtained. The photosensitivity and photovoltaic action in the fabricated device indicate photoexcitation of carriers and photocurrent generation at the graphene/n-Si interface. Figure 5.2.8d shows a quantum efficiency curve of the fabricated Schottky junction with Ag-NPs decorated graphene. I observed considerable phototresposnce and external quantum efficiency (EQE) in the shorter wavelength range as well, which can be attributed to the surface plasmon resonance scattering of Ag-NPs.
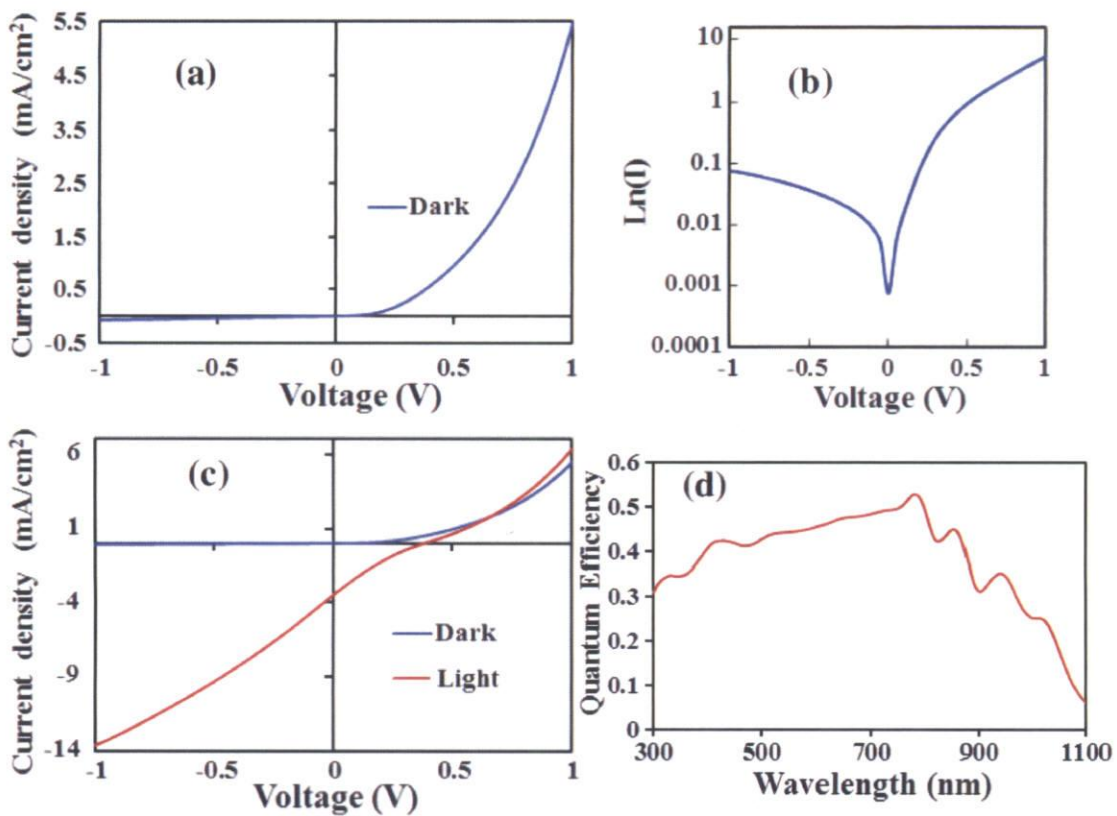
Figure 5.2.8   **(a)** J-V characteristic of the graphene/n-Si heterojunction and **(b)** log plot under dark condition. **(c)** J-V characteristic of the fabricated device with (100 mW/cm^2) and without light illumination. **(d)** EQE of the fabricated Schottky junction.

5.2.5   Photoresponsivity of Graphene-Si Schottky Junction Photodetector

Photoresponsivity of the presented device was further examined with illumination of different light intensities and wavelengths. Time-dependent photocurrent measurements are performed in the near-IR (1000 nm), visible (550 nm) and near-UV (350 nm) wavelengths. Figure 5.2.9a_c shows time-dependent photocurrent of the

fabricated device with illumination of 3.6, 5.1 and 2.1mW/cm^2 light at 1000, 550 and

350 nm wavelengths. I observed significant on/off current with low illumination light

intensity. The graphene/n-Si Schottky junction photodetector device presents

photoresponse of 78, 122 and 98mAW^{-1} in the near-IR, visible and near-UV,

respectively. Previously, it has been reported observation of photoresponsively of about

10mAW^{-1} in graphene based device with an optical pumping as high as 10^{8}mW/cm^2.

Recently, a maximum photoresponsively of 62.95mAW^{-1} at 445 nm wavelength has

been achieved in a reduced GO/Si heterojunction device [17].
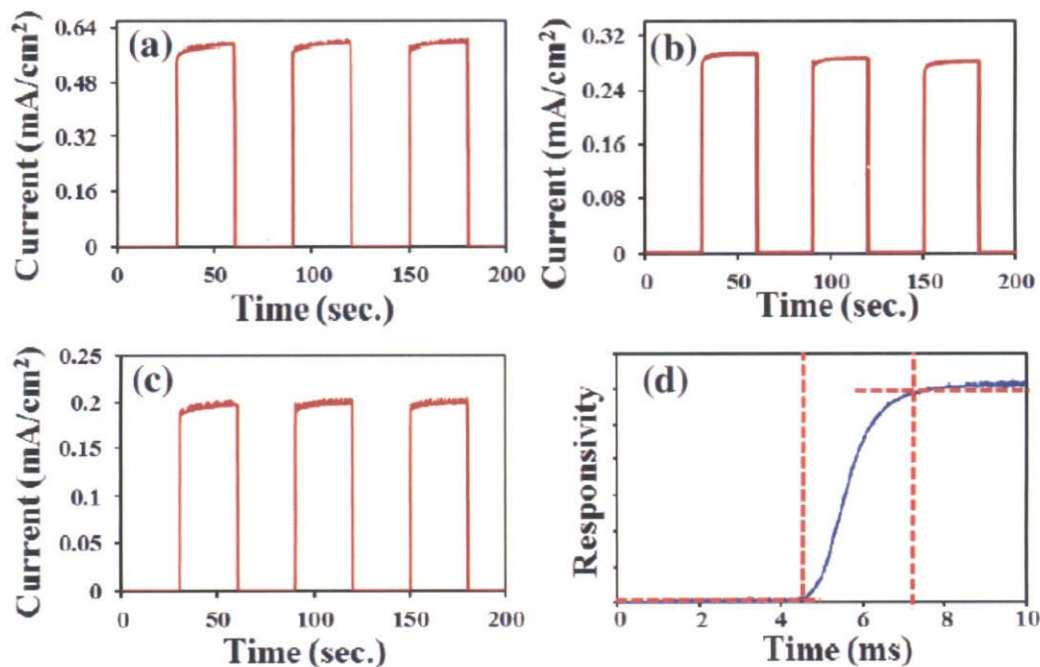
Figure 5.2.9   Time-dependent photocurrent of the fabricated device with illumination of 5.1, 3.6 and 2.1mW/cm^2 light at **(a)** 550 **(b)** 1000 and **(c)** 350 nm wavelengths. The graphene/n-Si Schottky junction photodetector shows photoresponse of **(a)** 122 **(b)** 98 and **(c)** 78 mAW^{-1} in the visible, NIR and near-UV, respectively. **(d)** Response time with illumination at 550 nm wavelength.

Figure 5.2.9d shows a photoresponse curve measured with illumination at 550 nm wavelength. The photoresponse time in the fabricated device is measure to be around 2.85 ms, which is comparable to CVD graphene/Si based photodetectors [18-22]. Considering these previous results, I demonstrate that the Schottky junction fabricated with Ag-NPs decorated graphene and n-Si shows significant photoresposne at quite low illumination intensity and zero bias voltage. Figure 5.2.10 shows a schematic illustration of the demonstrated photodetector device, illustrating the effect of plasmonic Ag-NPs on photoresponsivity. The strong photoresponce can be attributed to light interaction with the plasmonic Ag-NPs and formation of an effective Schottky junction.
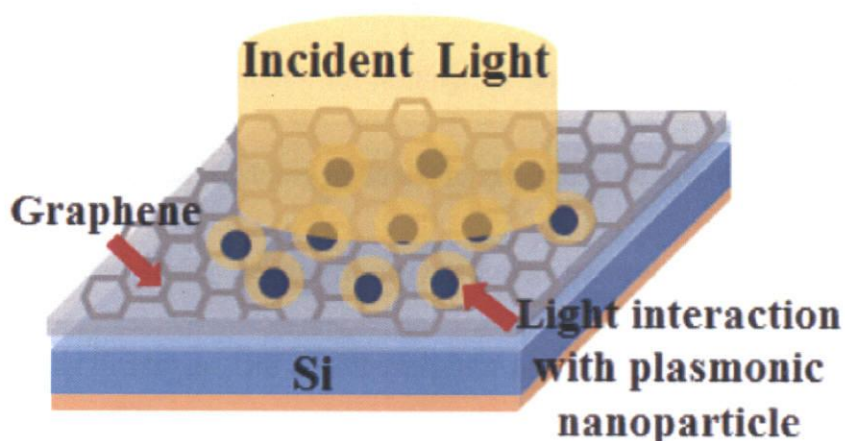
Figure 5.2.10   Schematic cartoon of the fabricated device, illustrating the effect of plasmonic Ag_NPs on photoresponsivity.

The Ag-NPs in the graphene can enhance near-field oscillation of conduction electrons and scattering of incident light. With oscillation, light can trapped around surface of Ag-NPs, leading to enhance local electrical field and thereby improving light absorption. Further enhancement of the overall photoresponsivity can be expected with higher quality graphene and optimized device structure and contact electrodes. Al can be used as an ohmic back contact, rather than Au:Sn to reduce dark current. My findings can be significant to obtain high performance broad-band photodetecotors with plasmonic silver nanoparticles decorated graphene Schottky junction device.

5.3   Conclusion

I have demonstrated formation of Ag-NPs in a CVD synthesized graphene by dissolving the base Ag foil and their integration for Schottky junction fabrication. Ag-NPs of the size 20-100 nm were directly obtained in graphene surface by dissolving the base Ag foil of as-synthesized graphene in a diluted HNO_3 solution. The Ag nanoparticles decorated graphene was transferred on a SiO_2 patterned n-Si substrate to fabricate a Schottky junction. Significant photoresponse has obtained with illumination of 3.6, 5.1 and 2.1mW/cm^2 of near-IR (1000 nm), visible (550 nm) and near-UV (350 nm) light, respectively. The Ag-NPs decorated graphene-Si Schottky junction showed photoresponse of 122, 98 and 78mAW^{-1} at 550, 350 and 1000 nm, respectively. The

strong photoresponce is attributed to light interaction with the plasmonic Ag-NPs and

efficient Schottky junction formation. In the fabricated device plasmonic Ag-NPs can

enhance light absorption and thereby enabling detection of the faintest incident light for

a broad-wavelength range.

5.4   Reference

[1]   A. K. Geim and K. S. Novoselov, *Nature mater,* **6**, 183, (2007)

[2]   S. V. Morozov , K. S. Novoselov , M. I. Katsnelson , F. Schedin , D. C. Elias , J. A. Jaszczak and A. K. Geim, *Phys. Rev. Lett.*, **100**, 016602, (2008)

[3]   R. R. Nair, P. Blake, A. N. Grigorenko, K. S. Novoselov, T. J. Booth, T. Stauber, N. M. R. Peres and A. K. Geim, *Science*, **320**, 1308, (2008)

[4]   F. Xia, T. Mueller, Y. m-. Lin, A. V. Garcia and P. Avouris, *Nat. Nano.* **4**, 839, (2009)

[5]   T. Mueller, F. Xia and P. Avouris, *Nat. Photon.*, **4**, 297, (2010)

[6]   N. M. Gabor, J. C. W. Song, Q. Ma, N. L. Nair, T. Taychatanapat, K. Watanabe, T. Taniguchi, L. S. Levitov and P. J. Herrero, *Science*, **334**, 648, (2011)

[7]   M. C. Lemme, F. H. L. Koppens, A. L. Falk, M. S. Rudner, H. Park, L. S. Levitov and C. M. Marcus, *Nano Lett.*, **11**, 4134, (2011)

[8]   Y. Zhang, T. Liu, B. Meng, X. Li, G. Liang, X. Hu and Q. J. Wang, *Nature Comm.*, **4**, 1811, (2013)

[9]   Y. Liu, R. Cheng, L. Liao, H. Zhou, J. Bai, G. Liu, L. Liu, Y. Huang and X. Duan, *Nature Comm.*, **2**, 579, (2011)

[10]   M. E. Ayhan, G. Kalita, S. Sharma, M. Tanemura, *Phys. stat. sol. RRL*, **7**, 1076, (2013)

[11]   B. Kiraly, E. V. Iski, A. J. Mannix, B. L. Fisher,   M. C. Hersam and N. P. Guisinger, *Nature Comm.*, **4**, 2804, (2013)

[12]   Z. Zhang, F. Xu, W. Yang, M. Guo, X. Wang, B. Zhanga and J. Tang, *Chem. Comm.*, **47**, 6440, (2011)

[13]   G. Kalita, R. Hirano, M. E. Ayhan and M. Tanemura, *J. Phys. D: Appl. Phys.*,

46, 455103, (2013)

[14]   E. C. Garnett, W. Cai,   J. J. Cha, F. Mahmood, S. T. Connor, M. G. Christoforo, Y. Cui, M. D. McGehee and M. L. Brongersma, *Nature Mater.*, **11**, 241, (2012)

[15]   M. A. M. Khan, S. Kumar, M. Ahamed, S. A. Alrokayan and M. S. Alsalhi, *Nano. Res. Lett.*, **6**, 434, (2011)

[16]   N. Jain, A. Bhargava, S. Majumdar, J. C. Tarafdar and J. Panwar, *Nanoscale*, **3**, 635, (2011)

[17]   M. Zhu, X. Li, Y. Guo, X. Li, P. Sun, X. Zang, K. Wang, M. Zhong, D. Wu and H. Zhu, *Nanoscale*, DOI: **10.1039**/x0xx00000x, (2014)

[18]   M. Zhu, X. Li, Y. Guo, X. Li, P. Sun, X. Zang, K. Wang, M. Zhong, D. Wu and H. Zhu, *Nanoscale*, **6**, 4909, (2014)

[19]   P. Lv, X. Zhang, X. Zhang, W. Deng and J. Jie, *IEEE Electron Dev. Lett.*, **34**,1337, (2013)

[20]   C. Xie, X. Zhang, Y. Wu, X. Zhang, X. Zhang, Y. Wang, W. Zhang, P. Gao, Y.Hana and J. Jie, *J. Mater. Chem. A*, **1**, 8567, (2013)

[21]   Z Zhang, Y Guo, X. Wang, D. Li, F. Wang and S. Xie, *Adv. Funct. Mater.*, **24**,835, (2014)

[22]   X. An, F. Liu, Y. J. Jung and S. Kar, *Nano Lett.*, **13**, 909, (2013)

CHAPTER VI

Transfer-Free Synthesis of Graphene with Carbon Diffusion Barrier by Solid Phase Process Using Tri-block Co-Polymer

Graphene has been derived or synthesized by various approaches, including, micromechanical cleavage of highly oriented pyrolytic graphite (HOPG) [1], epitaxial growth on silicon carbide (SiC) [2], reduction of chemically exfoliated graphene oxide [3] and chemical vapor deposition (CVD) on transition metals [4-6]. However, in terms of many practical device applications, high quality CVD derived graphene have to be transferred to insulting arbitrary substrates. To overcome drawback of the additional transfer process, direct synthesis of graphene on the target substrate has been investigated for practical device applications [7-10]. Previously, Ismach et al. has demonstrated direct synthesis of few-layer graphene on dielectric surface by a CVD approach owing to evaporation of Cu catalytic layer during growth process [11]. Similarly, direct graphene growth has been achieved on germanium (Ge) in a CVD process [12]. Previously, our group have also demonstrated synthesis of bi-layer and few-layer graphene on SiO_2/Si substrate by Co catalytic layer assisted crystallization of a-C thin film [13].

Transfer free synthesized few-layer graphene has been combined with n-Si substrate for fabrication of a Schottky junction. However, control carbon diffusion and graphitization process at the metal catalytic layer and substrate interface were inhomogeneous to obtain a single layer graphene. Crystallization of the a-C thin film at the substrate interface remains a challenge to obtain high quality monolayer graphene.

In this study, I used the Pluronic F127 ($EO_{106}PO_{70}EO_{106}$) co-polymer as the carbon source to synthesis graphene directly on a SiO_2/Si substrate. The co-polymer can be easily dissolved in common organic solvents such as acetone, ethanol and methanol or water considering the low molecular weight. Monolayer graphene is successfully synthesized by a solid phase reaction from a co-polymer thin film by metal (Ni) catalyzation. The developed process for monolayer synthesis of graphene can be remarkable to overcome the drawback of unwanted impurities and formation of wrinkle during extra transfer process.

6.1 Experimental

PluronicF127 ($EO_{106}PO_{70}EO_{106}$)was purchased from Wako Chemicals and used as received for thin film deposition by spin coating. Figure 6.1.1a shows a molecular structure of the block co-polymer used for graphene synthesis. The co-polymer was dissolved in water (0.1wt %) and spin coated onto SiO_2/Si substrate at 5000 rpm for 2 min. The top Ni thin layer is deposited by pulsed laser deposition (PLD)

technique using Nd:YAG laser (λ = 355 nm, energy density of 30mJ and f=10 Hz). Highly carbon soluble Ni metal layer (100 nm) is used as catalyst layer. Subsequently, NiO carbon diffusion barrier layer was created on top of Ni layer by ozone UV irradiation. In-situ annealing of the NiO/Ni/co-polymer stack layers on SiO_2/Si substrate is performed at 1000 ^oC in 50 sccm of H_2 atmosphere using infrared heater with rapid cooling process. Finally, NiO/Ni layer is removed by chemical etching with diluted nitric acid solution 35%) and graphene film was obtained directly on the SiO_2/Si substrate. Schematic of transfer-free graphene synthesis by the solid phase reaction process is demonstrated in figure 6.1.1b.
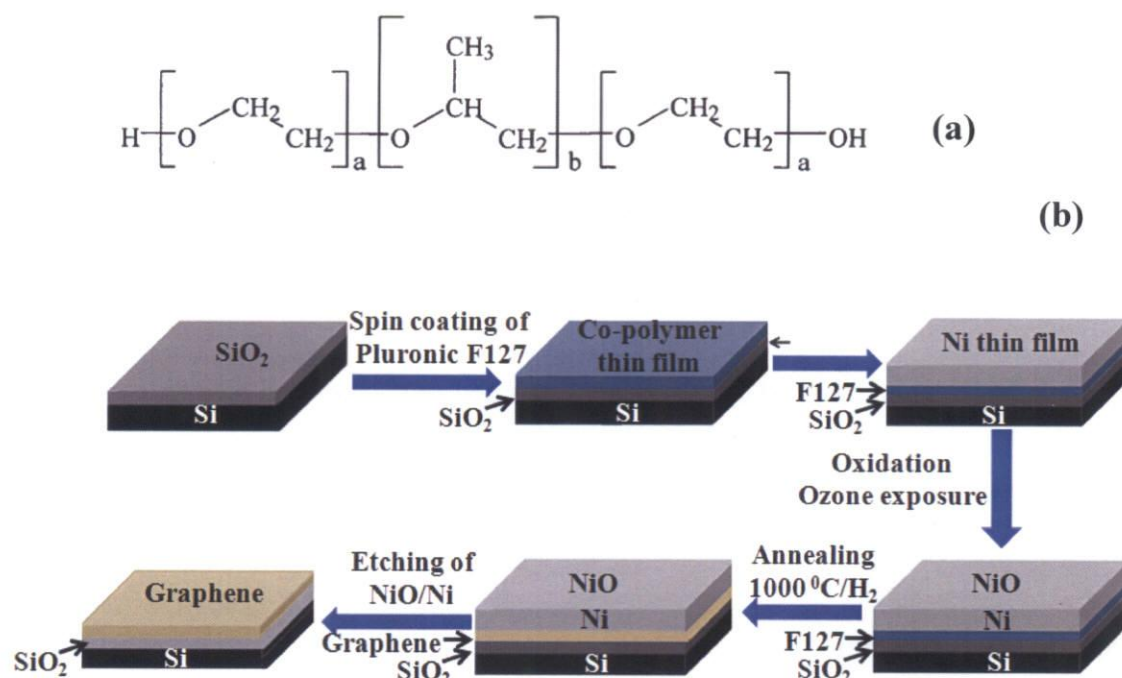
Figure 6.1.1   (a) Chemical formula of triblock co-polymer Pluronic F127 (b) schematic diagram of the transfer-free graphene synthesis on SiO2/Si substrate by the solid phase reaction process.

Morphological and structural analysis of the deposited material on SiO_2/Si

substrate is carried out with Raman spectroscopy, optical and atomic force microscopy

(AFM). Raman studies were performed with NRS 3300 laser Raman spectrometer with

laser excitation energy of 532.08 nm. The optical microscopy studies are carried out

with VHX-500 digital microscope. AFM study was performed with a JSPM-5200

scanning probe microscope. Scanning electron microscope (SEM) analysis was carried

out by ultra-high resolution Elionix ESM-9000 to identify the graphene layer.

6.2   Result and Discussion

Thermally decomposable block co-polymer Pluronic F127 is highly soluble in

water due to presence of plenty of hydroxyl groups (-OH) in the carbon chain.

Deposition of a thin film of the co-polymer is possible due to high solubility. Formation

of graphene and graphitization process using a block co-polymer as precursor is

explored considering presence of a long carbon chain.

6.2.1   The Effect of The Amount of Tri-Block c-opolymer Pluronic F127

Graphene growth is investigated with different concentration of the tri block

co-polymer to optimize thickness of the thin film. Figure 6.2.1 shows Raman spectra of

the graphene directly obtained on SiO_2/Si substrate by the solid phase reaction approach

using 100 and 200 μl of co-polymer Pluronic F127 precursor. Raman spectroscopy is the most common way to study the quality and number of the synthesized graphene layer. The most pronounced peaks in the spectra are observed at 1350, 1580 and 2695 cm^{-1}, corresponding to disorder-induced D, graphitic G and second order 2D peak, respectively.

The synthesized graphene with 100 μl co-polymers shows a strong D peak and higher I_D/I_G ratio of 1.03. Whereas, synthesized graphene using 200 μl co-polymers shows much better graphitization with low intense D peak with I_D/I_G ratio of 0.54. This result shows that the amount of carbon source significantly affect the graphene growth in the solid phase reaction. Thickness of the tri-block co-polymer films is controlled by simply adjusting the amount of Pluronic F127 precursor. The study signifies that less quantity of the polymer is not sufficient for good graphitization and graphene growth on the substrate surface. A higher amount of tri-block co-polymer effectively decomposes and precipitates on the SiO2/Si substrate to obtain single layer and bilayer graphene formation.
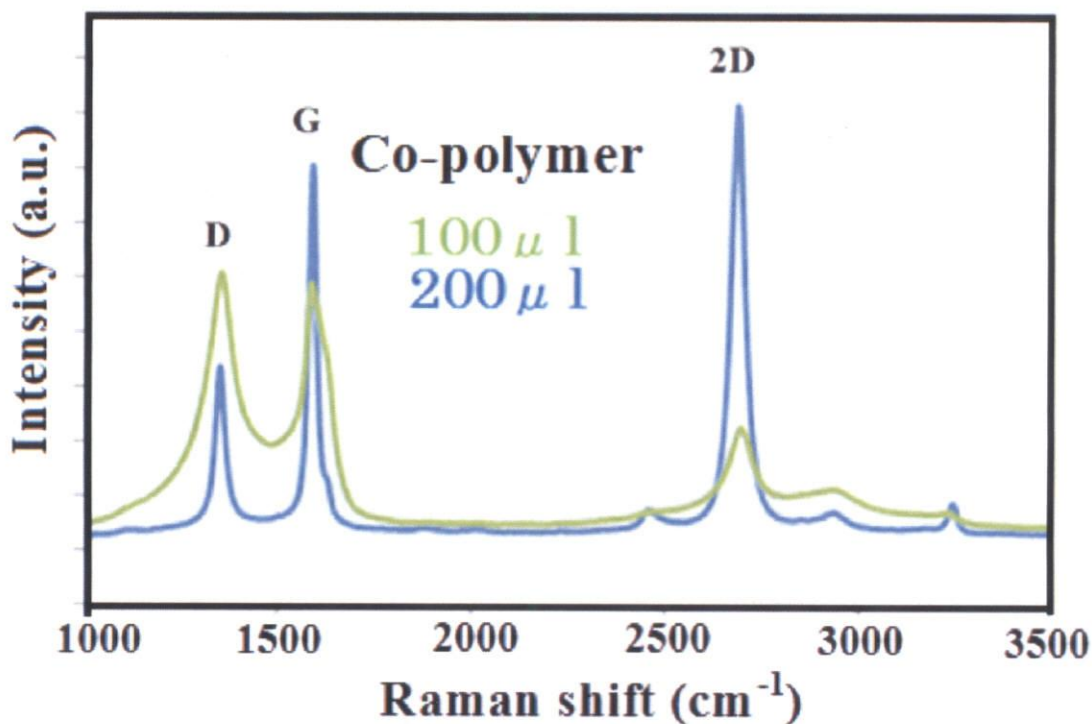
Figure 6.2.1   Raman spectra of synthesized graphene directly on SiO$_2$/Si substrate using 100 and 200 µl of tri-block co-polymer Pluronic F127.

6.2.2   The Effect of Annealing Time

Figure 6.2.2 shows Raman studies of the synthesized graphene with different annealing time. Good graphitization and uniform graphene formation is not observed with an annealing time for 10 min. Synthesized carbon material shows a strong D peak and less intense second order 2D peak, corresponding to disordered few-layer graphene growth. Increasing the annealing time from 10 to 15 and 30 min, better quality single layer and bilayer graphene formation is obtained as shown in figure 6.2.2. For a monolayer graphene full width at half maximum (FWHM) of G and 2D peak is found to be 23.5 and 41 cm^{-1}, respectively. Synthesis of monolayer graphene is observed to be homogenous and uniform for 15 min annealing duration.
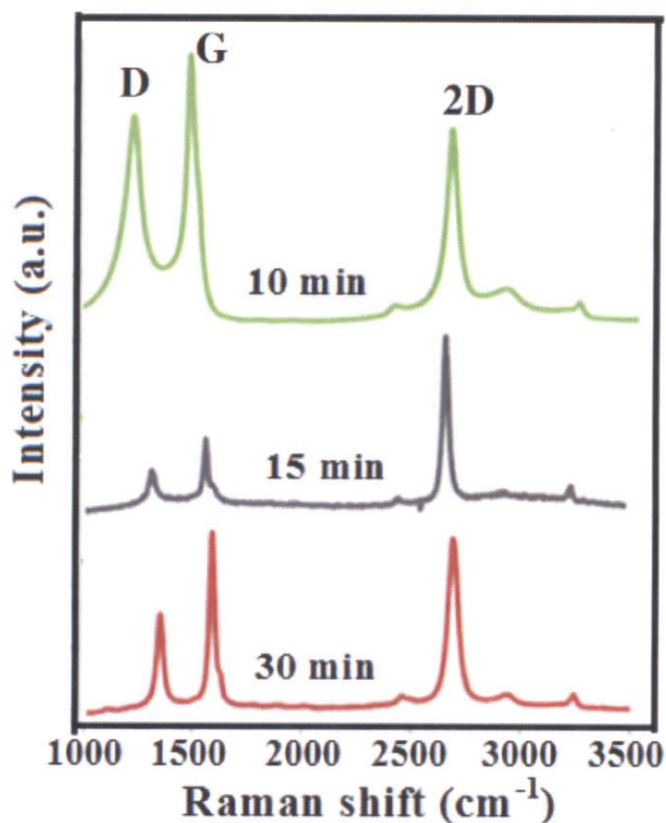
Figure 6.2.2   Raman spectra of directly synthesized graphene on SiO_2/Si substrate for the annealing duration of 10, 15 and 30 min.

Figure 6.2.3 shows the optical microscopy images of the graphene formation on the SiO_2/Si substrate. Cluster like structure of the graphene domains observed by the optical microscope analyses. Increasing the annealing time formation of larger graphene clusters were observed. Again, increasing the annealing duration more than 30 min, irregular carbonization was observed. Subsequently, by increasing the annealing temperature up to 1000°C, Ni metal layer become much harder and become difficult to remove from the substrate. My studies showed that in the solid phase reaction process graphene layer number can be easily controlled by changing the annealing time and thickness of the co-polymer layer.
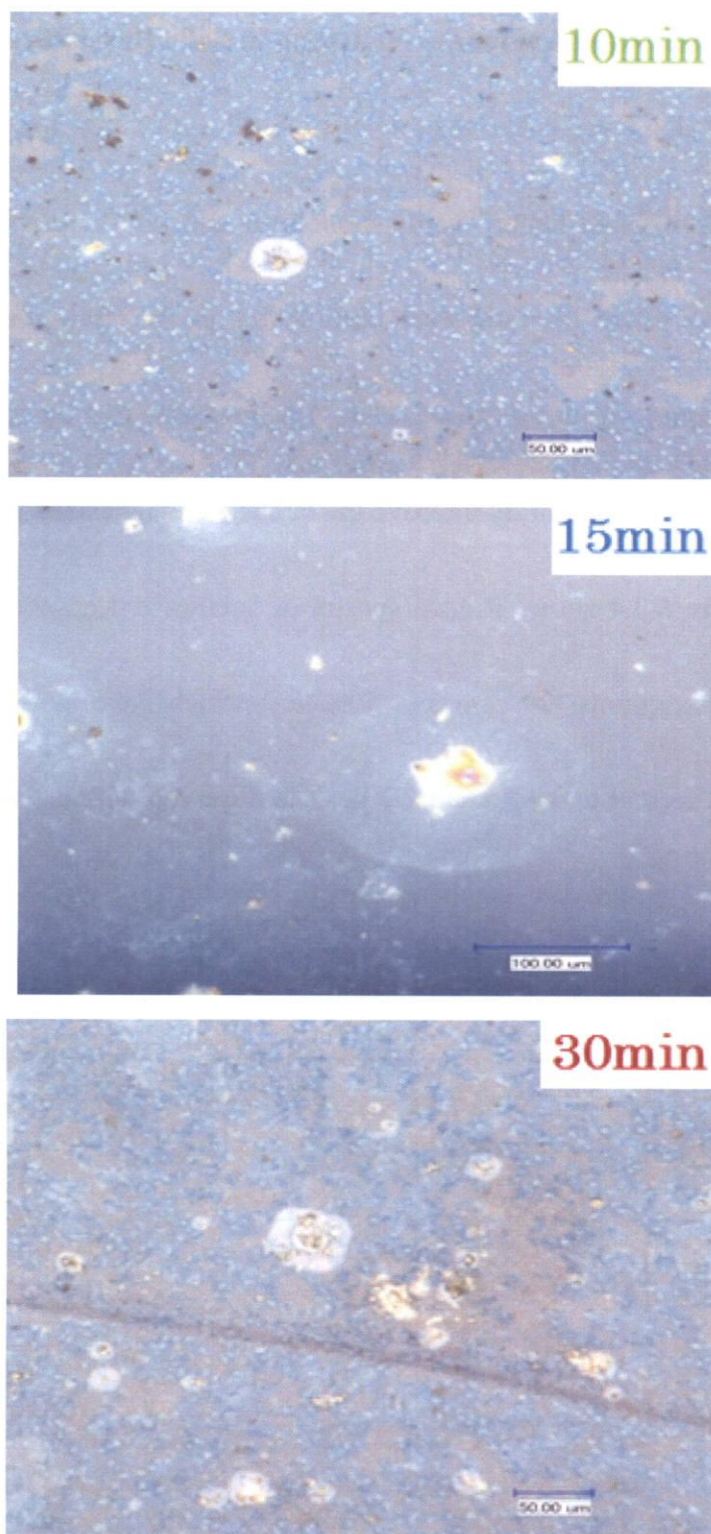
Figure 6.2.3   Optical microscope images of directly synthesized graphene on SiO₂/Si substrate for the annealing duration of 10, 15 and 30 min.

6.2.3   The Effect of the Amount of Hydrogen in Solid Phase Reaction

I have also investigated the role of H_2 for the graphitization process in the solid phase reaction to obtain better quality monolayer and bilayer graphene. My previous studies of solid phase reaction were carried out in Ar atmosphere and monolayer graphene formation was not achieved. Here, I demonstrate that the annealing process in presence of H_2 can significantly improve the quality of synthesized graphene on SiO_2/Si substrate. Figure 6.2.4 shows Raman spectra of synthesized graphene in two different hydrogen concentrations (20sccm and 50scmm) which gave better quality graphene. Higher intense second order Raman 2D peak is observed with a FWHM of around 41 cm^{-1}. I observed monolayer graphene growth directly on SiO_2/Si substrate with the annealing process using 50 sccm of H_2.
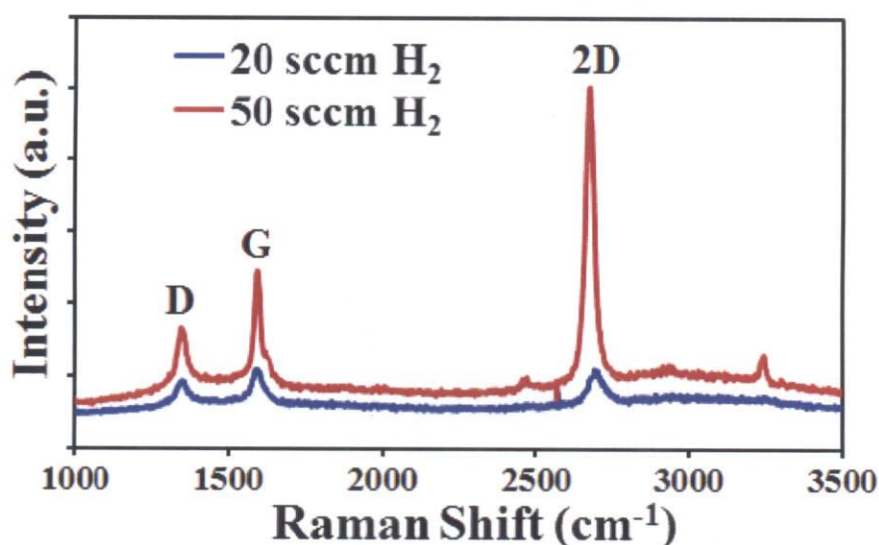
Figure 6.2.4   Raman spectra of transfer-free graphene synthesized on SiO_2/Si substrate using 20 and 50 sccm of H_2.
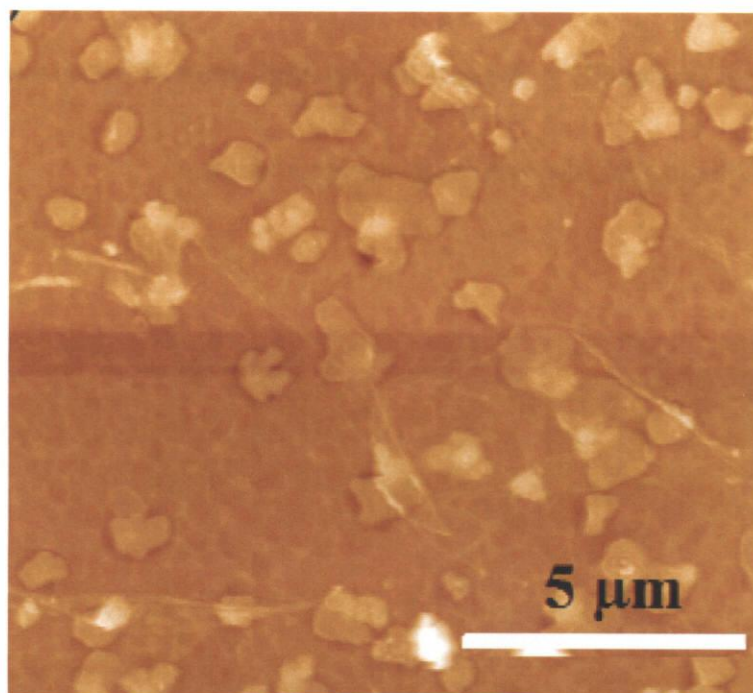
Figure 6.2.5 AFM image of as-synthesized graphene flakes on SiO$_2$/Si substrate.

Figure 6.2.5 shows an atomic force microscope (AFM) image of the directly obtained graphene on SiO$_2$/Si substrate by the solid phase reaction. Flake like morphology of graphene on the substrate surface was observed. Figure 6.2.6 shows scanning electron microscope (SEM) images of the graphene obtained by ERA-9000, which provide ultra-high resolution in the direction of 1nm height. The directly synthesized graphene layer is evidently identified (figure 6.2.6) on the SiO$_2$/Si substrate. At present, evaluation of certain thinness of the graphene is quite difficult due to rough base substrate. The synthesized graphene films by the developed method shows several

discontinuous domains like structure. In this technique, graphene obtained on SiO_2/Si

substrate can be directly integrated for the fabrication of transistors, Schottky junction

devices, photodetector like energy device applications.
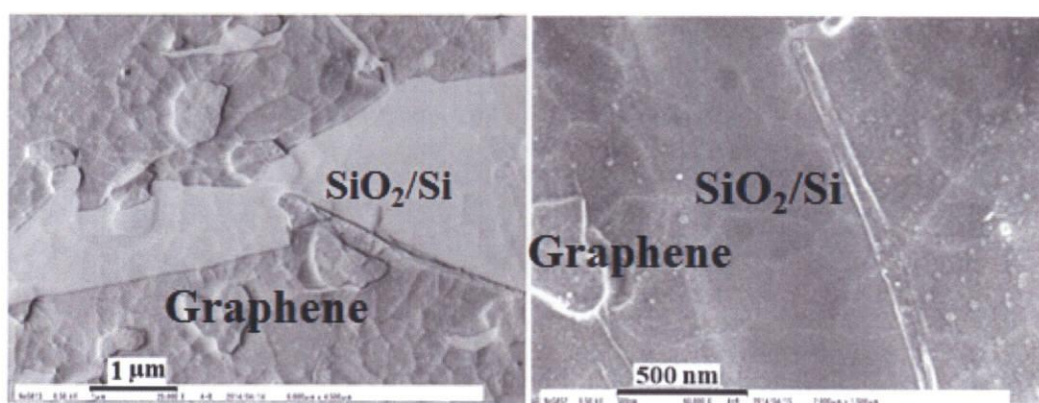
Figure 6.2.6   Ultra high resolution SEM image of as-synthesized graphene flakes on

SiO_2/Si substrate.

Figure 6.2.7 shows a schematic representation of graphene growth mechanism

in the developed process. In the annealing process, tri-block co-polymer decomposed

and dehydrogenated at a high temperature. Subsequently, carbon atoms diffuse to the Ni

catalytic layer and graphene formation occurs with segregation during cooling process.

The top NiO thin layer acts as a carbon diffusion barrier, like that carbon atoms do not

diffuse to upper surface. Hereby, most of the diffused carbon atoms segregate at the

interface of Ni and SiO_2/Si substrate. NiO layer has a critical role in the graphene

growth process as in absence most of the carbon diffed and segregate at upper surface. NiO layer prevent carbon diffusion to top surface thereby making it possible to get better quality graphene on directly SiO_2/Si substrate. In our previous studies of a solid phase reaction bilayer and few layer graphene growth was obtained by using Co and CoO as the catalytic layer and diffusion barrier layer, respectively.

While, in this study synthesis of monolayer graphene is achieved by the solid phase reaction process using a tri-block polymer in H_2 atmosphere annealing by infrared heating system. This approach can be significant to achieve monolayer and bilayer graphene or to control the growth process. The demonstrated transfer-free synthesis can be significant for various device applications such field effect transistors, Schotkky junction, photo diodes, barristors and other solar photovoltaic devices by accurately controlling the layer numbers.
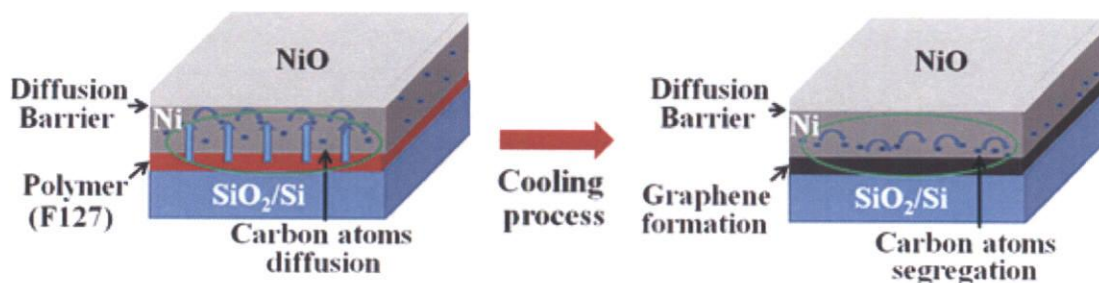
Figure 6.2.7   Schematic illustration of carbon atoms diffusion and segregation in presence of Ni and NiO catalytic and carbon diffusion barrier layer, respectively for the graphene growth process.

6.3 Conclusion

I demonstrate, successful synthesis of monolayer graphene by a solid phase reaction approach using the triblock co-polymer Pluronic F127 as carbon source. The amount of Pluronic F127 precursor used for thin film deposition by spin coating, significantly affects the formation of graphene. I obtained that the number of layers can be controlled by optimizing the thickness of the co-polymer film, annealing duration time and the amount of H_2 gas. Monolayer graphene were obtained directly on the SiO_2/Si substrate by graphitizing the triblock co-polymer in presence of the Ni and NiO catalytic and carbon diffusion barrier layer, respectively. The findings revealed that the NiO/Ni stacked thickness of polymer layer and reaction process in H_2 atmosphere strongly affect the quality of synthesized graphene.

6.4 References

[1] K. S. Novoselov, D. Jiang, F. Schedin, T. J. Booth, V. V. Khotkevich, S. V. Morozov, and A. K. Geim, *Proc. Natl. Acad. Sci.* **102, 10451** (2005).

[2] C. Berger, Z. Song, X. Li, X. Wu, N. Brown, C. Naud, D. Mayou, T. Li, J. Hass, A. N. Marchenkov, E. H. Conrad, P. N. First, and W. A. de Heer, *Science* **312, 1191**(2006).

[3] S. Stankovich, D. A. Dikin, G. H. B. Dommett, K. M. Kohlhaas, E. J. Zimney, E. A. Stach, R. D. Piner, S. T. Nguyen, and R. S. Ruoff, *Nature* **442, 282** (2006).

[4] P. R. Somani, S. P. Somani and M. Umeno, *Chem. Phys. Lett.* **430, 56** (2006).

[5] Q. Yu,J. Lian, S. Siriponglert, H. Li, Y. P. Chen and S. S. Pei, *Appl. Phys. Lett.* **93, 113103** (2008).

[6] A. Reina, X. Jia, H. John, D. Nezich, H. Son, V. Bulovic, M.S. Dresselhaus, and J. Kong, *Nano Lett.* **9, 30** (2009).

[7] Yan Z, Peng Z, Sun Z, Yao J, Zhu Y, Liu Z, Ajayan P M andTour J M, *ACS Nano* **5 8187** (2011)

[8] Su C Y et al *Nano Lett.* **11 3612,** (2011)

[9] GKalita, M SKayashta, K Wakita and M Umeno,*RSCAdv.,* **2 3225**(2012)

[10] J Kwak et al,*Nature Commun.,* **3 1**(2012)

[11] Ismach, A.; Druzgalski, C.; Penwell, S.; Schwartzberg, A.;Zheng, M.; Javey, A.; Bokor, J.; Zhang, Y.,*Nano Lett.,* **10, 1542–1548** (2010.)

[12] Gang Wang et al., Scientific Reports **3, 10,1038** (2013)

[13] G. Kalita, R. Hirano, M.E.Ayhan, M.Tanemura, *J.Phys. D. Appl Phys.* **46, 455103** (2013)

CHAPTER VII

SUMMARY and FUTURE PLAN

7.1   Overall Summary

Needs of the next generation energy sources increase day by day increasing the cost of fossil fuels, as well as decreasing the source of fossil fuels. Unfortunately, only 19% of global energy consumption of the world supplied from renewable energy according to 2013 energy trends. To leave a livable World to our children we have to reconsider again about renewable and clean energy sources.

Graphene is one of the most promising candidate for renewable energy device applications. Graphene based composite nanomaterials can be used for various energy device applications, considering extraordinary electronic, mechanical, optical and chemical properties. There are many obstacles in conventional applications that employed in renewable energy. Among these problems, I have tackled to solve two main problem in energy related devices. The first problem is the low light absorption and low photoresponsivity in monolayer graphene. The second problem is transfer of graphene in many energy device applications that has to be solved.

In this dissertation, two different approaches of synthesis of graphene and an Ag-NPs decorated grahene based photodetector device were demonstrated to solve above mentioned problems. First is synthesis of graphene on noble metal silver by chemical vapor deposition and second is transfer-free graphene synthesis with carbon diffusion barrier by solid phase reaction process using tri-block co-polymer.

In the first chapter, current energy trends, importance of renewable energy, current issues of graphene and integration of graphene with next generation energy device applications are discussed. Motivation of work has also discussed in terms of synthesis of graphene by chemical vapor deposition (CVD), solid phase reaction approaches and their applications.

The second chapter presents the classification of frontier carbonaceous materials such as fullerenes, carbon nanotubes and graphene. Structure, properties, applications, and synthesis methods of graphene were presented in this chapter.

The third chapter, experimental facilities like chemical vapor deposition (CVD) systems and solid phase reaction systems were presented. Furthermore characterization facilities such as Raman spectroscopy, scanning electron microscopy (SEM), transmission electron microscopy (TEM), atomic force microscopy (AFM) were also presented.

Fourth chapter demonstrates the synthesis of graphene on Ag foil by the AP-CVD process as a tarnish-resistant coating. Although most essential substrate for catalytic decomposition of hydrocarbon are Ni, Cu and Co; Ag as substrate in CVD technic can be very interesting substrate material considering its unique optical properties and surface plasmonic resonance. For the first time I have demonstrated the synthesis of graphene on noncatalytic Ag metal by CVD approach using solid carbon source.

My results based on optical and morphological evidence which are obtained by optical and scanning electron microscopy studies, as well as correlating with XPS analyses showed that coating of silver surface with graphene film effectively preserve the silver material from sulfurization and tarnishing. Synthesized graphene can be significant for solar panels, reflector coating process, Schottky junction devices. Graphene synthesized on Ag is electrically conductive and nearly transparent and having to capability of absorbing different wavelength of light give an opportunity to be employed in solar photovoltaic industry. Furthermore synthesized continuous few-layer graphene can be used as electrode materials in next generation batteries and supercapacitor technologies, as well.

Chapter fifth demonstrates formation of Ag-NPs in a CVD synthesized graphene by dissolving the base Ag foil and their integration for Schottky junction fabrication. Combination of graphene and noble metal silver nanoparticles showed that excellent optical absorption compare to previously reported devices thus fabricated Schottky junction device enabled to detect of the faintest incident light. Ag-NPs of the size 20-100 nm were directly obtained in graphene surface by dissolving the base Ag foil of as-synthesized graphene in a diluted HNO_3 solution. Significant photoresponse has obtained with illumination of 3.6, 5.1 and 2.1mW/cm^2 of near-IR (1000 nm), visible (550 nm) and near-UV (350 nm) light, respectively. The Ag-NPs decorated graphene-Si Schottky junction showed photoresponse of 122, 98 and 78mAW^{-1} at 550, 350 and 1000 nm, respectively.

Ag-NPs can enhance light absorption and thereby enabling detection of the faintest incident light for a broad-wavelength range. In contrast to previous reports, I demonstrated a one-step approach to obtain Ag-NPs decorated graphene rather than using any other reagent or stabilizer. The photoresponse time in the fabricated device is measure to be around 2.85 ms, which is comparable to other CVD graphene/Si based photodetectors. Previously, facile one-pot synthesize of Ag-NPs and graphene composite with GO and $AgNO_3$ solution in presence of a reductant and stabilizer has

been achieved. The nanoparticles obtained in our demonstrated process remain highly disperse in the graphene sheets. Considering these previous findings, I demonstrate that the Schottky junction fabricated with Ag-NPs decorated graphene and n-Si shows significant photoresposne at quite low illumination intensity and zero bias voltage. However, dark current is still high in my photodetector device. If device structure can be optimized and by using Al as ohmic back contact rather than Au:Sn, much better dark current characteristics and higher photoresponsivity can be achieved. For the first time demonstrated one step approach to obtain Ag-NPs decorated graphene without using any other reagent can be used for various device applications such as solar cell, fuel cell, photodetectors, photodiodes, next generation batteries and supercapacitors.

Chapter sixth demonstrates direct synthesis of single layer and bilayer graphene with carbon diffusion barrier by solid phase reaction process using tri-block co-polymer. One of the main obstacle in graphene technology is high quality CVD graphene must be transferred to insulting arbitrary substrates to fabricate practical device applications. For the first time monolayer graphene were obtained directly on the SiO_2/Si substrate by graphitizing the tri-block co-polymer in presence of the Ni and NiO catalytic and carbon diffusion barrier layer, respectively Selection of precursor was the critical factor for this work.

Number of graphene layers can be controlled easily by only changing the amount of precursor. A higher amount (200 µl) of tri-block co-polymer effectively decomposes and precipitates on the SiO2/Si substrate to obtain monolayer and bilayer graphene formation in solid phase reaction. My studies also showed that in the solid phase reaction process, number of graphene layer can be easily controlled by changing the annealing time and optimize annealing duration is estimated as 15min for uniform monolayer and bilayer graphene formation. The role of the amount H_2 was also investigated in solid phase reaction process.

In my preliminary experiments in-situ annealing carried out in Ar atmosphere in solid phase reaction process. However single layer and bilayer graphene formation was not observed. Presence of H_2 gas can provide much better graphitization and monolayer and bilayer graphene formation in the solid phase reaction process. Graphene formation and graphitization process using a 100% active, thermally decomposable block co-polymer as carbon source is investigated considering presence of a long carbon chain. The developed process for monolayer graphene growth can be significant to overcome the drawback of undesirable impurities and wrinkle formation during an additional transfer process.

Chapter seventh presents the overall summary about above mentioned approaches of graphene synthesis and their applications results which are discussed in Chapter IV, Chapter V and Chapter VI in details. Future prospects were also discussed in this chapter.

In conclusion, based on the above discussed results; remarkable solutions have been presented to solve two major problem, which are low light interaction, low photoresponsivity properties of monolayer graphene and additional graphene transfer process in energy device application. Surface plasmonic Ag nanoparticles have been successfully integrated with continuous graphene film to increase light absorption in fabricated photodetector device. Combination of Ag-NPs with graphene was achieved by one-step approach without using any other reagent as explained in chapter 4. By this novel one-step approach, simple energy device architecture and high light sensitivity was achieved. Compare to other conventional photodetectors and other graphene based photodetector devices, my demonstrated Ag-NPs decorated graphene based photodetector device shows significant photoresponse properties.

To solve graphene transfer problem in energy devices, purposed direct synthesis of graphene by solid phase reaction process using common type block co-polymer was successfully carried out. Uniform monolayer and bilayer graphene were synthesized

directly on insulating substrates. Undesirable impurities, wrinkle formations and inhomogeneous interface formation problems can be avoided by this solid phase reaction process. Transfer free synthesized monolayer and bilayer graphene can be employed in Schottky junction devices, photodetectors, electrode materials in supercapacitors, solar photovoltaic devices and so on.

In this dissertation, to solve above mentioned problems in next generation energy device application, proposed study was successfully carried out. This thesis may open up new wide range research in renewable energy device applications.

7.2   Future Prospects

First time I have been demonstrated the synthesis of graphene on noble metal silver by chemical vapor deposition process [1]. Recently, B.Kiraly et. al. was reported decoupled graphene growth on single-crystal Ag(111) substrate by a CVD process using solid carbon source [2]. In despite of regarding to solubility of carbon in Ag is considerably low as that of Cu compare to Ni catalytic metal, the unique optical properties are remarkable for next generation photovoltaic device applications.

As a future prospect, synthesis of single and bilayer graphene on silver have to be investigated using different precursors both gas based and solid carbon sources. Ag-NPs decorated monolayer graphene based solar cells, other photo detector like devices and transparent conductors can be very interesting. On the other hand synthesized graphene on Ag by CVD approach can be combined with other materials like carbon nanotubes, mesoporous carbons, MoS_2 etc. to develop nano composite materials.

To overcome drawback of the transfer process in CVD approach, demonstrated direct synthesis of graphene by solid phase reaction method can be developed by increasing the thickness of Ni catalytic layer and using different block co-polymers. Thus we can increase the domain size of graphene. On the other hand noble silver can be employed as catalytic metal in solid phase reaction process.

7.3   References

[1]   M. E. Ayhan, G. Kalita, S. Sharma, M. Tanemura, *Phys. stat. sol. RRL*, **7, 1076**, (2013)

[2]   B. Kiraly, E. V. Iski, A. J. Mannix, B. L. Fisher,   M. C. Hersam and N. P. Guisinger, *Nature Comm.*, **4, 2804**, (2013)

List of Publications

1) **Muhammed Emre Ayhan**, Golap Kalita, Subash Sharma, Masaki Tanemura; "Chemical vapor deposition of graphene on silver foil as a tarnish resistant coating", *Physicsa Status Solidi RRL*, **1076–1079**, (2013)

2) **Muhammed Emre Ayhan**, Golap Kalita, Ryo Hirano, Masaki Tanemura, "Synthesis of transfer-free graphene by solid phase reaction process in presence of a carbon diffusion barrier", **Materials Letters.**, (2014) in press (Volume 129, 15 August 2014, Pages 76-79; DOI: 10.1016/j.matlet.2014.05.007).

3) **Muhammed Emre Ayhan**, Golap Kalita, Masaharu Kondo, Masaki Tanemura, "Photoresponsivity of silver nanoparticles decorated graphene-silicon Schottky junction", **RSC Advance,** (2014) in press. (DOI: 10.1039/C4RA02867H, received 01 Apr 2014, accepted 09 Jun 2014, first publish online 2014)

4) Kalita Golap, **Ayhan Muhammed E.**, Sharma Subash, Shinde Sachin M., Ghimire Dilip, Wakita Koichi, Umeno Masayoshi, Tanemura Masaki; "Low temperature deposited graphene by surface wave plasma CVD as effective oxidation resistive barrier", *Corrosion Science vol. 78 p. 183-187*, (2014)

5) Kalita, Golap, Hirano Ryo, **Ayhan Muhammed E**, Tanemura Masaki; "Fabrication of a Schottky junction diode with direct growth graphene on silicon by a solid phase reaction", *Journal of Physics D: Applied Physics* vol. **46 issue 45, p. 455103-455103,**(2013)

6) Sharma Subash, Kalita Golap, **Ayhan Muhammed Emre**, Wakita Koichi, Umeno Masayoshi, Tanemura Masaki, "Synthesis of hexagonal graphene on polycrystalline Cu foil from solid camphor by atmospheric pressure chemical vapor deposition", *Journal of Materials Science* **vol. 48 issue p. 7036 – 7041** (2013)

7) Tatsuo Kimura, **Ayhan M.Emre**, Kazumi Kato, Yasuhiko Hayashi; "Phenol resin carbonized films with anisotropic shrinkage driven ordered mesoporous structures", *Journal of Material Chemistry. A,,***1, 15135-15141,** (2013)

Presentations

1) Subash Sharma, Golap Kalita, **Ayhan Emre**, Ryo Hirano, Masaki Tanemura, "Evolution of chemical vapor deposited graphene domains on Ni and Cu foils using camphor precursor", **60th JSAP Spring Meeting**, Japan, (2013)

2) **Muhammed Emre Ayhan**, Kalita Golap, Sharma Subash, Shinde Sachin, Masaki Tanemura, "Synthesis of graphene on silver (Ag) foil by chemical vapor deposition (CVD) as a tarnish resistant coating", *74th Japan Society of Applied Physics Autumn Meeting*, Japan (2013)

3) Subash Sharma, Golap Kalita, Remi Papon, **Emre Ayhan**, Ryo Hirano, Masaki Tanemura, "Graphene growth on polycrystalline Cu foil using solid carbon source by atmospheric pressure chemical vapor deposition", *74th Japan Society of Applied Physics Autumn Meeting,*, Japan (2013)

4) **Muhammed Emre Ayhan**, Kalita Golap, Ryo Hirano, Sharma Subash, Masaki Tanemura, "Transfer-Free Synthesis of Graphene by Solid Phase Reaction",**12th International Conference on Atomically Controlled Surfaces, Interfaces and Nanostructures**, Japan (2013)

ACKNOWLEDGEMENTS

Author Profile

Personal Information

AYHAN Muhammed Emre

Department of Frontier Materials, Nagoya Institute of Technology

Gokiso-cho, Showa-ku, Nagoya, Aichi, Japan

E-mail: m.emreayhan@gmail.com

Nationality: Turkey

Date of birth: Apr.17, 1981

Languages: Turkish, English, Japanese

Education History

2011-2014	Ph.D Course, Synthesis of graphene by chemical vapor deposition and solid phase reaction process towards next generation energy applications, Department of Frontier Materials, Nagoya Institute of Technology, Nagoya, JAPAN
2009-2011	Master Course, Nanoscale Characterization of Metal-Filled Carbon Nanotubes, Department of Frontier Materials, Nagoya Institute of Technology, Nagoya, JAPAN
2008- 2009	Research Student, Carbon Nano Materials for Next Generation Energy Source, Department of Frontier Materials, Nagoya Institute of Technology, Nagoya, JAPAN
1998- 2004	Bachelor in Electrical and Electronic Engineering, Faculty of Engineering, University of Inonu, Malatya, TURKEY

AVARD and SCHOLARSHIPS

2013-2014	Heiwa Nakajima Foundation Scholarship
2011-2013	NGK Foundation Scholarship
2009-2011	Yoneyama Rotary Club Scholarship